REPORT DOCUMENTATION PAGE

Form Approved
OMB No. 0704-0188

2. REPORT DATE	3. REPORT TYPE AND DATES COVERED
October 1991	Final Report 1 Apr 88 - 30 Jun 91

4. TITLE AND SUBTITLE
Ceramics Derived from Organo-Metallic Precursors

5. FUNDING NUMBERS
61102F 2303/A3

6. AUTHOR(S)
Donald R. Uhlmann

7. PERFORMING ORGANIZATION NAME(S) AND ADDRESS(ES)
University of Arizona
Department of Material Science
Tucson, AZ 85721

8. PERFORMING ORGANIZATION REPORT NUMBER
AFOSR-TR 91 0887

9. SPONSORING/MONITORING AGENCY NAME(S) AND ADDRESS(ES)
AFOSR/NC
Bolling AFB, DC 20332-6448

10. SPONSORING/MONITORING AGENCY REPORT NUMBER
F49620-88-C-0064

11. SUPPLEMENTARY NOTES

12a. DISTRIBUTION/AVAILABILITY STATEMENT
Approved for public release; distribution is unlimited

12b. DISTRIBUTION CODE

13. ABSTRACT (Maximum 200 words)

See Back

14. SUBJECT TERMS

15. NUMBER OF PAGES
153

16. PRICE CODE

17. SECURITY CLASSIFICATION OF REPORT	18. SECURITY CLASSIFICATION OF THIS PAGE	19. SECURITY CLASSIFICATION OF ABSTRACT	20. LIMITATION OF ABSTRACT
UNCLASSIFIED	UNCLASSIFIED	UNCLASSIFIED	SAR

13. Work carried out under the present grant was directed principally to the wet chemical synthesis of various oxide ceramics in film, fiber and powder forms. These include (1) chemical synthesis of high temperature oxide superconductors, the formation of glasses of such superconductors, their subsequent crystallization behavior, and the wet chemical synthesis of barrier layers for use with superconducting thin films; (2) ceramic-organic hybrid composites (POLYCERAMS); (3) synthesis and dielectric properties of POLYCERAMS, (4) novel optical materials comprising of non-linear organic dyes in POLYCERAM hosts; (5) wet chemical coating of fibers for composites and synthesis of bulk transformation - toughened ceramics; (6) seeded transformation of alumina gels from different precursors; (7) ferroelectric powders, films and fibers; and (8) second harmonic generation from ferroelectric thin films.

Progress in these areas are summarized in the present report. Taken in toto, the results demonstrate clearly the utility of wet chemical methods for preparing oxide ceramics with exceptional properties. They also demonstrate the critical role of chemical insight and the ability to tailor chemistry and process conditions in the synthesis of ceramics.

Research carried out under the grant resulted in 22 publications (journal articles or book chapters) A listing of these publications is presented on the following pages

FINAL TECHNICAL REPORT

on

CERAMICS DERIVFD FROM ORGANO-METALLIC PRECURSORS

(GRANT NO. F49620-88-C-0064)

for the period

April 1, 1988 - March 31, 1991

submitted to

AIR FORCE OFFICE OF SCIENTIFIC RESEARCH

by

UNIVERSITY OF ARIZONA

Professor D.R. Uhlmann
Principal Investigator

DISCLAIMER NOTICE

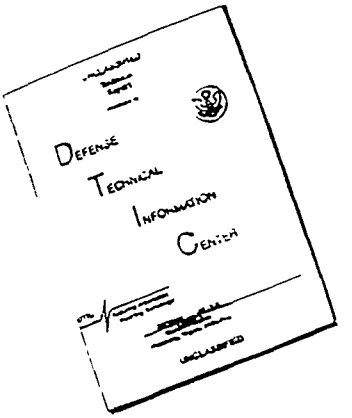

THIS DOCUMENT IS BEST QUALITY AVAILABLE. THE COPY FURNISHED TO DTIC CONTAINED A SIGNIFICANT NUMBER OF PAGES WHICH DO NOT REPRODUCE LEGIBLY.

INTRODUCTION

Work carried out under the present grant was directed principally to the wet chemical synthesis of various oxide ceramics in film, fiber and powder forms. These include (1) chemical synthesis of high temperature oxide superconductors, the formation of glasses of such superconductors, their subsequent crystallization behavior, and the wet chemical synthesis of barrier layers for use with superconducting thin films; (2) ceramic-organic hybrid composites (POLYCERAMS); (3) synthesis and dielectric properties of POLYCERAMS; (4) novel optical materials comprising of non-linear organic dyes in POLYCERAM hosts; (5) wet chemical coating of fibers for composites and synthesis of bulk transformation - toughened ceramics; (6) seeded transformation of alumina gels from different precursors; (7) ferroelectric powders, films and fibers; and (8) second harmonic generation from ferroelectric thin films.

Progress in these areas are summarized in the present report. Taken in toto, the results demonstrate clearly the utility of wet chemical methods for preparing oxide ceramics with exceptional properties. They also demonstrate the critical role of chemical insight and the ability to tailor chemistry and process conditions in the synthesis of ceramics.

Research carried out under the grant resulted in 22 publications (journal articles or book chapters). A listing of these publications is presented on the following pages.

PUBLICATIONS REPORTING WORK CARRIED OUT UNDER THE GRANT

1. "Wet Chemical Processing of High T_c Superconducting Films," B. Dutta, B. Samuels, J.P. Cronin, G. Dale, G. Teowee, G. Rajendran, E.D. Zanotto, E.V. Uhlmann, B.D. Fabes and D.R. Uhlmann, pp. 501-510 in M.F. Yan, ed., Ceramic Superconductors II (American Ceramic Society, Ohio, 1988).

2. "Melt Processing of Bi-Ca-Sr-Cu-O Superconductors," E.D. Zanotto, J.P. Cronin, B. Dutta, B. Samuels, S. Subramoney, G.L. Smith, G. Dale, T.J. Gudgel, G. Rajendran, E.V. Uhlmann, M. Denesuk, B.D. Fabes and D.R. Uhlmann, pp. 406-418 in M.F. Yan, ed., Ceramic Superconductors II (American Ceramic Society, Ohio, 1988).

3. "Bi-Ca-Sr-Cu-O Superconductors of (2122) Composition by Melt Processing," T.J. Gudgel, E.D. Zanotto, G.L. Smith, G. Dale, S. Subramoney, E.V. Uhlmann, M. Denesuk, J.P. Cronin, B. Dutta, G. Rajendran, B. Fabes and D.R. Uhlmann, pp. 419-427 in M.F. Yan, ed., Ceramic Superconductors II (American Ceramic Society, Ohio, 1988).

4. "Wet Chemistry-Derived Barrier Layers for Ceramic Superconductor Films," J.P. Cronin, T.J. Gudgel, L. Zanotto, B. Dutta, G.P. Rajendran, G. Dale, E.D. Zanotto, E.V. Uhlmann, G.L. Smith, M. Denesuk, B.D. Fabes and D.R. Uhlmann, pp. 511-523 in M.F. Yan, ed., Ceramic Superconductors II (American Ceramic Society, Ohio, 1988).

5. "Crystallization of Gel-Derived Glasses," D.R. Uhlmann, M.C. Weinberg and G. Teowee, Journal of Non-Crystalline Solids, 100 (1988) 154-161.

6. "TEM Study of Boehmite Gels and Their Transformation to α-Alumina," X. Yang, A.C. Pierre and D.R. Uhlmann, Journal of Non-Crystalline Solids, 100 (1988) 371-377.

7. "Sol-Gel Processes, a Route to Nano-Hybridization and Creation of New Functions," D.R. Uhlmann, G. Teowee, J.M. Boulton, H.H. Fox and D.R. Ulrich, pp. II 1 - II 38 in SYMPOSIUM ON HYBRID MATERIALS FOR NEW FUNCTIONALITY (Japan Assoc. for New Chemistry, Tokyo, 1989).

8. "Ceramic-Organic Hybrid Composites," D.R. Uhlmann, J.M. Boulton and H.H. Fox, pp. III 1 - III 22 in SYMPOSIUM ON HYBRID MATERIALS FOR NEW FUNCTIONALITY (Japan Assoc. for New Chemistry, Tokyo, 1989).

9. M.C. Weinberg, B.J. Zelinski, D.R. Uhlmann and E.D. Zanotto, Journal of Non-Crystalline Solids, 123 (1990) 90-96.

10. M.C. Weinberg, D.R. Uhlmann and E.D. Zanotto, Journal of the American Ceramic Society, 72 (1989) 2054-2058.

11. D.P. Birnie and D.R. Uhlmann: "Microstructure-Property-Processing Relationships in Microelectronic Thin Films", in Materials and Processes for Microelectronic Systems, Ceramic Transactions, Volume 15 (ACerS, 1990), pp. 503-525.

12. J.M. Boulton, S. Subramoney and D.R. Uhlmann: "Sol-Gel Synthesis of Alumina-Zirconia and Mullite-Zirconia", to appear in Proceedings of 4th International Conference on Ultrastructure Processing.

13. J.M. Boulton, S. Subramoney and D.R. Uhlmann: "Seeded Transformation of Aluminum Chlorohydrate Gels", to appear in Proceedings of 4th International Conference on Ultrastructure Processing.

14. C.L. Schutte, J.R. Fox, R.D. Boyer and D.R. Uhlmann: "Initial Evidence for Si-O-Ti Bond Formation in Organically Modified Silicon Titanates by Solid State Si^{29} Nuclear Magnetic Resonance Spectroscopy", to appear in Proceedings of 4th International Conference on Ultrastructure Processing.

15. J.M. Boulton, H.H. Fox, G.F. Neilson and D.R. Uhlmann: "Synthesis and Structural Characteristics of Polycerams", to appear in BETTER CERAMICS THROUGH CHEMISTRY IV, ed. B.J.J. Zelinski, C.J.Brinker, D.C. Clark and D.R. Ulrich (MRS, 1990).

16. G. Teowee, J.M. Boulton, H.H. Fox, A. Koussa, T. Gudgel and D.R. Uhlmann: "Dillectric Characterization of Polyceram Films", to appear in BETTER CERAMICS THROUGH CHEMISTRY IV, ed. B.J.J. Zelinski, C.J. Brinker, D.E. Clark and D.R. Ulrich (MRS, 1990).

17. J.M. Boulton, J. Thompson, H.H.Fox, I. Gorodisher, G. Teowee, P.D. Calvert and D.R. Uhlmann: "Non-Linear Organic Dyes in Polyceram Hosts", to appear in BETTER CERAMICS THROUGH CHEMISTRY IV, ed. B.J.J. Zelinski, C.J. Brinker, D.E. Clark and D.R. Ulrich (MRS, 1990).

18. D.R. Uhlmann, G. Teowee, J.M. Boulton and B.J.J. Zelinski: "Wet Chemical Derived Films for Electrical Applications", to appear in BETTER CERAMICS THROUGH CHEMISTRY IV, ed. B.J.J.Zelinski, C.J. Brinker, D.E. Clark and D.R. Ulrich (MRS, 1990).

19. D.R. Uhlmann, B.J.J. Zelinski, G. Teowee, J.M. Boulton and A. Koussa: "Wet Chemical Synthesis of Bulk Optical Materials", accepted for publication, Journal of Non-Crystalline Solids.

20. D.R. Uhlmann, G. Teowee and J.M. Boulton: "Dielectric Relaxation in Ferroelectrics", accepted for publication, Journal of Non-Crystalline Solids.

21. D.R. Uhlmann, J.M. Boulton, G. Teowee, L.W. Weisenbach and B.J.J. Zelinski: "Sol-Gel Synthesis of Optical Thin Films and Coatings": SPIE Proceedings 1328 (1990) 270-295.

22. D.R. Uhlmann, G. Teowee, J.M. Boulton, M. Denesuk and W.M. Bommersbach: "Wet Chemical Synthesis of Optical Films" to appear in Proceedings of 5th International Conference on Ultrastructure Processing.

I. HIGH TEMPERATURE SUPERCONDUCTORS

The research activity concerned with high temperature superconductors was directed to three principal areas. These are (1) wet chemical synthesis of high temperature superconductors, (2) the formation of glasses of high temperature superconductors and their subsequent crystallization behavior, and (3) chemical synthesis of barrier layers for use with superconducting thin films.

A. Wet Chemical Synthesis of High Temperature Superconductors

The discovery of superconductivity at temperatures above liquid nitrogen temperature has opened up new vistas of possible industrial application. Processing of thin films is a very important step in many technological exploitations of these superconducting materials. The techniques for depositing superconducting films on various substrates comprise electron beam evaporation, molecular beam epitaxy, sputtering and pulsed laser evaporation. These techniques invariably require high vacuum (as 10^{-6} - 10^{-7} Torr) and expensive equipment. The superconductive transitions that have been reported in these studies are generally in the range 60° - 95°K depending on the type of substrate and the firing and annealing procedures employed.

The high vacuum conditions required for the existing techniques for depositing superconducting films require skilled operators. The evaporation or sputtering targets have to be prepared in the form of alloys which are expensive to prepare. Moreover, it is economically unattractive to coat large and intricate objects with these techniques. These problems can be overcome by wet chemical processing which involve inexpensive machinery and relatively unskilled operators.

Prior to the present work, there was one unsuccessful attempt to process superconducting films on ceramic substrates by spraying, using solutions of yttrium, barium and copper compounds. Attempts to measure the resistivity of the annealed films were unsuccessful because the films were extensively cracked. In other words, superconductivity was not observed; and a continuous film, covering the surface of the substrate, was not achieved.

In the present work, techniques have been developed for processing homogeneous films by spraying or otherwise depositing nitrate solutions of cation combinations such as Y, Ba and Cu or Bi, Sr, Ca, Cu or ceramic

substrates. After firing, the resulting oxide films exhibit superconductivity up to temperatures similar to those of films obtained by vacuum deposition techniques.

The cations, preferably in the stoichiometric ratio (e.g., for the Y-Ba-Cu system, the ratio is 1,2,3) are incorporated in a clear solution. The solution can be aqueous, whether acidic, neutral or basic. Compounds, such as the oxides, nitrates, carbonates or hydroxides or a combination of these, can be dissolved in acids or water. Mild heating associated with stirring may be necessary to obtain a clear solution. It is beneficial to have a saturated solution, but care must be taken to ensure that no precipitate is formed.

The substrate can be a metal, a ceramic or a glass. The substrate should be cleaned and heated to a suitable temperature such that a drop of solution will evaporate relatively rapidly on contact. There exists an optimum temperature range for a substrate-solution combination which facilitates formation of a good film. For the Y-Ba-Cu (1,2,3) system, this temperature range is 170-190°C; and for the Bi-Sr-Ca-Cu (4,3,3,4) system, the temperature range is 210-230°C. An unduly low substrate temperature results in a wet film, and the desired stoichiometry is difficult to maintain. The less soluble components tend to precipitate, whereas the more soluble components tend to remain in solution and get washed away during successive depositions. Moreover, problems arising from local non-stoichiometry arise if an unduly low substrate temperature is used. An unduly high substrate temperature has also been found to result in defective films which are patchy in texture and may contain numerous cracks.

Several methods of depositing films have been employed. These include:

Technique I: The deposition of the film may be carried out by depositing the solution onto hot substrates in the form of small drops. The substrate is kept flat on a heat source such as a hot plate, and drops of the solution are added at regular intervals to the substrate. The liquid spreads over the substrate on contact and dries rapidly, leaving a film on the substrate. The number of drops required to form a film depends on the surface area of the substrate, the solute concentration of the solution and the size of the drop.

Technique II: Solutions may be sprayed with a spray gun onto suitable substrates, the surfaces of which are heated and maintained at a pre-determined temperature. The substrate is kept flat on a hot plate, and

spraying is preferably done from a point located vertically on top of the substrate. To prevent loss of the more soluble components, spraying is preferably performed intermittently, making sure the already deposited film is at the pre-determined high temperature. The number of spraying cycles which is required depends on parameters such as the type of spray gun, the area of the substrate being coated, the concentration of the solution and the film thickness required.

Technique III: An assembly of spray guns may be positioned on the periphery of a circle and the substrate is placed at its center. A heating device heats the substrate to a desired temperature and all the sprayers are activated at the same time. Spraying from all directions will ensure the desired stoichiometry of the film being processed. The number of spray guns will be determined by the area of the substrate.

Technique IV: Spraying a small substrate from a vertical direction may entail some loss of solution. To reduce this wastage, a guard wall around the substrate may be placed. The sprayer is positioned at the top opening of the guard well, and spraying in this configuration will minimize wastage of the solution.

A number of other deposition techniques such as dip-coating, ultrasonic spraying, and roller-coating may also be used to good effect.

The films deposited by any of these techniques are ready to be fired immediately thereafter. The firing may conveniently be carried out in horizontal tube furnaces, but other furnace geometries may be used as well. The furnaces should have attachments for flowing oxygen gas during the heat treatment. Each superconducting system has its own firing and annealing schedules. These depend on the chemical composition of the oxides as well as the physical and chemical nature of the respective superconducting phases.

In general, slow heating rates are desired to allow the film and the substrate to adjust to the thermal expansion mismatch. An extended soaking period from 400° to 620°C seems important because in this temperature range the gases resulting from the decomposition of the nitrates evolve. Sintering of Y-Ba-Cu films starts at temperatures in the range of 650°C. If all the gaseous products of nitrate decomposition are not allowed to diffuse away from the film, the porosity of the film may increase, resulting in increased resistivities of the samples. A prolonged soaking at 880°C facilitates improved sintering

of the film, giving it a good connective texture. The films are black in color and no cracks or apparent defects are observed.

For systems other than Y-Ba-Cu or for starting materials other than nitrates, the temperature range at which the starting compounds decompose can readily be determined; and a soak in that temperature range should be allowed. Similarly, the highest sintering temperature and the subsequent annealing range of temperature should be tailored for each superconducting system.

Standard four-probe electrical measurements were performed on the films. Silver electrodes were pasted on the film with silver paint. A representative resistance vs. temperature plot for a $YBa_2Cu_3O_7$ film shows a critical temperature of 94°K. X-ray diffraction studies using CuKα radiation were performed on the films. The variation of intensity with scattering angle indicated that the majority phase in the film was $YBa_2Cu_3O_7$.

In the case of Bi-Sr-Ca-Cu-O (4-3-3-4) films deposited on partially stabilized zirconia substrates, black films, without any apparent cracks or pores, were formed (similar in appearance to the Y-Ba-Cu-O films). Standard four-probe electrical measurements showed that these films were superconducting and that their critical temperatures were in the range of 85°K.

It has thus been demonstrated that it is possible using wet chemical synthesis routes to produce dense, crack-free films with superconducting critical temperatures similar to those of the best vapor-deposited films. The wet chemical route offers great potential for highly cost-effective processing; and the critical issue for its wide-scale implementation is that of critical current density, which is presently being addressed in another context in a separate Air Force-sponsored program. Because of the technological potential of the wet chemical route to high temperature superconductors, a patent disclosure has been prepared and filed with the University patent section.

B. Glass Formation and Crystallization Behavior of High Temperature Superconductors

In our exploration of processing techniques which offer important potential for cost-efficient synthesis of high temperature ceramic superconductors, attention was also directed to melt processing. It was recognized that melt processing techniques are potentially very interesting

because, in principle, they can be used to fabricate complex geometries, such as wires, films and odd-shaped articles. They also can provide great flexibility for microstructural control, as well as for enhancing properties through chemical homogeneity.

In the present work, attention was focused on glass formation and crystallization behavior as a function of composition and thermal history in the Bi-Ca-Sr-Cu-O system. The system was selected for detailed investigation because of the attractive high temperature superconducting characteristics of several Bi-Ca-Sr-Cu compositions, and because preliminary exploration in our laboratory demonstrated the surprising result that several of the compositions were reasonable glass-formers.

Four different compositions in the Bi-Ca-Sr-Cu-O system, with compositions 2122, 2223, 4334 and 4223, were melted in Al_2O_3 or Pt crucibles at temperatures varying from 1050C to 1200C for 15 minutes. The numbers indicate the atomic compositions of Bi, Ca, Sr and Cu. Further designations A and P refer to samples melted in Al_2O_3 and Pt crucibles respectively.

The batch materials were reagent grade Bi_2O_3, $CaCO_3$, $SrCO_3$, $Sr(NO_3)_2$ and CuO. The first three compositions were chosen based on reports which identify two superconducting phases in the new system: the T_c=110K phase (2223) and the T_c=85K phase (2122). Both of these phases could not be obtained in isolation by sintering powders having the exact stoichiometric compositions, the recommended starting composition being 4334. In the present work, we attempted to make glasses and subsequently to crystallize single phase HTSC materials. The fourth composition, 4223, was made in order to test the effect of Bi on glass formation in this system.

The melts were very fluid and highly corrosive, and hence a substantial amount of Al is expected to be dissolved in the liquid when melting is carried out in Al_2O_3 crucibles. Composition 2223P was melted in a Pt crucible and no sign of chemical attack was observed. In this case, $Sr(NO_3)_2$ was used instead of $SrCO_3$ to prevent reduction of Bi and consequent alloying with Pt.

The liquids were cast on graphite molds or quenched between two steel plates. The thickness of the as-cast plates was typically about 1 cm. Table I summarizes the compositions investigated and the rough glass-formability of the materials melted and cooled in different ways. For purposes of this table, the glass yield is defined as the thickness of the bottom layer (which first

touched the mold on casting) and appeared glassy to the eye. It should be noted, however, that SEM observations and X-ray diffraction analysis have shown a small degree of crystallinity in the "glassy" layers of the cast 2223 and 4334 compositions. The glassy layers in the 2122 and 4223 samples were X-ray amorphous.

The heat treatments were carried out in a muffle furnace. The specimens were inserted into the cool furnace which was then slowly heated to the desired temperature, between 845C and 885C; and held at that temperature for periods of up to 40 hours. After the holding periods, the specimens were allowed to cool inside the furnace. In some cases, an optical microscope provided with a hot stage was used to carry out the heat treatments.

The resulting microstructures were analyzed by optical and scanning electron microscopy, as well as by X-ray diffraction. Four probe d.c. electrical measurements were performed by the linear 4-point and the Van de Paaw configurations. A current of 1 mA was used during the measurement. Silver paste was used to attach indium leads to the samples.

The as-cast 2122 material, having a thickness of about 1 cm., was glassy in appearance (no evidence was found for internal crystals visible at magnifications of 100-200X), save for a thin skin on the top surface (the melt-vapor interface). This surface skin had crystalline material, was typically less than 0.1 mm in thickness, and was also observed on much thinner samples (samples whose thickness was in the range of 1 mm). No such crystalline skin was found on the surfaces which had been in contact with the graphite mold. X-ray diffraction of the bulk of the cast material indicated only a broad diffraction maximum typical of an amorphous material.

When placed in a furnace provided with an oxygen atmosphere and maintained at 865°C, the samples were observed to have crystallized completely in periods of less than 1 hour. During such times, pronounced slumping of the samples was observed. In addition, marked evolution of gas took place during such crystallization treatments, presumably from the raw materials used in preparing the original melts. This evolution of gas produced a pumice-like appearance of the samples.

X-ray diffraction analysis of the crystallized samples indicated that an important crystallization product was the second phase(s) seen in crystallized

samples of the (2223) and (4334) compositions - see below - rather than the expected dominance of the tetragonal (2122) phase. There was, however, a significant fraction of the tetragonal (2122) phase included in the body.

The resistance vs. temperature relation for material crystallized at 865°C for 1 hour indicated a sharp drop in resistance over the temperature range 133-91°K, but the condition of zero resistance was not achieved at temperatures above 91°K.

When the as-cast material ws remelted in a Pt crucible at 900C, gas evolution was complete within 15 minutes. When the temperature was lowered to 865°C and maintained at that temperature for 10 minutes, complete crystallization of the sample was observed. In this case, however, the sample had a monolithic character, without the presence of large numbers of gas bubbles. X-ray diffraction of this body indicated the presence of only the other phases(s) seen in crystallized samples of (2223) or (4334) composition. No diffraction peaks were seen which corresponded to the (2122) phase.

The resistance vs. temperature relation for this remelted and crystallized material shows a sharp drop in resistance with decreasing temperature, beginning at about 103°K. The state of zero resistance is, however, not observed at temperatures above 87°K.

SEM observations of 2223 material which had been melted in Al_2O_3 crucibles and cast of the same material melted in Pt crucibles rapidly quenched between steel plates showed a notably greater thickness of the "glassy" layer in the sample melted in the Al_2O_3 crucible - despite the more rapid cooling used with the sample melted in Pt. The "glassy" regions were seen to contain a few small crystals, which appear to be associated with bubbles (seed) in the material. These crystals were identified by X-ray diffraction as consisting entirely of the 2122 phase. The crystalline top surface regions in these as-cooled specimens consist of plate-shaped crystals as well as a matte-appearing second phase. X-ray diffraction confirmed the presence of two phases.

After subsequent heat treatment of the "glassy" 2223 material to produce crystallization, the presence of micaceous (plate-like) crystals was clearly seen, as are crystals of a second, matte-appearing phase.

Observations of cast samples of the 4334 material which had been melted in Al_2O_3 indicated a "glassy" layer which is larger than that in the 2223

material. As with the 2223A samples, some small crystals are seen in the "glassy" regions; and these crystals are the 2122 phase. The crystalline regions again consist of two phases, one of which is the plate-like in appearance and which was identified by diffraction as the 2122 phase.

When heated in an oxygen atmosphere while viewed in an optical microscope, crystallization of the "glassy" 2223A material was observed to occur rapidly at temperatures in the range of 850°C (growth rates were in the range of mm/sec). On further heating, partial melting was observed in the range of 925°C. At higher temperatures, none of the plate-like crystals were seen; but the matte-appearing fine-grained crystals persisted until temperatures approaching 1200°C.

By comparison, the 2223P material was observed to crystallize in periods as short as 10 sec. at temperatures in the range of 860-870°C. On further increasing of the temperature, melting was observed to begin at about 890°C; and by about 1050°C, the sample was molten save for a small volume fraction of the matte-appearing phase. This phase persisted to temperatures above 1220°C.

The relative resistances of composition 2223A (initially "glassy") which had been heat treated respectively at 845°C for 4 hours, 865°C for 40 hours and at 860°C for 28 hours were measured. The absolute values of the resistance at 273°K (for similar geometries) were typically 0.02, 0.004 and 0.12 (arbitrary units), respectively. The as-cast "glassy" specimen had a resistance of 24. Hence, there is a difference of 4 orders of magnitude between the least and the most resistive specimens at 273°K. The resistivity at 300°K of sample 2223A heated at 840°C is 5700 Ω-cm.

Dramatic changes in behavior caused by different heat treatments were also observed. For treatment at 845°C, a metallic behavior is observed, with a superconductive onset at T_{on} = 110°K, although zero-resistance behavior was not detected at temperatures above 85°K. With a long treatment (40 hours) at 865°C, the specimen warped slightly and was dark black. The resistance drops continuously with decreasing temperature and undergoes a clear transition with T_c = 85°K. The "anomaly" reported by several authors between 110°K and 120°K is clearly seen and indicates the presence of another superconducting phase. When the "glassy" specimen is heated at 885°C, it partially melts, a shiny surface is obtained, and it fails to exhibit superconducting behavior, at least at temperatures down to 85°K.

The relative resistance was also determined for three different compositions (2223A, 2223Pt and 2223B) heated to 865°C for several hours. Sample 2223A was melted in a rather porous Al_2O_3 crucible, while sample 2223B was melted in an impervious Al_2O_3 crucible. The amount of attack on the crucible by the melt was much greater for 2223A than for 2223B. In spite of the differences in chemical compositions (different Al_2O_3 contents), they all show metallic behavior and have zero resistance at approximately 85°K.

The relative resistances of composition 4334 as-quenched (crystalline side) and heated to 845°C for 4 hours and to 875°C for 2 hours were likewise determined. Both as-quenched sides ("glassy" and crystalline) do not superconduct down to 10°K. The glassy layer has a much higher resistance. The "glassy" specimen heated to 845°C has a much lower resistance which does not vary significantly down to 85°K. The "glassy" specimen heated to 875°C shows a superconducting onset at about 110°K, but did not superconduct at temperatures above 85°K.

The present work has demonstrated that melting, quenching and subsequent crystallization plus annealing provides a useful alternative route to powder or vapor-phase processing for forming superconducting Bi-Ca-Sr-Cu-O materials. The present results provide support for such processing as an attractive route to forming high-T_c superconductors in useful shapes. This route offers the attractive features which accompany liquid state processing.

A significant aspect of the present study is the ability to quench the liquid into the glassy state. In this regard, it was found that the incorporation of Al_2O_3 in the 2223 melt has a clearly beneficial effect in promoting glass formation without deleteriously affecting the critical temperature for superconducting behavior. Similar beneficial effects of Al_2O_3 on glass formability are expected for the other Bi-Ca-Sr-Cu-O compositions as well. In the work reported here, the Al_2O_3 was obtained by partial dissolution of the crucible in the melt; but in on-going work, it is provided by additions to the batch. The effect of such additions on critical current density also needs clarification.

Considering the high fluidity of these melts at temperatures near the liquidus (they pour rather like water), it is remarkable that they can be formed as substantially amorphous materials by simple casting. This likely reflects a sizable barrier to crystal nucleation and/or a large temperature dependence of the viscosity -or alternatively a relatively small interval between the upper

temperature limit of stability of the 2122 phase (T_L) and the glass transition temperature (T_g). Based on observations of the cast/quenched specimens, it appears that the matte-appearing phase on the liquidus is not the first to nucleate on cooling. Rather, it is the 2122 phase, which presumably reflects its smaller crystal-melt interfacial energy. On this basis, the relative factor in considering glass formation is not $T_{liquidus} - T_g$, but rather $T_L - T_g$.

The addition of Al_2O_3 has only a modest effect on the viscosity at a given temperature (judging from the pouring behavior). The effect of Al_2O_3 on glass formability must then be related to its role in reducing T_L and/or the crystal-melt interfacial energy, or in decreasing the crystal growth rate via its effect on the interdiffusion coefficient in the melt.

The observation of small crystals associated with pores in the "glassy" cast material very likely reflects nucleation on second-phase impurities, rather than simply on the liquid-vapor interfaces of the pore surfaces. The nature of the suggested second-phase impurities remains to be identified. The subsequent crystallization of such "glassy" material is being further investigated to elucidate the role of the observed crystallites and thermal history of the glass.

It is noteworthy that X-ray diffraction of the "glassy" material in both the 2223 and 4334 samples indicates the presence of a small amount of only the 2122 phase (the phase suggested as responsible for high temperature superconducting behavior). After complete crystallization, however, both samples show the presence of two crystalline phases with distinctive morphologies. The crystallization process as observed in the optical microscope took place too rapidly to permit detailed observation of the sequence of phase development, but presumably growth of the small 2122 crystals present in the "glassy" material was accompanied/followed by nucleation and growth of the matte phase.

Based on the present observations, it appears that the preferred heat treatment schedules in the literature for preparing superconducting samples of the 2223 and 4334 compositions involve partial melting of the 2122 phase. In particular, it appears that these heat treatments involve a reorganization via dissolution/re-precipitation, which may involve some increase in the volume fraction of the 2223 phase at the expense of the 2122 phase, but almost certainly involves the development of more favorable interconnected morphologies of the preferred phase(s).

The times required for complete crystallization of the samples at 865°C are much shorter than the heat treatment times used to prepare the superconducting samples (less than a minute vs. several hours).

It appears that superconducting material of the 2223 composition can only be prepared by crystallization in a narrow range of temperature (845C<T<885C). The origin of this behavior is not satisfactorily understood at the present time, but must involve the development of different phase assemblages/microstructures at the different temperatures. X-ray diffraction indicates a similar distribution of diffraction peaks in material crystallized at 865°C. Also of note is the marked difference in conductivity behavior over the temperature range 275K-125°K among glasses crystallized at 845°C, 865°C, and 885°C.

Regardless of the details of the crystallization process, it appears that extended heat treatments - much longer than those required to develop a substantial degree of crystallinity - are required to obtain superconducting samples. Whether these extended heat treatments are required for reasons of oxygen stoichiometry, or for the development of appropriate crystalline-phase assemblages, is presently being explored.

C. Wet Chemical Synthesis of Barrier Layers

It is well established that substrate composition and orientation play crucial roles in determining the properties of thin film ceramic superconductors. The substrate can affect both the epitaxial quality of the superconductor coating and interdiffusion between the substrate and coating; these, in turn, affect superconducting properties (e.g., transition temperature and critical current density).

The importance of substrate diffusion in thin film ceramic superconductor has inspired many investigators to coat the substrates with barrier layers, in the hope of effectively separating the coating from the diffusing substrate cations. ZrO_2, SiO_2, Ta_2O_5, LaF_3, MgO, VN, $La_2O_3 \cdot Al_2O_3$, Ag, Au (and some other compositions) have been tried. Many of these coatings -- especially ZrO_2, Ag, and Au -- have resulted in significant improvements in the electrical properties of ceramic superconductor coatings. In general, these barrier layers have been used with superconductor coatings which are applied by vacuum deposition techniques, such as magnetron sputtering, evaporation, and electron beam evaporation. As a result, the

barrier layers have also been deposited using high vacuum processes. For chemically derived superconducting coatings, however, the advantages in cost and versatility would be lost if the substrates had to be first coated with a barrier layer in a vacuum chamber. Hence, there is a need to develop barrier layers which can be deposited by more simple, versatile techniques, such as wet-chemical, or sol-gel, techniques. In initial work under the program, wet chemical methods were used to deposit ZrO_2 barrier layers on sapphire substrates. Onto such coated substrates, a second barrier layer of Ag was deposited. This combination allowed superconducting $YBa_2Cu_3O_{7-x}$ films to be sputter-deposited on sapphire. Without the barrier layer, the films were not superconducting; and with the composite barrier layer, a T_c onset of 89°K with a T_c completion of 65°K was observed.

In subsequent work, we investigated a broader range of sol-gel barrier layers. These include Ta_2O_5, since it forms a nominally dense sol-gel coating at low temperatures (450-500C); Y-stabilized ZrO_2 (YSZ), which is one of the preferred bulk substrate materials and which (without yttria stabilization) is a commonly used vacuum deposition barrier layer; $Y_2Cu_6O_9$, which may provide not only a barrier layer but also serve as a source of excess copper, which is often deficient after heat treatments; and $BaTiO_3$ and $SrTiO_3$, which were studied because of the superiority of $SrTiO_3$ as a bulk substrate material. Each barrier layer was investigated with and without silver overcoats.

Results reported to date under the program included the development of synthesis procedures for two of these barrier layers (Ta_2O_5 and Y-stabilized ZrO_2) as well as the effects of these barrier layers on coating adhesion, coating/substrate interdiffusion, and resistivity measurements for $YBa_2Cu_3O_{7-x}$ films sprayed from nitrate solutions onto barrier-coated sapphire substrates.

Barrier Layer Synthesis

The coating solutions were made from alkoxide precursors. All solvents were purified by standard procedures before use. Single crystal sapphire slides, 90° cut (1cm x 1cm x 1mm) were used as the substrate material. The slides were cleaned using the Huang process before coating. All samples were coated using a spin coater, 2000 rpm, for 20 sec.

Ta_2O_5 coatings were obtained from $Ta(OC_2H_5)_5$ solutions. A 5 wt% $Ta(OC_2H_5)_5$ solution in dry ethyl alcohol was prepared in a three-neck flask equipped with a nitrogen inlet, condenser, drying tube, and stirring and heating

accessories. Water was added to this solution so as to maintain a 1:1.3 water to alkoxide ratio. The solution was stirred at room temperature for one hour, and then coated onto the sapphire substrates. To increase the thickness, this coating was heated at 80C for 10 minutes, and then a second Ta_2O_5 layer was spun on. The dual coatings were finally fired for 4 hours at 950C in air. Rutherford Backscattering (RBS) analysis showed the resulting coatings to be ~600 Å thick.

To prepare Y-stabilized ZrO_2 barrier layers, zirconium n-propoxide and anhydrous yttrium chloride were weighed into a three-neck flask, equipped as described above. The weight of components was adjusted in such a way that ZrO_2 containing 9 wt% Y_2O_3 would be obtained. Dry isopropyl alcohol (30 ml) was added to this solution, and the resulting mixture was heated until a solution free from any solid particles was obtained. To hydrolize the alkoxide mixture, 1 mole% of the amount of water required for complete hydrolysis was added to one ml isopropyl alcohol. This hydrolysis solution was then added the the alkoxide solution and refluxed for about five hours. The solution was then spin coated onto the pre-cleaned sapphire substrates. A second coating was deposited after the first had been fired at 400°C in air for one hour. Then, the dual coating was given a final heat treatment at 900°C for four hours. RBS analysis showed the product coating to be ~800 Å thick, and X-ray diffraction analysis showed the coating to be a cubic crystalline phase.

Superconductor Coatings

Y-Ba-Cu-O films were sprayed onto the barrier layers using a nitrate solution technique which was described in detail above. Basically, the process involves mixing nitrate solutions of the cations in the stoichiometric ratio (1:2:3 Y:Ba:Cu) and spraying this solution onto heated (170-190°) substrates. The sprayed coatings were then given a complicated heat treatment, part of which involved heating at 925°C for 6 hours. The details of the spraying procedure and firing schedule are both important in obtaining good superconducting properties.

For 15 μm coatings sprayed on bulk yttria-stabilized zirconia substrates, a superconducting onset is obtained at 94°K, with a transition width of about 12°K (zero resistivity at 82°K). For thinner coatings, the onset temperature decreases and the transition width increases. It is apparent, therefore, that the extent of substrate poisoning can be very large -- i.e., microns in extent -- with the nitrate-derived coatings.

Coating Adherence

For bulk YSZ substrates, the nitrate deposition technique formed very robust, well adhering coatings. When the oxide barrier layers were added, the coatings became somewhat more fragile, and could be partially scraped off with a razor blade In our previous work on sputtered films, no such effect was observed with the sol-gel barrier layers. It is apparent that the complex chemical interactions at the coating/substrate interface make the nitrate-deposited coatings more sensitive to substrate chemistry than the vacuum deposited coatings. This difference was particularly evident when nitrate coatings were sprayed onto the silver-coated barrier layers. Here, films could not be formed at all. The coatings coalesced into small islands, apparently the result of chemical attack of silver by nitric acid from the coating solution.

In some cases, the barrier layers could be used to enhance coatability. For example, the nitrate coatings did not adhere to unpolished polycrystalline Al_2O_3. With the addition of a $BaTiO_3$ barrier layer, however, adhering coatings could be formed. Hence, in addition to providing diffusion barriers, the sol-gel barrier layers can significantly affect coatability by changing the substrate chemistry and morphology, in both the positive and negative directions.

Substrate Diffusion

SEM micrographs of the Ta_2O_5 coating show a very smooth surface. Except for what seems to be cracking in the gold coating, there is no apparent structure (porosity) in the film down to at least 300 Å. The RBS spectrum of a fired Ta_2O_5 coating shows a very sharp Ta peak, indicating that there is very little interdiffusion between the Ta_2O_5 and Al_2O_3 during the 950°C firing. Assuming the coating is dense, these RBS measurements correspond to a Ta_2O_5 coating thickness of about 600 Å. Auger sputter depth profiles of the same sample confirm the sharpness of the interface, but suggest a coating thickness of about 1550 Å, more than twice the RBS estimate. This discrepancy implies that, although coating shrinkage has long since stopped by 950°C, the Ta_2O_5 coating is not completely dense. For use as a barrier layer, this may have a significant, negative effect.

The RBS spectrum of the same Ta_2O_5 film after coating with the nitrate solution (1-2 μm) and firing shows an extension of the Ba peak, and especially of the Ta peak, indicating that interdiffusion between the superconductor and

barrier coatings has taken place. The interdiffusion is more dramatically observed in an Auger sputter depth profile of the same sample. The barium has diffused into the substrate, leaving the bulk of the film deficient in Ba; the tantalum is evenly distributed throughout the bulk of the superconductor film; and, most importantly, the aluminum has diffused through almost the entire superconducting coating.

It is interesting that the sputter rate is significantly faster through the superconductor film than through the Ta_2O_5, suggesting that the mechanical integrity of the nitrate-sprayed superconductor coating on a Ta_2O_5 barrier layer is rather poor. This is consistent with our observation of reduced adhesion for nitrate films on barrier layers.

X-ray diffraction patterns of fired nitrate coatings on bulk YSZ indicate that only the superconducting 1-2-3 phase is present. Diffraction patterns of a fired nitrate coating on a Ta_2O_5/sapphire substrate indicate the presence in addition to the 1-2-3 material, of impurity phases (Y_2BaCuO_5, $BaCuO_4$, and possibly others), as well as $BaCO_3$. The presence of phases other than the 1-2-3 is not surprising, in light of the extreme substrate/barrier layer/superconductor interdiffusion seen in the RBS and Auger results. The $BaCO_3$, however, is quite unexpected, since the barrier layers were fired to 950°C before coating with the nitrate solutions.

SEM micrographs of the YSZ coating show that the YSZ coatings are also smooth and featureless, at least down to the 300 Å level. When coated with the nitrate solutions and fired, however, the XRD pattern shows the presence of the same impurity phases, including $BaCO_3$ as in the Ta_2O_5 barrier layer. It is apparent that disruption of the 1:2:3 stoichiometry is just as severe with the YZS barrier coatings as with the Ta_2O_5 barrier coating.

This chemical interaction could be caused by incomplete densification before the nitrate coatings are applied, or by chemical attack of the superconductor during the rigorous heat-treatment to which the entire superconductor coating/barrier layer/substrate system was subject. Since YSZ is well established as one of the best (least reactive) substrates, it seems unlikely that the superconducting coating would severely attack these coatings. Hence, there is strong indication that the YSZ coatings were not fully densified by the 900°C heat treatment, and that this relaxed porosity limits their effectiveness as barrier layers.

Resistivity vs. temperature measurements were made for all nitrate-coated and fired barrier layers. Since the thickness of the superconductor coatings can vary by multiple microns across a sample, however, it is difficult to quantify the effects of the different barrier layers. Qualitatively, minor improvements in electrical properties (such as a slight increase in onset temperature) have been observed when sapphire substrates are coated with these barrier coatings.

II. CERAMIC-ORGANIC HYBRID COMPOSITES (POLYCERAMS)

Besides offering an attractive route for preparing novel glasses and ceramics, wet chemical processing can be used to obtain novel materials with combined organic and inorganic functionality. These materials are known as POLYCERAMS, CERAMERS or ORMOSILS. Three structural types of POLYCERAMS have been identified. These types are shown schematically in the figures on the following pages.

The simplest case, a Type I structure, corresponds to an individual organic group being bonded to a single metal cation with one end tied. Such organic modification could theoretically give organic-rich domains within the inorganic network as shown in Figure 1(b). In the second type of organic modification, the organic group is bonded to more than one metal cation. This leads to the formation of organic polymers directly bonded through two or more groups to an inorganic network as shown for the Type II structures in Figure 2. With such POLYCERAMS, it is also possible to form an independent organic network, as shown schematically in Figure 2(c).

In contrast to these types of organic modified oxides, Type III POLYCERAMS represent a case where there is no direct bonding between the inorganic and organic components. They can take the form of two interpenetrating networks or composite structures (see Figure 3).

A variety of Type I POLYCERAMS have been prepared, and applied to areas ranging from gas-sensitive layers in MOSFET's and MIS capacitors to hot melt adhesives and materials for immobilizing antibodies, as well as surfaces for immobilizing homogeneous transition-metal catalysts. They have also been used effectively in the form of coatings.

In the case of coatings, such organic network modification has considerable advantages over normal alkoxide-derived coatings. Organic modification enables the refractive index, microhardness and thermal expansion coefficient of the film as well as the polar contribution to its surface characteristics to be modified and tailored to specific applications.

It has also been shown that the nature of the organic group bonded to a silicon cation can have a profound effect on the properties of the final material. In particular, the use of phenyl groups often leads to thermoplastics which are soluble in organic solvents. Due to the steric hindrance brought

Figure 1-Structural Features of Type I POLYCERAMS

(a) Simple Organic Modification of Inorganic Network (One End Tied)

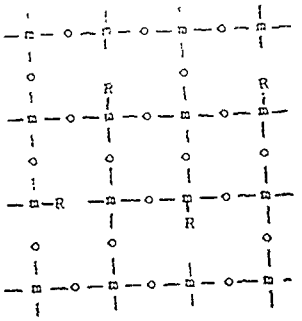

(b) Formation of Domains with Simple Organic Modification

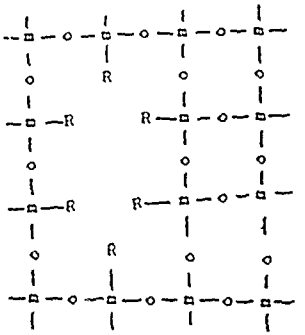

□ ≡ metal cation; R ≡ alkyl, aryl

Figure 2-Structural Features of Type II POLYCERAMS

(a) Organic Modification of Inorganic Network (Both Ends of Organic Tied)

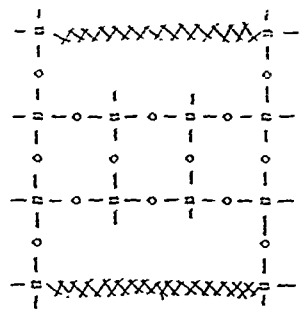

(b) Formation of Domains with Organic Modification (Both Ends of Organic Tied)

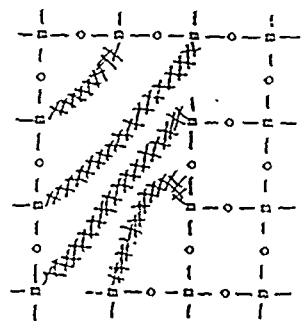

□ ≡ metal cation ⩘ ≡ polymer chain

Figure 2-(continued)

(c) Organic Network Modification of Inorganic Network

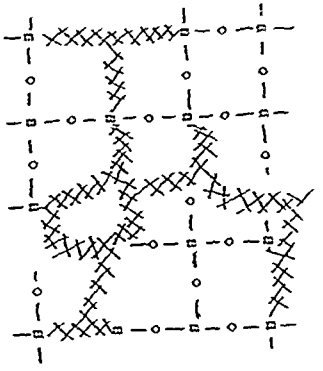

u ≡ metal cation ≡ polymer chain

Figure 3-Structural Features of Type III POLYCERAMS

(a) Interpenetrating Networks

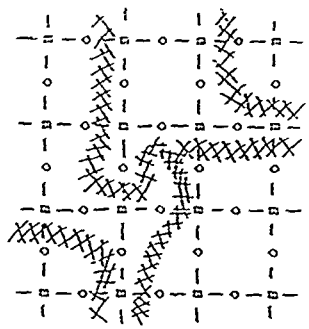

(b) Composite Structure

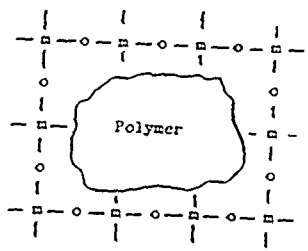

▫ ≡ metal cation XXX ≡ polymer chain

about by the bulky phenyl groups, a low degree of polymerization typically occurs. This results in the formation of soluble, low molecular weight polymers which are useful for preparing coatings.

In the case of Type II POLYCERAMS, complex organic modification can be effected by organic networks cross-linked with inorganic networks or by the incorporation of organic components bonded to more than one metal cation. Organically cross-linked networks can be prepared from a variety of precursors where the organic component has the ability to polymerize materials having vinyl, epoxy or methacryloxy functionalities. Organic components bonded to more than one metal cation can be introduced by reacting alkoxides with polyols or with polymers containing reactive functional groups such as silanol terminated polydimethylsiloxane.

A variety of organic modified silicates based on (3-glycidoxypropyl) trimethoxysilane have been extensively studied and considered for use in preparing hard contact lenses. In these cases, the methacryloxy-substituted alkoxysilane functions as a hook between the inorganic network and the polymer chain. Also studied extensively has been the incorporation of polymers with reactive functional groups into sol-gel networks. Perhaps the classic example of this is the incorporation of poly(dimethylsiloxane) into silica-titania glasses by reacting silanol-terminated PDMS, silicon ethoxide and a titanium alkoxide. Optically clear, monolithic samples can be prepared under a range of conditions.

It is interesting to note that in this and other POLYCERAM systems, dense structures can be obtained at room temperature - likely because of exceptional relaxation and flow in the sample due to the presence of the polymer. Several items of evidence indicate that the PDMS is chemically incorporated into the forming inorganic network by reaction of the terminal silanol groups with the alkoxides or their hydrolysis products.

In the case of Type III POLYCERAMS, interpenetrating networks and composite structures can be formed by two synthetic routes. A polymer can be dispersed in an alkoxide solution which is subsequently gelled. Alternatively, organic monomers can be impregnated into the connective pores of an inorganic gel and then polymerized. A variety of examples of each of these types of POLYCERAMS have been synthesized and applied to a number of interesting applications.

In summary, organic modified oxides represent a new class of inorganic-organic hybrid materials with unique properties. While they are prepared by methods similar to those used in the sol-gel synthesis of glasses and ceramics, the incorporation of organics allows a much wider variety and range of synthetic chemistry to be applied. That is, POLYCERAMS can be tailor-made with regard to specific properties. In addition, organic modification allows many of the problems associated with conventional sol-gel processing to be avoided. Thick (tens of microns) crack-free coatings can be obtained, due to the relaxation and flexibility of the network; and dense monoliths can also be formed at ambient temperature.

POLYCERAMS with applications as diverse as contact lens materials, sensors, abrasives, adsorbents, functional coatings, scratch-resistant coatings, adhesives, ionic conductors and optical hosts for dye molecules have been prepared. At present, the majority of POLYCERAMS have been derived from a limited number of silicon-based precursors and organic components. Further structural insights are critically needed if anything like the real potential of these materials is to be achieved.

Considering the relatively unexplored character of POLYCERAM materials and the outstanding potential which they offer for providing new combinations of properties, one can be confident that the coming decade will see a considerable expansion of activity directed to these fascinating examples of the chemical art.

III. SYNTHESIS AND DIELECTRIC PROPERTIES OF POLYCERAMS

Organic-modified ceramics (POLYCERAMS) represent an emergent class of hybrid, multifunctional materials which combine the properties of organic and inorganic materials. A wide variety of precursors can be used to tailor both the type and degree of organic modification of the inorganic material.

We have carried out work on the synthesis and structural characteristics of bulk POLYCERAMS and the dielectric characterization of POLYCERAM films prepared via the hydrolysis and co-condensation of tetraethoxysilane and the following functionalized polymers: triethoxysilyl modified 1,2 polybutadiene (MPBD), (N-triethoxysilylpropyl) o-polyethylene oxide urethane (MPEOU) and trimethoxysilyl propyl substituted polyethyleneimine (MPEI).

Tetraethoxysilane (TEOS) and modified polymers were obtained from Petrarch (Bristol, PA). The MPBD was received as a 50 wgt. pct. toluene solution; the MPEI was 50 wgt. pct. in iso-propanol (IPA); and the MPEOU was neat. The characteristics of the modified polymers are compared and contrasted in Table I.

The first step in preparing MPBD and MPEOU POLYCERAMS was the same: TEOS and H_2O (acidified with 0.19 M p-toluene sulfonic acid) were reacted by refluxing at a 2:1 H_2O: TEOS molar ratio for 15 min. in tetrahydrofuran (THF) with 1g TEOS: 3 ml THF. The MPEI reactions were similar except IPA was the solvent (MPEI is insoluble in THF). Next the modified polymer was added. With MPBD and MPEOU, the reaction mixture was refluxed for 30 min., whereas with MPEI the solution was cooled to room temperature. This was due to the short gelation times of MPEI solutions. The reaction mixtures were poured into polypropylene beakers and loosely covered with foil. The MPBD and MPEOU solutions all gelled within 36 hrs, while those of MPEI gelled within an hour. POLYCERAMS were formed from all three modified polymers, with weight ratios of reactants, TEOS: polymer of 1: 0.25, 0.5, 1 and 2.

In preparing coating solutions to be used in preparing films for dielectric characterization, for MPBD [triethoxysilyl modified 1,2 polybutadiene] and MPEOU [(N-triethoxysilylpropyl) 0-polyethylene oxide urethane], tetramethoxysilane (TMOS) was directly hydrolyzed with H_2O resulting in an

Table 1 - Properties of Modified Polymers

	MPBD	MPEI	MPEOU
Structure	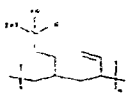	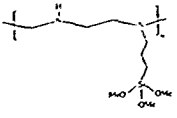	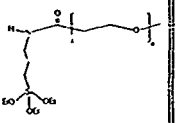
Approximate M.W.	3500-4000	1500-2000	300-400
Chain Length (no. of monomers)	~74	~32	~4
Modification	triethoxysilyl	trimethoxysilyl	triethoxylsilyl
Degree of Modification	One silane for every 20 monomers	One silane for every 20 monomers	One silane for every 4 monomers
Polarity	Non-polar (insoluble alcohol)	Relatively polar (soluble in alcohol)	Relatively polar (soluble in alcohol)
Apparent pH	7.2	9.4	7.6

exothermic reaction and the formation of a clear solution. The water was acidified to 0.15M HCl, and a molar ratio of 1 TMOS: 4 H_2O was used. The solution was stirred at room temperature for 10 min. and the polymer was added in THF (1 g TMOS: 6 ml THF) to give a wgt. ratio of 2 TMOS: 1 polymer. The resulting solution was stirred for 30 min. prior to coating. This reaction scheme was unsuitable for MPEI [thriethoxysilylpropyl substituted polyethyleneimine], as the basic polymer solution (pH 9.4) resulted in rapid gelation. Therefore tetraethoxysilane (TEOS) was hydrolyzed with 0.15M HCl at a molar ratio of 1 TEOS: 2 H_2O in THF (1 g TEOS: 4.38 ml THF). The solution was refluxed for 15 mins and cooled; polymer was added and then directly used for coating.

Coatings of each solution were applied to Pt-coated Si substrates at 2000 rpm for 20 sec. Films of neat polymer and silica were prepared by similar methods. The substrates were fabricated by sputtering Pt for 10 min. at 200 watt RF power under 20 m Torr Ar pressure onto oxidized Si wafers, resulting in films 1700Å thick. These were annealed for 30 min. at 700C. Coatings were dried at 50C for 24 hr. prior to electrical characterization. After drying, Pt dots with radius of about 0.70 mm were sputtered onto the coating using a shadow mask.

In the other experiments, the effects of the TMOS: PBD ratio on dielectric properties were determined. Coating solutions were prepared as above, except the solutions were refluxed for 30 mins prior to coating at various speeds for 20 sec. Si wafers were also coated for FTIR analysis.

Monolithic materials, in the range 2.5 to 20g, were obtained from all the compositions explored. All the samples were highly transparent. Those of MPBD were pale yellow, while those of MPEI and MPEOU were clear (e.g., Figure 4). A variety of techniques were employed to investigate the structural characteristics of the materials. These included SEM, BET, density measurements, FTIR and SAXS. SEM examination of the fracture surfaces of the Polycerams indicated that the samples appeared similar, even at a magnification of 10,000X. The fracture surfaces were smooth and pore-free within the resolution of the microscope. Little contrast was observed, suggesting little or no variation in composition within a resolution of $\sim 0.1\mu m$.

The pore-free character of the Polycerams was confirmed by BET measurements, in which no specific surface areas could be detected. This

Figure 4. A transparent TEOS-MPEOU POLYCERAM
(1 division = 1 cm)

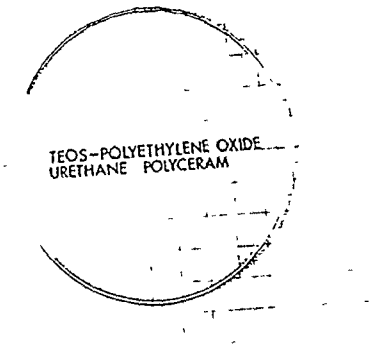

characteristic of organically modified materials is quite remarkable, and has been observed by other workers.

Room temperature densification was assessed by density measurements using displacement methods. Theoretical densities were calculated from the density values of the individual components of the gels: MPBD, 0.90 g/cm^3; MPEI, 0.91 g/cm^3; and MPEOU, 1.13 g/cm^3. The density of the silica component was taken to be 2.05 g/cm^3, a value reported for the skeletal density of SiO_2 gels prepared under acidic conditions. The POLYCERAMS had theoretical densities of 80 to 100%. Higher theoretical densities were obtained with increasing polymer volume fractions. The MPEI and MPEOU gels had higher theoretical densities compared to materials of similar polymer contents containing MPBD. Organic modification therefore results in very different densification behavior compared to inorganic gels where high temperature treatment is necessary to achieve anything like full density. The organics allow the network to relax at low temperature, resulting in a dense, pore-free body.

FTIR analysis of the MPEOU Polycerams showed shifts in the vibrational frequencies of the organic species upon incorporation into the silicate network. Specifically, the carbonyl stretching frequency shifted to a lower wavenumber in the gel (1730 to 1700 cm^{-1}), indicating a weaker bond, most likely due to hydrogen bonding between the carbonyl and other hydroxyl groups. No major shifts were observed for the MPBD and MPEOU POLYCERAMS.

Homogeneity of the Polycerams was investigated by SAXS. Clear, free-standing films were cast from solution with the composition 1g TEOS: 0.5 g polymer. This composition corresponds to 79.8%, 79.6% and 75.9% volume fractions of polymer for the MPBD, MPEI and MPEOU systems respectively. A high degree of homogeneity was anticipated (at least for sizable spatial scales), since even bulk samples were transparent and large differences exist between the refractive indices of the organic and inorganic phases.

The SAXS intensities, corrected for background and absorption, are shown in the form of Guinier plots in Figure 5. As shown there, the scattering was in the order MPBD > MPEI > > MPEOU. The scattering from the MPBD and MPEI POLYCERAMS was notably higher than that from homogeneous silicate glasses; while the scattering from the MPEOU POLYCERAM was comparable to but somewhat larger than that from silicates. The slopes of the

Figure 5. SAXS profiles of POLYCERAMS

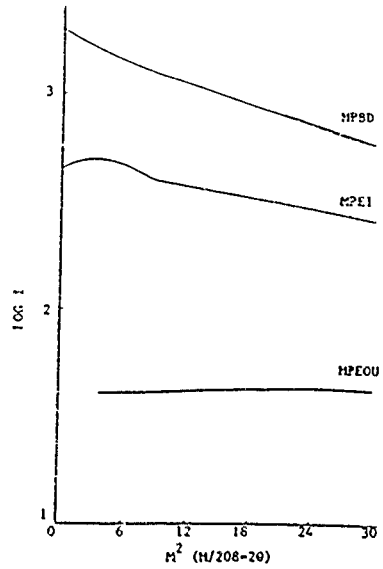

curves in Figure 5 are proportional to R^2, where R is the radius of the inhomogeneity (assumed to be spherical in shape).

For MPBD, the data indicate a range of particle diameters from 66-44Å; while for the MPEI POLYCERAM, data indicate a diameter of 34Å. The maximum in intensity at low angles in this system very likely reflects a correlation distance resulting from nanophase separation. The absence of such a maximum in the MPBD data may simply reflect the dispersivity in sizes of the inhomogeneities.

The horizontal intensity vs. M^2 plot for the MPEOU Polyceram may reflect the asymptotic scattering from simple compositional fluctuations (similar to that seen in homogeneous melted glasses but higher because of the higher compressibility of the POLYCERAMS compared with inorganic glasses). The overall scattering from the MPEOU Polyceram is consistent with a material having a high degree of chemical homogeneity.

The structures of POLYCERAMS are expected to depend on a number of factors relating to the precursors and synthesis conditions. Several are pertinent to the reactive modified polymer. Molecular weight is of considerable importance, and influences directly the level of homogeneity that can be obtained.

The type and number of reactive functional groups are also expected to have important effects on the final structural characteristics. Alkoxysilyl modification provides almost - ideal functional groups for incorporation into alkoxide-derived gels due to the similarity in reaction rates which they provide. Silyl functions on the polymer would also increase the mutual solubility of the polymer and the alkoxide, thereby promoting homogeneity. The number of reactive groups would affect the number of tie-points of the polymer into the inorganic network, thus affecting its relaxation behavior.

Polarity is a key concern, since inorganic oxide networks are polar while most organic polymers show a range of polarities depending on the type of functionality. Note in this regard that MPEOU is the most polar, and MPBD the least polar, of the organics used in the present study. Similar polarities and mutual solubility seem required for forming chemically homogeneous POLYCERAMS. The pH of the polymer in solution can also dramatically affect the network structure, as demonstrated for alkoxide-derived silica gels prepared under acidic and basic conditions.

The properties of the modified polymers are consistent with the results obtained in this work. Shorter gelation times were obtained with MPEI due to its basic nature and the presence of trimethoxysilyl compared with triethoxysilyl groups. The effective pH's of the solutions before gelation were 9.2 for the MPEI, 3.2 for the MPBD and 3.6 for the MPEOU. Homogeneity was dependent both on the molecular weight and polarity of the polymer. The highest homogeneity was obtained with MPEOU due to its low molecular weight and high polarity. The higher molecular weight and lower polarity polymers, MPEI and MPBD, formed POLYCERAMS exhibiting microphase separation on a nanoscale.

In preparation for the dielectric characterization work, FTIR spectroscopy was used to monitor the drying of MPBD based POLYCERAM films on Si wafers. The coatings were heated at various temperatures using the schedule: room temperature, 24 hrs; heating temperature, 24 hrs; heating temperature, 24 hrs under vacuum (23.4 mm Hg). The results presented in Figure 6 show that a 100C treatment in vacuum is necessary to dry the films.

Data on dielectric constant and tan δ at 10 kHz and 0.005 V rms signal level for the different POLYCERAM films are presented in Table 2. Among the modified polymers, MPEOU is the most polar while MPBD is non-polar. Furthermore, MPEOU is conjugated, contributing an added polarizability arising from electron delocalization within the molecule. Hence it is to be expected, as reflected in Table 2, that the MPEOU-modified film has the highest dielectric constant while the MPBD-modified film has the lowest value.

Three compositions of MPBD-modified films were investigated with different relative amounts of TMOS and MPBD. They all exhibit a similar dielectric constant ($\approx$5.7) and tan δ ($\approx$0.04), as can be seen in Table 3.

Note that the values of dielectric constant shown in Table 3 (5.7) are notably higher than the value for the MPBD-based films presented in Table 2 (4.4). This difference very likely reflects the difference in film thickness and process conditions used to prepare the films. Such variations are deserving of further exploration, which is presently underway.

The dielectric properties of neat SiO_2 and MPBD films at 10 kHz and 0.005 V rms signal level which have been annealed at 100C under vacuum for 48 hrs are tabulated in Table 4.

Figure 6. Infrared absorption for PBD based POLYCERAMS dried under vacuum at room temperature, 50, 75, and 100C.

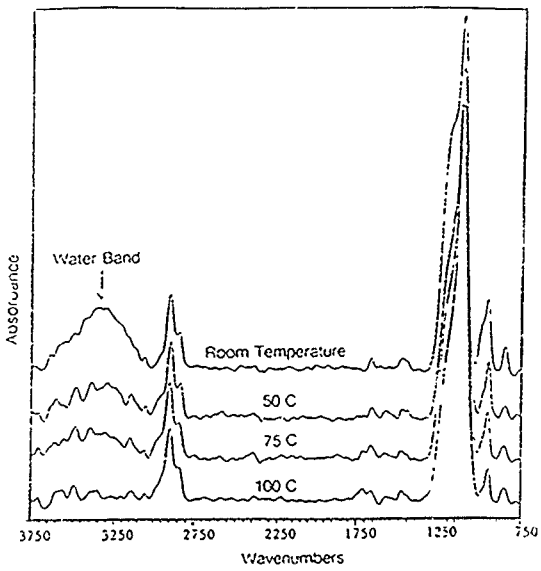

Table 2 - Dielectrical Properties of POLYCERAM Films

POLYCERAM system	Dielectric constant	Tan δ
74.3 vol% MPBD	4.4	0.02
74.0 vol% MPEI	7.2	0.06
69.7 vol% MPEOU	7.8	0.16

Table 3 - Dielectrical Properties of MPBD POLYCERAM Films

Volume % PBD	Dielectric Constant at 10 kHz, 0.005 V rms	Tan δ at 10 kHz, 0.005 V rms	Dielectric Constant Calculated from End Members
59.1	5.7	0.03	6.9
68.4	5.7	0.05	6.0
74.3	5.8	0.03	5.3

Table 4 - Dielectric Properties of Neat SiO_2 Films

Film	Dielectric Constant
TMOS-derived SiO_2	13.0
TEOS-derived SiO_2	13.0
neat MPBD	2.7

Assuming for simplicity that the dielectric constant of the POLYCERAM reflects the volume fractions of the constituents and using the end-member values in Table 4, the calculated dielectric constants for the MPBD-modified POLYCERAMS shown in Table 3 were obtained.

There is a strong increase in tan δ at low frequencies for the POLYCERAM films (Figure 7). Such behavior can be attributed to DC conduction since there is no strong dispersion in dielectric constant, which would be present in the case of relaxation. To investigate the nature of the charge carriers within the film, capacitance vs. applied bias measurements were taken. If ionic impurities were present, then peaks or hysterisis would be expected. Figure 8 shows a straight line, however; and hence the conduction is assumed to be electronic in nature.

The dielectric constants obtained for the MPBD-based Polyceram films lie between values for the end-members, MPBD and SiO_2, and are reasonably predicted by a simple volume fraction additive relation. In detail, the measured dielectric constants vary less with composition than predicted by the simple relation.

More generally, the dielectric constants of about 13 obtained for TEOS- and TMOS-derived films which had been vacuum dried at 100C appear to limit the ability to obtain POLYCERAM films with exceptionally low dielectric constants (assuming reasonable fractions of the inorganic constituent and TMOS/TEOS as precursors for that constituent).

The results obtained in this phase of the study illustrate the capability of wet chemical processing for tailoring the structures of organic-modified inorganics on a scale of nanometers. By control of chemistry and processing, POLYCERAMS can be formed as novel hybrid materials with considerable potential for providing new combinations of functionality. It is also clear from the present results that it is possible -- by control of chemistry and process conditions -- to vary the dielectric constants of POLYCERAM films over a wide range. Such films offer improved adhesion to inorganic surfaces and better abrasion resistance compared with polymer films (as observed here for MPBD-based films on platinized surfaces).

Figure 7. Dielectric Constant and Tan δ vs. Frequency 2 TMOS: 1 MPBD Film at 0.005 V_{RMS}

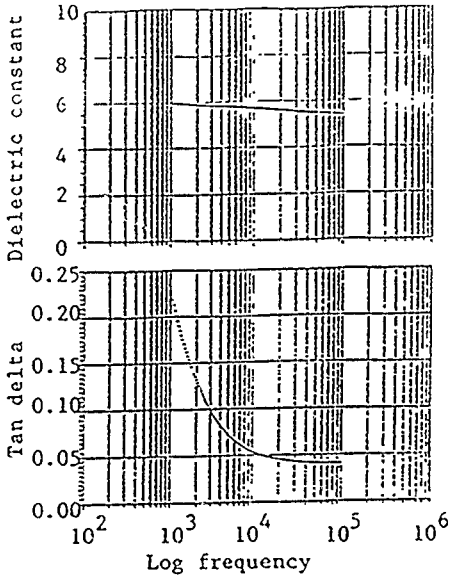

Figure 8. Dielectric Constant and Tan δ vs. Applied Bias for 4 TMOS: 1 MPBD Film at 1 kHz, 0.005 V_{RMS}

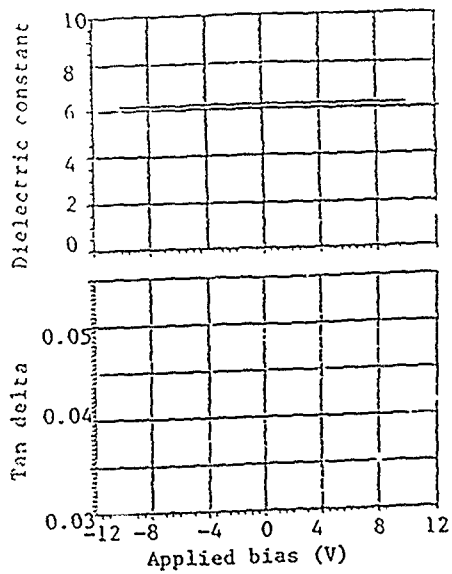

IV. NOVEL OPTICAL MATERIALS COMPRISING NON-LINEAR ORGANIC DYES IN POLYCERAM HOSTS

Wet chemically derived organically modified inorganic materials (POLYCERAMS) are logical host materials for organic dyes. The organic component can act as a solvent phase in the network, increasing the solubility of the dye and also protecting the dye from acidic silica surfaces. The inorganic component of the POLYCERAM can improve the stability of the material by providing structural support and protecting the organic groups from inter-reaction. A further advantage of using POLYCERAMS as hosts is that the organic modification of the inorganic gel network minimizes the cracking problems associated with conventional alkoxide-derived inorganic gels.

The present work was undertaken to explore the incorporation of the exceptional non-linear organic dyes, 2-methyl-4-nitroaniline (MNA) and p-nitroaniline (pNA) in POLYCERAM films and monoliths prepared by the hydrolysis and co-condensation of tetraethoxysilane and trimethoxysilylpropyl - substituted poly(ethyleneimine) (MPEI) of MW = 1500-2000. The poly(ethyleneimine) system was selected primarily due to the compatibility between the imine groups of the polymer and the amino groups of the dye molecules. Protonation of the amine groups would be undesirable.

Sample preparation consisted of refluxing TEOS and H_2O (acidified to 0.15M HCl) in iso-propanol (IPA) at a H_2O:TEOS molar ratio of 2:1 for 15 min. The reaction mixture was cooled, and the MPEI and organic dye were added. In all cases, the weight ratio of the MPEI solution to added IPA was 1.4. Solutions were passed through a 0.8 μm syringe filter and coated onto pre-cleaned glass slides by spin-coating at 1000 rpm for 10 sec. The coatings were dried in air for 5 min. before coating again. Multiple coatings were applied to give the desired thickness. Thickness measurements were obtained using a Dektak 11A profilometer. The remaining solution was cast into poly(propylene) beakers and allowed to gel and dried slowly at room temperature. Films dried in air for 48 hours were investigated for second harmonic generation using the Maker fringe method.

Film thicknesses of about 30 μm were readily obtained; and much thicker films could be formed. Additionally, under slow drying conditions monoliths could be prepared: a typical example of a 1 TEOS: 1 MPEI: 0.1 MNA (wgt. ratio) doped POLYCERAM is shown in Figure 9.

Figure 9. Monolithic 1 TEOS: 1 MPEI: 0.1 MNA POLYCERAM.

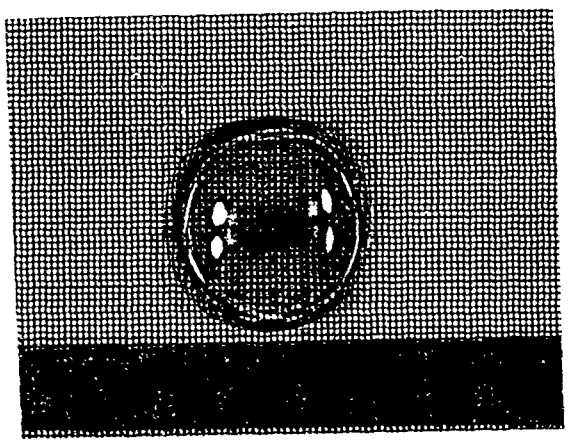

The effect of the TEOS: MPEI ratio on second harmonic generation (SHG) was investigated, with the results shown in Table 5. As shown there significant SHG signals were observed for all samples. By comparison, crystalline MNA powder (approx. 100 μm thick) gave an SHG signal of around 1100 mV under these experimental conditions. all the coating compositions listed in Table 5 resulted in optically clear, crack-free, X-ray amorphous films.

The intensity of the normalized SHG signal (SHG signal divided by thickness) is plotted in Figure 10 vs. the TEOS: MPEI ratio at a constant MNA: MPEI ratio of 0.1. An increase in TEOS: MPEI ratio is seen to produce a dramatic increase in the SHG signal, despite the fact that since the MNA: MPEI ratio is constant, an increase in TEOS: MPEI serves effectively to dilute the MNA. This suggests there is interaction between the silica surfaces in the POLYCERAM and the MNA molecules, producing local orientation.

The effect of the MNA: MPEI ratio on SHG was next determined at a constant MNA: TEOS ratio of 2. SHG signals obtained from optically clear, crack-free and X-ray amorphous films are shown in Table 6; normalized SHG signals as a function of MNA: MPEI ratio are plotted in Figure 11.

As seen in the figure, increases in the MNA: MPEI ratio result in marked increases in the normalized SHG signal. At higher MNA: MPEI ratios than those shown in Figure 11, substantial crystallization of the MNA occurred. An MNA: MPEI ratio of 0.28 resulted in an X-ray amorphous film. At the higher ratio of 0.284, substantial crystallization of MNA on the free surface of the film was observed; however, the characteristic MNA diffraction peaks could be removed by washing the film in IPA. Increasing the MNA: MPEI ratio to 0.3 resulted in substantial crystallization, both on the free surface and in the bulk.

The principal question arising from these results is whether the high SHG signals obtained from the clear films arose from the presence of microcrystalline MNA regions in the film, or whether alignment of the MNA molecules had occurred resulting in a non-centrosymmetric structure, or possibly both of these phenomena. As stated above, the results presented in Tables 5 and 6 were derived from optically clear, X-ray amorphous films. Investigation by cross-polarized optical microscopy revealed small crystals at the film-glass slide interface in some cases. A typical micrograph is shown in Figure 12. While crystalline MNA was present on the surface of at least some

Table 5 - Effect of TEOS: MPEI Wgt. Ratio on Second Harmonic Generation (MNA: MPEI = 0.1)

TEOS: MPEI Ratio	Thickness (μm)	Maximum Second Harmonic Signal (mV)
0	28.2	62.4
1	32.3	167
2	27.6	224
3	25.8	374

Figure 10. Effect of TEOS. MPEI Ratio on Normalized SHG Signal for constant MNA: MPEI = 0.1

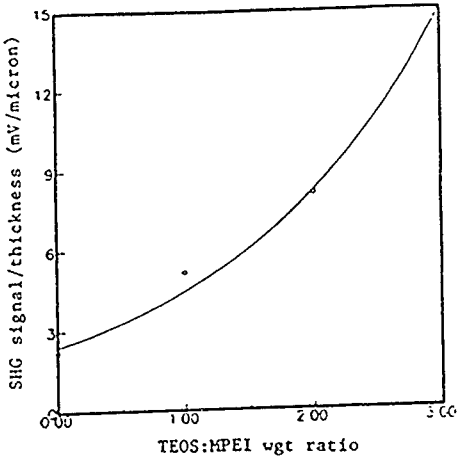

Table 6 - Effect of MNA: MPEI Wgt. Ratio on Second Harmonic Generation (TEOS: MPEI = 2)

MNA: PEI	Thickness (μm)	Maximum Second Harmonic Signal (mV)
0.1	27.6	224
0.15	26.1	390
0.2	27.6	660
0.24	31.0	953

Figure 11 - Effect of MNA: MPEI Ratio on Normalized SHG Signal for constant TEOS: MPEI = 0.2

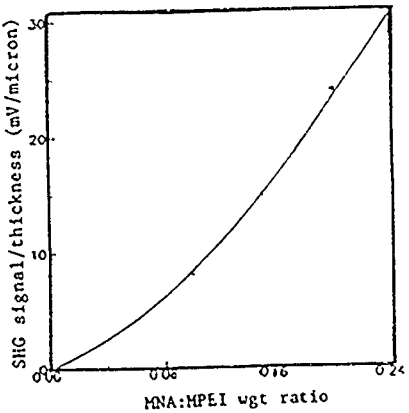

Figure 12. Optical Micrograph (Cross-Polarized) of 2 TEOS: 1 MPEI: 0.2 MNA Film (bar = 100μ)

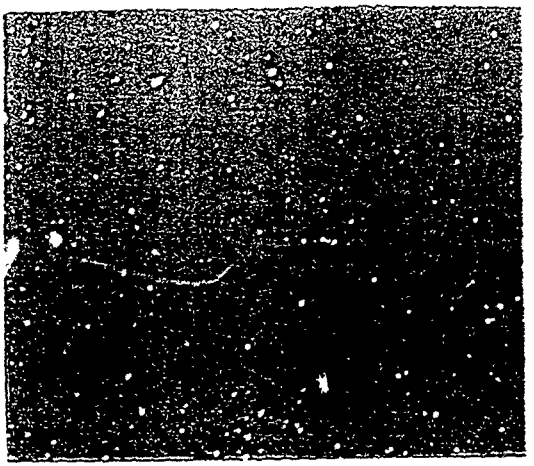

Figure 13. Optical Micrograph (Cross-Polarized) of Heated 2 TEOS: 1 MPEI: 0.2 MNA Film (bar = 100μm)

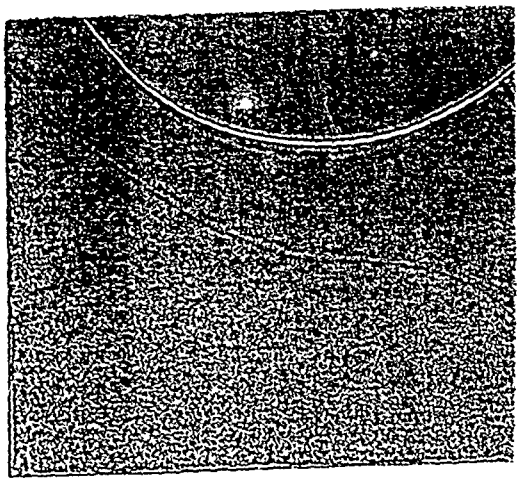

of the POLYCERAM films, the small size and number of crystals would not be expected to give rise to such strong SHG signals as were observed.

To elucidate further the basis of the observed second harmonic generation, a film with the composition 2 TEOS: 1 MPEI: 0.2 MNA was heated at 150C for 5 min., substantially higher than the melting point of MNA (131-133C). Heating resulted in substantial loss of the MNA due to its high volatility. Investigation of the heat-treated film showed the disappearance of the crystalline regions (see Figure 13). However, the sample still showed significant SHG: signals of approximately 287mV were obtained, which strongly suggests that MNA alignment had occurred in the film.

One final experiment was performed to confirm this finding: a 26μm film with the composition 2 TEOS: MPEI: 0.24 pNA was prepared. pNA undergoes centrosymmetric crystallization, whereas MNA undergoes non-centrosymmetric crystallization. Therefore, when pNA crystallizes, the oppositely charged molecular ends align in the crystal, canceling the net dipole moment and leading to zero quadratic hyperpolarizability, i.e., no SHG. The pNA-doped POLYCERAM film showed a SHG signal of 547 mV, which is very strong evidence for molecular alignment in the sample.

The present results indicate that POLYCERAMS are indeed fine hosts for non-linear organic dyes; and that by suitable tailoring the organic and inorganic species, it should be possible to carry out molecular engineering in the preparation of novel NLO materials. The results also provide evidence for a remarkable phenomenon - namely, the molecular alignment of the dye molecules in the samples.

V. WET CHEMICAL COATING OF FIBERS FOR COMPOSITES AND SYNTHESIS OF BULK TRANSFORMATION - TOUGHENED CERAMICS

Application of selected coatings on ceramic fibers allows the properties of fiber surface to be tailored for specific applications. One area which has gained considerable attention recently is the use of ceramic fibers in ceramic matrix and metal matrix composites. By use of appropriate coatings, it should be possible to modify the characteristics of the fiber-matrix interfaces and thereby to tailor the bonding between fiber and matrix and hence optimize composite performance.

Use of wet chemical methods to coat fibers is attractive because it offers wide latitude in coating chemistry and because it can be carried out in a continuous process, and hence in an economically effective manner. The present work was undertaken to explore the feasibility of such coating for application to both oxide (aluminum oxide) and non-oxide (silicon carbide and carbon) fibers. Most emphasis was placed on coating alumina fibers.

A variety of coating compositions were explored during the course of the work. These compositions and the precursors used in their synthesis are summarized in Table 7.

The preparation of a typical coating solution, in this case Al_2O_3-42.6 wt% ZrO_2, was carried out as follows: 3 g of $Al(O^iPr)_2C_6H_9O_3$ [0.011 moles] was weighed into a three-necked flask equipped with a nitrogen inlet, drying tube and stirring accessories. Dry iso-propanol (10 ml) was added, followed by a solution of 0.20 ml of 0.15 M aqueous hydrochloric acid and dry iso-propanol (5 ml) to give the ratio 1 mole alkoxide: 1 mole H_2O. The solution was then stirred at ambient temperature for thirty min. Then 1.1 g of $Zr(O^nPr)_4$ [0.003 moles] and dry iso-propanol (10 ml) was added. After thirty min., a final hydrolysis was carried out. This consisted of adding a solution of 0.45 ml of 0.15 m aqueous HCl and dry iso-propanol (5 ml) to give the ratios 1 mole aluminum alkoxide: 1 mole H_2O and 1 mole zirconium alkoxide: 4 moles H_2O. The resulting clear solution was then stirred at ambient temperature for thirty min. before being used for coating.

As necessary, the fibers were desized prior to coating. For Fiber FP (aluminum oxide), the desizing treatment consisted of firing at 600C for six hr. at a heating/cooling rate of 5C $min.^{-1}$ to remove the size. SiC and C fibers

Table 7 - Coating Compositions and Precursors Explored in the Present Study

Coating	Precursors
Al_2O_3	$Al_2(OH)_5Cl \bullet 2H_2O$ or $Al(O^iPr)_2C_6H_9O_3$ or $Al(O^sBu)_2C_6H_9O_3$
Y_2O_3 stabilized ZrO_2	YCl_3 and $Zr(O^nPr)_4$
$MgAl_2O_4$	$Mg[Al(O^sBu)_4]_2$
Al_2O_3-42.6 wt% ZrO_2 Al_2O_3-20 wt% ZrO_2 Al_2O_3-25 wt% ZrO_2	$Al(O^iPr)_2C_6H_9O_3$ and $Zr(O^nPr)_4$
$3Al_2O_3 \bullet 2SiO_2$+15 wt% ZrO_2	$Al(O^iPr)_2C_6H_9O_3$ and $Zr(O^nPr)_4$ and $Si(OEt)_4$
Al_2TiO_5 Al_2O_3+1.5 wt% TiO_2	$Al(O^iPr)_2C_6H_9O_3$ and $Ti(O^iPr)_4$
Al_2O_3-42.6 wt% ZrO_2 (stabilized with 7 mole% Y_2O_3) Al_2O_3-20 wt% ZrO_2 (stabilized with 7 mole% Y_2O_3) Al_2O_3-25 wt% ZrO_2 (stabilized with 7 mole% Y_2O_3)	$Al(O^iPr)_2C_6H_9O_3$, $Zr(O^nPr)_4$ and $Y(NO_3)_3 \bullet 5H_2O$

were desized by soaking in acetone overnight, followed by rinsing with acetone and drying at 60C.

The coating procedure consisted of cutting the fiber strands into three-inch long segments. Five three-inch segments were then mounted on a cardboard frame. The frame was immersed into the coating solution, and the coating solution was pumped out of the container at specific rates using a peristaltic pump. Various solution withdrawal rates were used, corresponding to linear withdrawal rates ranging from 0.5-7 cm $min.^{-1}$. The coatings were then allowed to dry; and as desired for thicker coatings, the coating was repeated. Finally, the fibers were fired at 1000C for 2 hr. using a heating/cooling rate of 5C $min.^{-1}$. After firing, the coated fibers were investigated by SEM and EDS analysis.

Bulk gels of the coating compositions were also obtained by allowing the coating solutions to gel by exposure to atmospheric moisture and solvent evaporation. The crystallization behavior of the gels was investigated by X-ray diffraction, SEM and EDS analysis.

It was found that high quality oxide coatings covering a broad range of composition could be deposited onto ceramic fibers using the solutions and coating methods described above. The thicknesses of the coatings depended on a number of factors including sol viscosity, the number of coatings applied and the withdrawal rates used. As expected, faster withdrawal rates gave rise to thicker coatings. Using optimized multiple coating procedures, defect-free and crack-free coatings with thicknesses ranging from 3000-4000 Å (after firing to 1000C) could routinely be obtained.

Examples of Al_2O_3 fibers coated with Y_2O_3-stabilized ZrO_2 and with Al_2O_3 (derived from $Al(O^iPr)_2C_6H_9O_3$) are shown in Figures 14 and 15 respectively. Attempts to coat fibers with coatings thicker than ~0.5 μm led to the introduction of defects and some cracking of the coatings. This thickness limit is common to all chemically derived coatings which are prepared without organic modification.

Investigation of the crystallization behavior of the bulk gels yielded interesting results. For example, in the case of Al_2O_3 gels, the subsequent phase development of the gel exhibited a marked dependence on the precursor material. This is shown by the results in Table 8. Gels synthesized using chelated aluminum alkoxides, $Al(O^iPr)_2C_6H_9O_3$ or $Al(O^sBu)_2C_6H_9O_3$, gave

Figure 14

SEM MICROGRAPH OF Al_2O_3 COATING
ON FP (Aluminum Oxide) FIBER

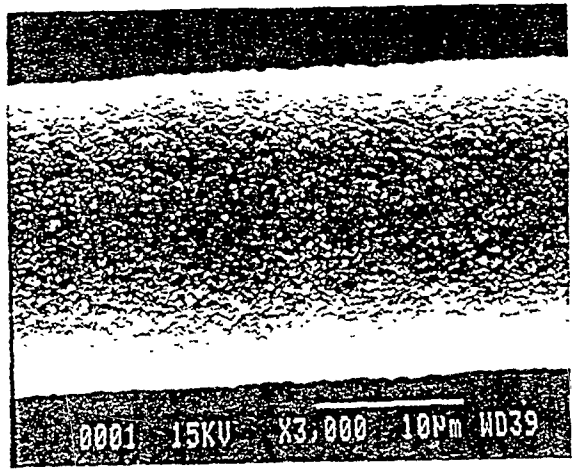

Figure 15

SEM MICROGRAPH OF YSZ COATING ON FP FIBER

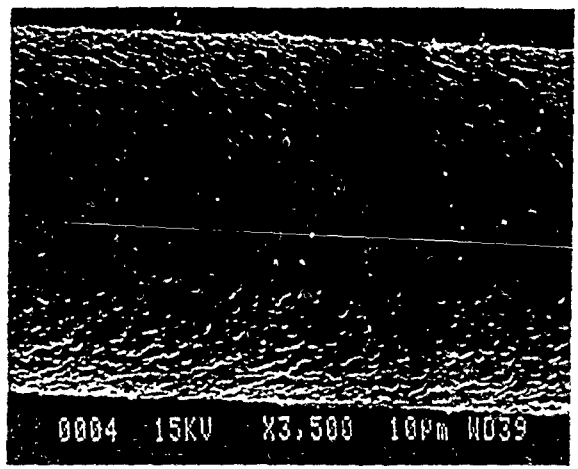

Table 8 -

EFFECT of Al_2O_3 PRECURSOR ON SUBSEQUENT PHASE DEVELOPMENT

$Al_2(OH)_5Cl \cdot 2H_2O$	$Al(O^sBu)_2C_6H_9O_3$	$Al(O^iPr)_2C_6H_9O_3$
~500C	~800C	~800C
transitional Al_2O_3 phases	transitional Al_2O_3 phases	transitional Al_2O_3 phases
~1000C	~900C	~900C
transitional Al_2O_3 phases $+\alpha$-Al_2O_3	transitional Al_2O_3 phases $+\alpha$-Al_2O_3	transitional Al_2O_3 phases $+\alpha$-Al_2O_3
~1100C	~1000C	~950C
$+\alpha$-Al_2O_3	$+\alpha$-Al_2O_3	$+\alpha$-Al_2O_3

much easier conversion to α-Al_2O_3 compared to gels prepared from aqueous aluminum chlorohydrate solutions. Additionally, when using the chelated aluminum alkoxides, the nature of the alkoxy ligand also affected the subsequent crystallization behavior: Single phase α-Al_2O_3 could be obtained from $Al(O^iPr)_2C_6H_9O_3$ at 950C; whereas firing at 1000C was necessary for gels derived from $Al(O^sBu)_2C_6H_9O_3$. This has important practical implications with regard to depositing coatings on Al_2O_3 fibers. Prolonged heating of the commercial alumina fibers at temperatures above 1000C leads to exaggerated α-Al_2O_3 grain growth in the fiber, causing a severe reduction in strength.

These considerations are likewise important for coatings on silicon carbide fibers, which exhibit a marked degradation in strength at even lower temperatures.

In the case of transformation-toughened ceramics, such as Al_2O_3-ZrO_2 and mullite-ZrO_2, optimum toughening is obtained with dense, uniform fine-grained microstructures. In addition, retention of ZrO_2 in the metastable, tetragonal phase is necessary for stress-induced transformation. Retention requires the ZrO_2 grain size to be less than 0.5-0.8 μm.

A variety of wet chemical procedures have been investigated for preparing Al_2O_3-ZrO_2 composites. These include evaporative decomposition of an α-Al_2O_3-$ZrO(NO_3)_2$ slurry; hydrolysis of $Zr(O^nPr)_4$ in a dispersion of α-Al_2O_3, colloidal processing; co-precipitation or spray-drying of aqueous sols or solutions; and sol-gel processing using alkoxides. Debsikdar prepared $80Al_2O_3 \bullet 20ZrO_2$ (wt.) powders by complexing $Al(O^sBu)_3$ with 2,4-pentanedione, partially hydrolysing this complex, reacting with $Zr(O^nPr)_4$, followed by further hydrolysis.

Less attention has been paid to the preparation of mullite-ZrO_2 composites. These have been prepared by conventional sintering; from $ZrSiO_4$ and Al_2O_3; from glass powders; and from reaction of Al_2O_3 and SiO_2 sols prepared from alkoxides and ZrO_2 powder.

In the present study, Al_2O_3-ZrO_2 gels were prepared from a chelated aluminum alkoxide, $Al(O^iPr)_2C_6H_9O_3$, and $Zr(O^nPr)_4$. Three compositions were investigated: 95 Al_2O_3-5 ZrO_2 (wt.); 80 Al_2O_3 - 20 ZrO_2 (wt.) and 57.4 Al_2O_3 - 42.6 ZrO_2 (wt.). The last is the eutectic composition in the Al_2O_3-ZrO_2 system. The approach was then extended to prepare a mullite +15 wgt.pct. ZrO_2 composition.

The synthesis procedures are illustrated by the preparation of 57.4 Al_2O_3-42.6 ZrO_2 and $3Al_2O_3 \cdot 2SiO_2$ + 15 wt.% ZrO_2 described below. In preparing $57.4Al_2O_3$ - $42.6ZrO_2$, 3.00 g of $Al(O^iPr)_2C_6H_9O_3$ [0.011 moles] was added to 10 ml of ^{i}PrOH in an inert atmosphere. The aluminum alkoxide was partially hydrolysed by the addition of 0.20 ml 0.15M aq.HCl in 5 ml of ^{i}PrOH giving the ratio 1 mole Al alkoxide: 1 mole H_2O. After 30 min. 1.100 g of $Zr(O^nPr)_4$ [0.003 moles] in 10 ml of ^{i}PrOH was added. After stirring for an additional 30 min., a final hydrolysis was carried out. A solution of 0.45ml of 0.15M aq.HCl and 5 ml of ^{i}PrOH was added giving the ratios 1 mole Al alkoxide: 1 mole H_2O and 1 mole Zr alkoxide: 4 moles H_2O. the resulting clear solution was poured into polypropylene beakers, loosely covered with foil, and allowed to gel. This took several days at ambient temperature. After drying, the gels were transparent and pale yellow in color.

In preparing the mullite +15 wt.% ZrO_2 material, 3.00 g of $Al(O^iPr)_2C_6H_9O_3$ was reacted with 0.3097 g of $Zr(O^nPr)_4$ [0.001 mole] as described above. a pre-hydrolysed solution of $Si(OEt)_4$ was then added. This consisted of 0.7595 g of $Si(OEt)_4$ [0.004 moles], 3.8 ml of ^{i}PrOH and 0.13 ml of 0.15M aq.HCl, giving the molar ratio 1 mole $Si(OEt)_4$:2 moles H_2O. The solution was stirred at ambient temperature for 30 min. prior to its addition to effect pre-hydrolysis.

The reaction mixture was stirred for 30 min. and then a final hydrolysis was carried out. This consisted of adding 0.40 ml of 0.15M aq.HCl in 5 ml ^{i}PrOH, giving the ratios 1 mole Al alkoxide: 1 mole H_2O, 1 mole Zr alkoxide:4 moles H_2O and 1 mole Si: alkoxide: 2 moles H_2O. Subsequent gelation and drying gave transparent, pale yellow samples.

Samples of dried gels were fired in air using a 2 hr. soak and a heating/cooling rate of 5C $min.^{-1}$. In the case of the mullite-ZrO_2 gel, firing led to undesirable blackening due to residual alkoxide groups. This was eliminated by pre-firing the gel in O_2 to 700C at 1C $min.^{-1}$. Fracture surfaces were investigated by SEM and EDS. Samples were also analyzed by X-ray diffraction. In all cases, the samples were ground to a fine powder prior to firing. Grinding was not conducted after heat treatment to avoid the stress-induced transformation of tetragonal ZrO_2. The ratio of tetragonal to monoclinic ZrO_2 was determined from the integrated intensities of the tetragonal (111) and the monoclinic (111) and (111) peaks.

For the Al_2O_3-ZrO_2 gels, XRD indicated that the α-Al_2O_3 transition occurred at ~ 1100C (see Table 9). This is considerably higher than the transformation temperature for an Al_2O_3 gel prepared from $Al(O^iPr)_2C_6H_9O_3$, where the transition occurred at ~900C and α-Al_2O_3 was the only phase observed after firing at 950C for 2 hr.

In the present work, the relative amount of ZrO_2 was also found to be an important factor in phase development. With $95Al_2O_3$-$5ZrO_2$, well developed α-Al_2O_3 was observed at 1200C; but this was observed only on firing to 1300C for the $57.4Al_2O_3$ - $42.6ZrO_2$ composition. Also observed for the latter composition, a high concentration of ZrO_2 inhibited the formation of transitional Al_2O_3 phases. No crystalline Al_2O_3 (γ-,θ - or α -) was formed until 1100C. Broad peaks corresponding to the (111) reflection of tetragonal ZrO_2 were apparent in the high ZrO_2 content gels at 1000C - i.e., before the $\gamma \rightarrow \theta$ - Al_2O_3 transition.

The ZrO_2 phase was principally the tetragonal form for all the samples and firing temperatures studied. Only minor amounts (6 wgt.%) of monoclinic ZrO_2 were detected. In all cases, the amounts of tetragonal ZrO_2 and α-Al_2O_3 crystallized increased substantially on firing between 1100 and 1400C. For example, in the 80 Al_2O_3-$20ZrO_2$ material, the integrated intensity of the (111) reflection of tegragonal ZrO_2 increased by a factor of 1.6 and that of the (012) reflection of α-Al_2O_3 by a factor of 4.5 between 1100 and 1400C.

For the mullite-ZrO_2 gel, poorly crystalline mullite was observed at 900C; at 1000C the mullite was well-crystallized. Very weak reflections corresponding to tetragonal ZrO_2 were detected at 1000C; and the ZrO_2 was well crystallized at 1300C. No monoclinic ZrO_2 was detected by XRD in any of the samples investigated here.

Fracture surfaces of fired gels were investigated by SEM in the back-scattered mode. Indistinct microstructures with a lack of ZrO_2-rich areas were observed at 1200C. However, in samples fired at 1400C, well-defined microstructures were observed. Representative micrographs are shown in Figures 16 and 17. After firing at 1400C, the samples appeared dense and virtually pore-free within the resolution limits of the SEM. Tetragonal-ZrO_2 particles (light areas in the micrographs) were well dispersed throughout the mullite matrix, both inter- and intragranular.

Table 9 -

CRYSTALLINE PHASES OBSERVED IN FIRED GELS

Temperature (C)	$95Al_2O_3$ - $5ZrO_2$	$80Al_2O_3$ - $20ZrO_2$	$57.4Al_2O_3$ - $42.6ZrO_2$	Mullite - $15ZrO_2$
900	γ	γ	amorphous	M
1000	γ,θ	γ,ZT	ZT	M,ZT
1100	γ,θ, α,ZT	γ,θ,α ZT,ZM	γ,θ,α ZT,ZM	M,ZT
1200	α,ZT,ZM	α,ZT,ZM	θ,α,ZT,ZM	M,ZT
1300	α,ZT,ZM	α,ZT,ZM	α,ZT,ZM	M,ZT
1400	α,ZT,ZM	α,ZT,ZM	α,ZT,ZM	M,ZT

γ = γ-Al_2O_3; θ = θ-Al_2O_3; α = α-Al_2O_3; ZT = tetragonal ZrO_2; ZM = monoclinic ZrO_2; M = Mullite

FIGURE 16

MICROSTRUCTURE OF CHEMICALLY DERIVED $80Al_2O_3$-$20ZrO_2$ FIRED AT 1400C (X10,000)

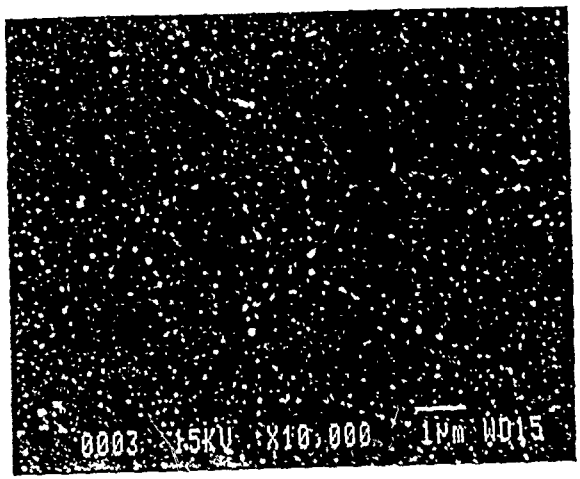

FIGURE 17

MICROSTRUCTURE OF CHEMICALLY DERIVED MULLITE-$15ZrO_2$ FIRED AT 1400C (X10,000)

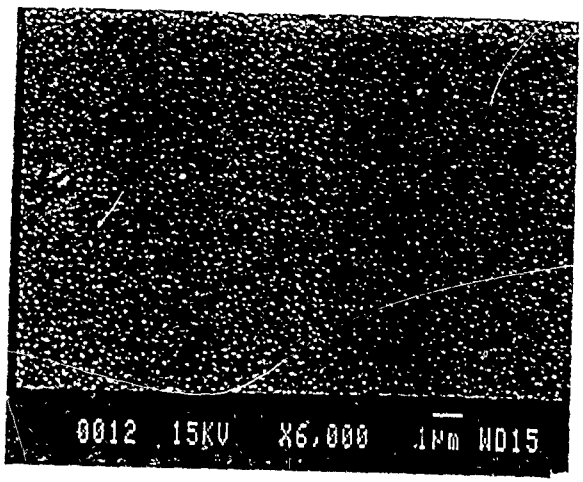

The present work has demonstrated the wet chemical methods can be used to provide coatings on ceramic fibers to modify their surface chemistry. a range of coating chemistries have been developed and found to yield dense, pore-free coating. The performance in composites of fibers with these coatings is presently being evaluated.

The wet chemical synthesis of transformation-toughening compositions in the alumina-zirconia and mullite-zirconia systems has also been demonstrated. Heat treatment at elevated temperatures led to the development of small precipitates of tetragonal ZrO_2 in ceramic matrices of alumina or mullite. Further work is on-going to evaluate the mechanical properties of the composites produced.

Also explored has been the role of chelating agents in the chemical synthesis of Al_2O_3-based ceramics. The selection of precursor and chelating agent was found to have a substantial effect in subsequent phase development, an effect with rather obvious technological consequences.

VI. SEEDED TRANSFORMATION OF ALUMINA GELS FROM DIFFERENT PRECURSORS

Seeding boehmite (γ-ALOOH) gels with tiny α-Al_2O_3 particles has been shown to have advantageous effects in terms of phase and microstructural development. Boehmite transforms to α-Al_2O_3 via the following steps:

$$boehmite \xrightarrow{\approx 450C} \gamma\text{-}Al_2O_3 \xrightarrow{\approx 850C} \delta\text{-}Al_2O_3 \xrightarrow{\approx 1000C} \theta\text{-}Al_2O_3 \xrightarrow{\approx 1200C} \alpha\text{-}Al_2O_3$$

The introduction of α-Al_2O_3 seed particles provides multiple nucleation sites for the θ-α Al_2O_3 transition. Boehmite seeded with ~1.5 wt% α-Al_2O_3 exhibits a reduction in the activation energy for α-Al_2O_3 formation by 71 KJ mol^{-1}, a lowering of the transformation temperature by as much as 170C, and the development of a submicron, aggregate-free microstructure which sinters to full density at 1200C.

The present study has been directed to exploring the effects of introducing α-Al_2O_3 seeds in the synthesis of gels from basic aluminum chlorides and chelated aluminum alkoxides.

The basic aluminum chloride, aluminum chlorohydrate, has the nominal formula, $Al_2(OH)_5Cl.2H_2O$. The high alumina content of this material coupled with its low cost (it is widely used as an ingredient in deodorants) render it highly attractive as a potential precursor for Al_2O_3-based materials; and it is presently used in the manufacture of ceramic fibers. Despite this attractiveness and commercial usage, aluminum chlorohydrate has been little studied in the literature concerned with chemical synthesis of ceramics.

As usually provided, aluminum chlorohydrate has a formal degree of hydrolysis (OH/Al ratio) of 2.5. The exact composition of highly hydrolyzed aqueous aluminum chloride solutions depends on factors such as aging. The principal species are polymeric, although smaller amounts of monomers and dimers also exist. The polymeric components have been identified as $[AlO_4Al_{12}(OH)_{24}(OH_2)_{12}]^{7+}$ (designated Al_{13}^{7+}), and higher molecular weight polymers, either structurally related to Al_{13}^{7+} or with a layer structure, similar to that of gibbsite, γ-$Al(OH)_3$.

In the present work, Al_2O_3 gels were prepared using both aluminum chlorohydrate and a chelated aluminum alkoxide, $Al(O^iPr)_2C_6H_9O_3$. In both cases, the solutions were seeded with small (0.15 μm) particles of α-Al_2O_3. The level of seeding corresponded to 5 mole % α-Al_2O_3/mole Al_2O_3 derived from the chlorohydrate or alkoxide. In the alkoxide route, gels were prepared from hydrolyzed iso-propanol solutions of the $Al(O^iPr)_2C_6H_9O_3$; while in the chlorohydrate route, aqueous solutions of the chlorohydrate were employed. After the seed particles were added to the respective solutions, sonication was applied to aid in the dispersion of the particles. Sonication was continued until gels were formed. After gelation, the respective samples were dried at 60C for 24 hrs.; and samples of the gels were fired at temperatures of 500, 700 and 900C for 2, 4 and 8 hour soak periods, using a heating/cooling rate of $5C^{-1}$ min. in all cases.

The efficacy of α-Al_2O_3 seeding was determined by a quantitative x-ray diffraction technique using quartz as an internal standard. The weight fraction of α-Al_2O_3 in the fired gels was determined by comparing the relative integrated intensities of the (102) reflection of α-Al_2O_3 and the (110) reflection of quartz to an α-Al_2O_3 - quartz calibration curve. Fracture surfaces of samples were investigated by scanning electron microscopy.

Unseeded gels derived from aluminum chlorohydrate showed a similar phase development as boehmite on firing. With two hour soak periods, transitional Al_2O_3 phases were detected between 500 and 1000C, and α-Al_2O_3 began to crystallize at approximately 1000C. On firing to 1100C, α-Al_2O_3 was the only phase detected.

Seeding had a dramatic effect on the transformation to α-Al_2O_3 in these gels. The weight fractions of α-Al_2O_3 in both seeded and unseeded fired gels are given in Table 10. On firing to 500C for 2 hours, 23.8 wgt. pct. α-Al_2O_3 (after subtracting the seed percentage) had been formed in the seeded gel. By comparison, only 17.5 wgt. pct. α-Al_2O_3 was formed in the unseeded gel on firing at the much higher temperature of 900C for the much longer time of eight hours. with the seeded gels, it can be seen that the fraction crystallized increases both with increasing temperature and with increasing time at temperature.

As indicated above, the seeding level investigated in these experiments is equivalent to 5 mole pct. α-Al_2O_3/mole Al_2O_3 derived from the aluminum chlorohydrate. This equates to approximately $3x10^{13}$ seed particles/cm^3 of θ-

Table 10 - Conversion to α-Al_2O_3 on Firing Gels Derived from Aluminum Chlorohydrate

Temperature (C)	Time (Hours)	Weight % α-Al_2O_3 in Gel	
		Unseeded	Seeded
500	2	-	23.8
	4	-	30.4
	8	-	43.4
700	2	-	35.3
	4	-	44.6
	8	-	63.0
900	2	-	60.9
	4	-	71.0
	8	17.5	88.3

Al_2O_3 derived from the aluminum chlorohydrate. As can be seen in Figure 18, which shows the fracture surface of a seeded, dried gel, the α-Al_2O_3 seed particles are well dispersed throughout the amorphous gel network, although in some instances agglomeration of the seeds had occurred. The rapid crystallization of α-Al_2O_3 on firing was accompanied by remarkable growth of the seed particles as indicated by SEM observations.

Micrographs of fracture surfaces of seeded gels fired at 500 and 700C for 4 hours are shown in Figures 19 and 20. As seen in Figure 19, the average diameter of the particles has grown to approximately 0.3 μm, indicating the occurrence of significant growth. Figure 21 shows the fracture surface of an unseeded gel fired at 700C for 4 hours. No α-Al_2O_3 crystals are seen. A comparison of Figures 20 and 21 illustrates clearly the dramatic effect of seeding on microstructural development.

For gels derived from the chelated aluminum alkoxide, seeding was also found to have a considerable on phase development - albeit perhaps not so dramatic as for gels derived from aluminum chlorohydrate. The results obtained on firing the alkoxide-derived gels are summarized in Table 11. As seen there, seeded gels develop about 30% α-Al_2O_3 in 4 hrs. at 700C, whereas unseeded 2-3 hours at the much higher temperature to develop the same α-Al_2O_3 content.

Seeding also had a dramatic effect on the microstructure of the fired gels. A representative comparison is shown in Figure 22, which shows the microstructures of seeded and unseeded gels which were fired at 1100C for 8 hours. The unseeded gel is seen to have a large grain size (~5 μm), whereas the structure in the seeded case is very fine-grained.

Based on these results, it is clear that seeding alumina gels with tiny α-Al_2O_3 particles has a dramatic effect on the conversion of the matrix to the desired α-Al_2O_3, whether the gels are derived from aluminum chlorohydrate or from a chelated aluminum alkoxide. The effect on microstructure is likewise dramatic, and undoubtedly reflects eptaxial transformation on the seed crystals. Further characterization using TEM is currently underway to gain insight into the seeding mechanism.

It will be interesting to extend these studies to more complicated systems such as lead zirconate titanate (PZT). In this case, seeding with the perovskite

Figure 18. Fracture Surface of Seeded, Dried Gel Synthesized from Aluminum Chlorohydrate. Light Areas are Seed Particles.

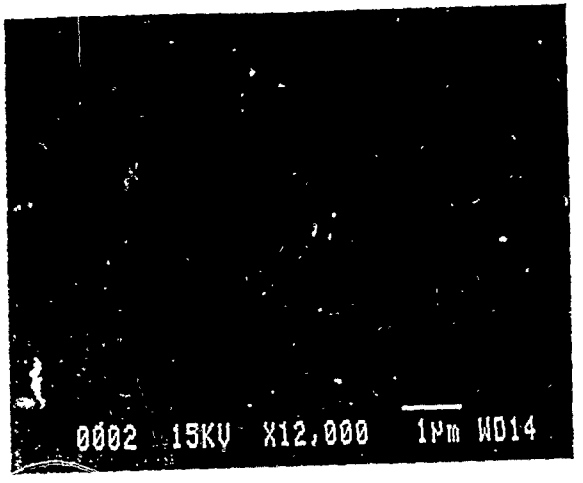

Figure 19. Fracture Surface of Seeded Gel, Synthesized from Aluminum Chlorohydrate and Fired at 500C for 4 Hrs. (x12000)

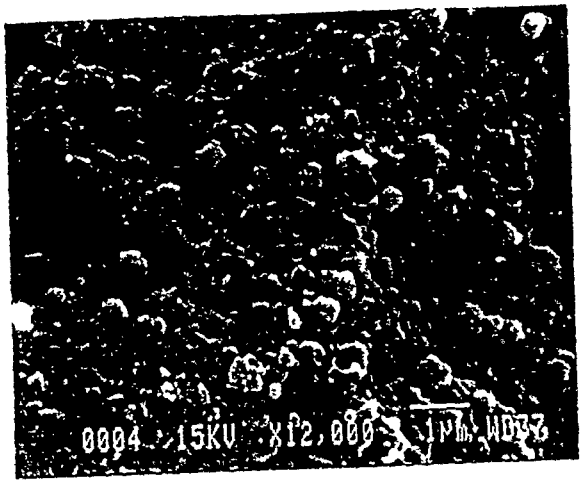

Figure 20 Fracture Surface of Seeded Gel, Synthesized from Aluminum Chlorohydrate and Fired at 700C for 4 Hrs. (x12000)

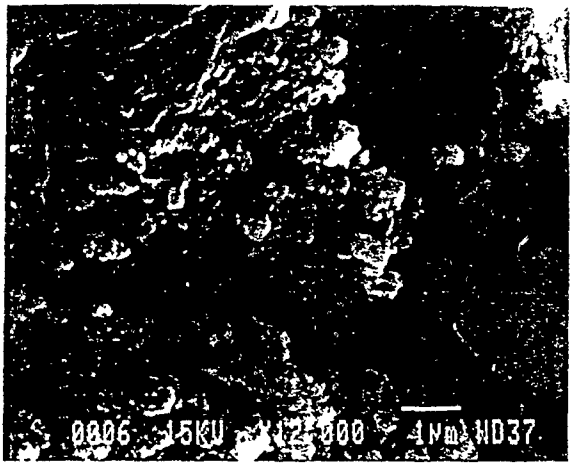

Figure 21. Fracture Surface of Unseeded Gel, Synthesized from Aluminum Chlorohydrate and Fired at 700C for 4 Hrs. (x12000)

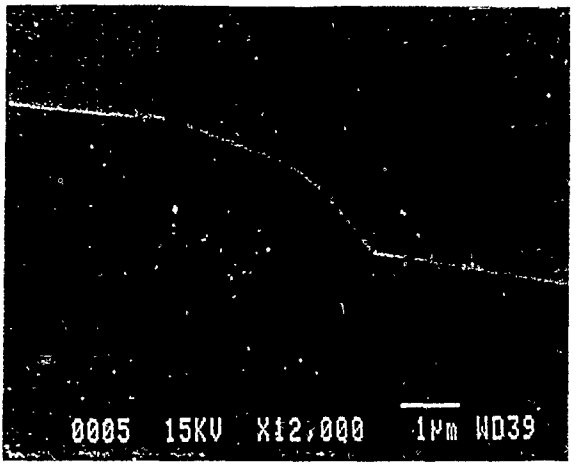

Table 11 - Conversion to α-Al_2O_3 on Firing Gels Derived from Chelated Aluminum Alkoxide

Temperature (C)	Time (Hours)	Weight α-Al_2O_3 in Gel	
		Unseeded	Seeded
500	2	0	5
	4	0	5
	8	0	10-15
700	2	0	20-25
	4	0	30-35
	8	0	40-45
900	2	0	70-75
	4	0	80-85
	8	0	90-95
1000	2	20-25	95-100
	4	50-55	95-100
	8	80-85	95-100
1100	2	95-100	95-100
	4	95-100	95-100
	8	95-100	95-100

Figure 22. Effect of Seeding on Gels Derived from Chelated Aluminum Alkoxide and Fired at 1100C for 8 Hours

Unseeded

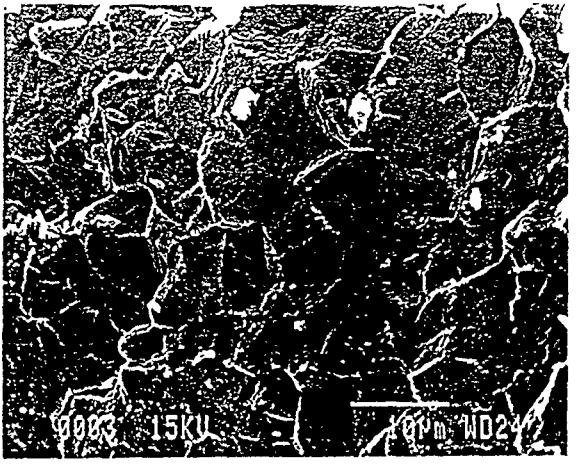

Seeded

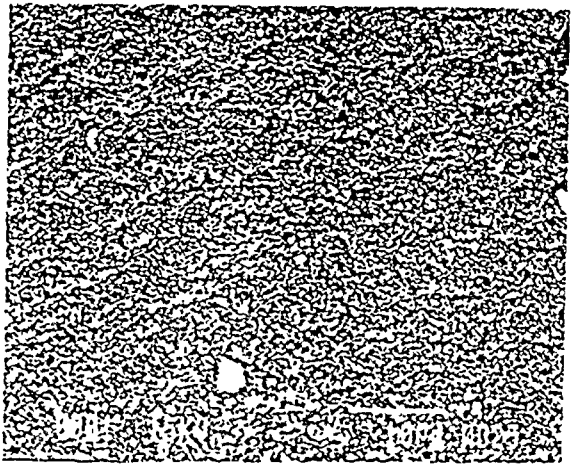

phase may well eliminate the formation of pyrochlore which has been a continuing problem with the wet chemical synthesis of PZT.

VII. FERROELECTRIC POWDERS, FILMS AND FIBERS

Ferroelectrics (FE's) are important electroceramic materials. Notable examples include lead zirconate titanate (PZT), lead lanthanum zirconate titanate (PLZT), barium titanate, lead magnesium niobate, strontium barium niobate and potassium niobate. PZT is used in a variety of applications, including tranducers, capacitors, waveguides, phase conjugators, composites and optical switches. An area of application for PZT thin fiims which has gained considerable attention is that of non-volatile memory devices or ferroelectric memory.

Conventionally, PZT is prepared by the solid state reaction of the constituent oxides at temperatures greater than 800C. Generally a variety of intermediate phases are formed prior to the ferroelectric perovskite, their exact nature and composition being dependent on the processing conditions.

Due to the inherently high level of chemical homogeneity of sol-gel derived materials, single phase PZT forms at much lower temperatures (around 550C) in chemically-derived systems. In this case, the reaction often proceeds via a metastable pyrochlore phase. This phase is paraelectric; and hence full conversion to perovskite via an optimized firing schedule is necessary to obtain desired properties.

Apart from ferroelectric memory applications, PZT thin films have potential as high dielectric constant dielectric materials. Ever-increasingly high density DRAMs necessitate miniaturization of microcircuitries to submicron levels, and hence there is an urgent need for high dielectric constant dielectric films to replace SiO_2 whose relative dielectric constant, E_r, is 3.8. By judicious choice of compositions (such as PZT- PLZT) or by incorporation of specific dopants, it is possible to design a paraelectric lead titanate system with linear dielectric characterisitics unlike that of typical ferroelectric compositions.

PZT films have been prepared by numerous methods, including evaporation, sputtering, laser ablation, CVD and MOCVD. It is expected, but not yet demonstrated in any detail, that the different deposition processes yield ferroelectric FE films with different microstructures and properties. With most of the methods, precise control of stoichiometry is difficult to achieve, and high temperature treatment is required to obtain good ferroelectric properties. Such thermal treatment restricts the choice of substrates and can damage the

underlying layer profiles of semiconductor devices. Most of the methods are also inherently expensive in terms of capital equipment. The deposition rate is usually quite slow, varying from 1 - 100 Å/min. Lattice damage due to the energetic bombardment of mobile species must also be considered. Desputtering of the deposited films has been reported, leading to depleted Pb especially near the plasma field edges. Thus inhomogeneity in the chemical profile across a large area is not uncommon. Incorporating excess Pb to compensate for Pb loss is at best an iterative, time-consuming approach.

Wet chemical methods offer clear and distinct advantages in the preparation of ferroelectric films of high purity and chemical homogeneity; and the attractiveness of these advantages - as well as the general lack of understanding of the chemical process variables and their effects on the microstructures and properties of the resulting films - provided important motivation for the present work.

The most widely used wet chemical method involves the formation of complex alkoxide-acetate species from Pb acetate and Zr and Ti alkoxides in 2-methoxyethanol. The highly toxic nature of the solvent (which is teratogenic, and causes neurological and hematological effects at the ppm levels) would seem, however, to limit its widespread use. An all-alkoxide route has also recently been reported. This route offers the potential of improved chemical homogeneity; but the synthesis of Pb alkoxides by normal routes invariably introduces a high level of Na^+ contamination, which is detrimental in microelectronic devices. Metallorganic decomposition (MOD) routes have also been studied using ethylhexanoate or neodecanoate precursors. Such routes are unattractive due to the low solids contents of the films, which tend to cause cracking and large shrinkages during pyrolysis.

Members of the present PI team have recently reported a detailed comparison of the various methods used to prepare PZT films [1]. Table 12 summarizes the electrical properties of PZT films prepared by vapor deposition methods; and Table 13 presents a comparable summary for wet chemically derived PZT films.

The preferred synthetic route of our team has utilized alkanolamine modification of Zr and Ti alkoxides to control the hydrolysis and subsequent condensation reactions of the alkoxides in a methanolic solution of Pb acetate. This route offers advantages in ease of processing and provides the ability to obtain films with exceptional microstructures and ferroelectric properties.

Table 12 - Ferroelectric Properties of PZT Films
Prepared by Various Techniques

Method	Dielectric Constant Er	Dissipation Factor Tan δ	Remanent Polarization P_r ($\mu c/cm^2$)	Coercive Field E_c (kV/cm)	Composition (Zr/Ti)	Ref.
Ion-Beam Sputtering			8		70/30	2
Pulsed Laser	658		12 (P_s)*		42/82	3
Laser Ablation	600		36		53/47	4
rf Sputtering	300-500	0.02-0.2	12.5	90	65/35	5
dc Magnetron Sputtering	194	0.26	12	40	54/48	6

*P_s Spontaneous Polarization

Table 13 - Ferroelectric Properties of Sol-Gel Derived PZT Films

Sol-Gel Methods on Various Substrates	Dielectric Constant, Er	Dissipation Factor Tan δ	Remanent Polarization P_s ($\mu c/cm^2$)	Coercive Field E_c (kV/cm)	Composition (Zr/Ti)	Ref.
Pt			36	40	53/47	7
ITO	260	0.1-0.7	6.6	26.7	40/60	8
Pt	1800	0.02	5	8	65/35+8 atom% La	9
Si			2.2	7.5	50/50	10
Pt	1200	0.01-0.02			50/50	11
Pt	1000	0.01-0.02			44/56	11
Pt (Amorphous PZT)	35-50	0.005-0.001				11
Pt	500	0.024	10	37	53/47+2 at % NB	12
Pt	300	0.03	21.8	81.6		13
Stainless Steel	400	0.4			50/50	14
Pt	500	0.06	12	60	50/50	15
Pt			15	25	50/50	16
Pt			12.5	57	50/50	17
n-Si			32	16	0.15% Nb 50/50	18
Pt	214	0.15			53/47	19
Pt	700	0.07			45/55	20
Pt	300-1200		32.5	30	53/47	21
Pt		27	34		53/47	22
Pt	**2000**	**0.1**	**18.3**	**37.5**	**53/47**	**UofA/AML**
Pt	505	--	12.0	100.0	50/50	23
Bulk Ceramics	625		33	6.5	50/50	10
Bulk Ceramics	750	0.004	45	17	53/47	24

A. Synthesis and Fabrication Procedures

In the present work, the reactivities of Zr and Ti alkoxides have been modified by reaction principally with ethanolamines: monoethanolamine (MEA), $H_2NC_2H_4OH$; diethanolamine (DEA), $HN(C_2H_4OH)_2$; and triethanolamine (TEA), $N(C_2H_4OH)_3$. Various other alkoxide-modifiers such as alkyl-substituted alkanolamines (e.g., dimethylethanolamine) and 2,4-pentanedione have also been investigated.

Such modification of the alkoxides produces species which are less reactive towards hydrolysis and condensation than their unmodified counterparts. This has many advantages for processing, including long shelf life, ease of handling and increased homogeneity of the final gel network.

The various wet chemical routes used in the present work are summarized in the flow chart of Figure 23. As indicated there, these routes have been used to prepare powders, pellets, films and fibers.

B. Synthesis and Characterization of PZT Gels

i) Synthesis and Experimental Procedure

As shown in Table 14 various alkoxide modifying agents have been investigated in preparing PZT gels. Major emphasis was placed on the MEA, DEA and TEA modifying agents.

To prepare PZT gels Pb acetate trihydrate ($Pb(OAc)_2 \cdot 3H_2O$) is dissolved in methanol (distilled over 5Å molecular sieve). Separately, freshly distilled Ti iso-propoxide is reacted with the modifying reagent (1 mole of alkoxide - 1 mole of modifying agent) at room temperature, resulting in an exothermic reaction and the formation of a yellow viscous liquid. Similarly, a solution of Zr n-propoxide in n-propanol is treated with the same procedure. The modified alkoxides are then added to the methanolic Pb acetate solution with vigorous stirring in appropriate quantities to give the desired stoichiometry of PZT, such as 53/47 ($Pb_1Zr_{.53}Ti_{.47}O_3$). The solutions are then stirred at room temperature overnight and cast into molds.

Among the chemical parameters which have been systematically varied in this work are the amount of water of hydrolysis (apart from the contribution due to the hydrated lead salt, $Pb(OAc)_2 \cdot 3H_2O$) and the amount of excess Pb

Figure 23. Schematic Representation of Synthetic Routes to PZT Gels, Powders, Pellets, Films and Fibers

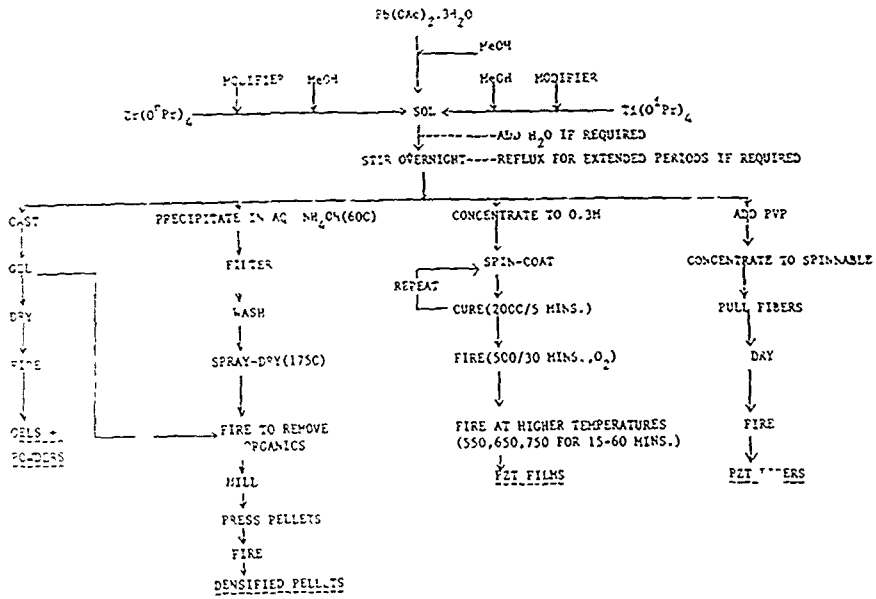

Table 14 - List of Modifiers Studied

Chemical Nature	Acronym Used
monoethanolamine	MEA
diethanolamine	DEA
triethanolamine	TEA
diethylethanolamine	DEEA
1-dimethylamino-2-propanol	DMAP
2-ethylaminoethanol	EAE
dimethylethanolamine	DMEA
2-methylaminoethanol	MAE
amino-2-propanol	AP
2,4-pentanedione	AcAc
ethylacetoacetate	EtAcAc

incorporated (to give $Pb_{1+x}Zr_{.53}Ti_{.47}O_3$ where x is the mole % excess Pb) in the gel network.

All the modified precursor solutions remained clear upon mixing. In the case of the unmodified alkoxides, the mixed solution stayed clear with the addition of the Ti iso-propoxide; but introduction of the Zr n-propoxide led to copious white precipitates (which were analyzed as Zr acetate from FTIR and EDAX). Interestingly, these precipitates were observed to re-dissolve upon vigorous stirring. The solutions were stirred overnight and then cast into PTFE molds and then partially covered with aluminum foil and allowed to gel. The unmodified precursor solution gelled overnight. The use of modifying agents significantly affected the gelation time, for example in the case of DEA the solution took about a week to gel.

After drying, the unmodified gel was opaque and quite brittle; the MEA-modified gel was translucent, and was less brittle than the unmodified gel; the DEA-modified gel was clear (transparent) and slightly rubbery; and the TEA-modified material remained a highly viscous liquid even after several weeks.

In some instances, the effects of refluxing the solution prior to gelation were also investigated. It was found that unmodified solutions turned cloudy on refluxing, whereas the DEA and TEA containing solutions remained clear.

ii) TGA and DTA Results

Unmodified gels and gels modified with 1-1 molar ratios of modifier to alkoxide of MEA, DEA, TEA, DMAP, DMEA, EAE, DEEA, MAE, AP (see Table 14 above for chemical identification of modifiers) were investigated by thermogravimetric analysis using a Perkin Elmer TGA-7 after drying at 50C overnight under vacuum. The results are tabulated in Table 15.

As seen in the Table, with the exception of the DEA and TEA cases, the gels were all essentially burned out at 630C. Gels containing DEA and TEA burned out at 480C and 520C respectively. The effects of varying amounts of DEA were also studied. Using a 1-0.5 molar ratio of alkoxide to DEA (rather than the 1-1 ratio shown in the Table), increased the burn-out temperature to 600C, establishing an effect of modifier concentration on burn-out (see Table 16). When a 1-2 molar ratio of alkoxide to DEA was used, the burn-out temperature increased to 520C, identical to that of a 1-1 molar ratio TEA-modified gel. One may speculate that there exists an optimum amount of

Table 15 - TGA Data on Various Gels Heated at $^{1}0C^{-1}$Min.

Modifier Used (1-1 Molar Ratio of Modifier to Alkoxide)	Final Decomposition Temperature (C)
MEA	630
DEA	480
TEA	520
unmodified	630
DMAP	630
DMEA	630
EAE	630
DEEA	630
MAE	630
AP	630

Table 16 - Effect of Alkoxide to DEA Molar Ratio on Decomposition Temperature

Molar Ratio of Alkoxide to DEA	Final Decomposition Temperature (C)
1-0.5	600
1-1	480
1-2	520

alkanolamine which helps in burning out organics within the gel network. In assessing these results, it should be noted that the number of active bonds responsible for modification in the 1-1 TEA- and 1-2 DEA-modified materials are almost equal, 3 and 4 respectively for each metal alkoxide; and this results in the same burn-out temperature. It can be further argued that the strength of such bonds in the modified alkoxides is important, e.g., "weak" modifiers such as EAE and MAE have no influence at all on the final burn-out temperature.

Differential thermal analysis (DTA) was carried out using a Perkin Elmer thermal Analysis System 7/4 at a heating rate of 10C min^{-1} in an oxygen atmosphere. Samples studied include various modified PZT (53/47) gels (having a molar ratio of alkoxide to modifier of 1-1), the unmodified gel, and Pb acetate trihydrate. Typical scans are shown in Figure 24. The results, in the form of locations of exothermic peaks in the DTA scans, are summarized in Table 17. As with the TGA results, the data on the unmodified gel is closely similar to those on many of the modified gels, e.g., those modified with MEA, EAE and EtAcAc. In contrast, while the first peaks of the DEA- and TEA-modified gels occur at similar temperatures to those of the unmodified gel, the larger second peaks are shifted to notably higher temperatures (to 460C and 430C, respectively).

The temperatures of the DTA peaks correspond to those of the differential TGA peaks, where the maximum rate of weight loss occurs. Hence the DTA peaks are associated with organic decomposition, rather than with crystallization. Any crystallization peaks (whether amorphous → pyrochlore or amorphous → perovskite) are overshadowed by these exothermic peaks. The effects of modifier concentration on the temperatures of the exothermic peaks are presented in Table 18 for DEA-modified PZT gels. As seen there, increasing concentrations of DEA lead to increasing temperature of the high temperature exotherm - and for the highest concentration of DEA, to a lowering of the temperature of the low temperature exotherm.

iii) FTIR Characterization of Gels

To help elucidate the structures of the fired gels, Diffuse Reflectance Fourier Transform Infra-Red (FTIR) spectra of the fired gels were obtained on a Galaxy FTIR Spectrometer. PZT (53/47) gels, both unmodified and modified (1-1) with MEA, DEA and TEA, were fired at 350, 450, 550 and

Figure 24. Representative DTA Scans on PZT (53/47) Gels, Obtained at a Heating Rate of 10C Min.$^{-1}$

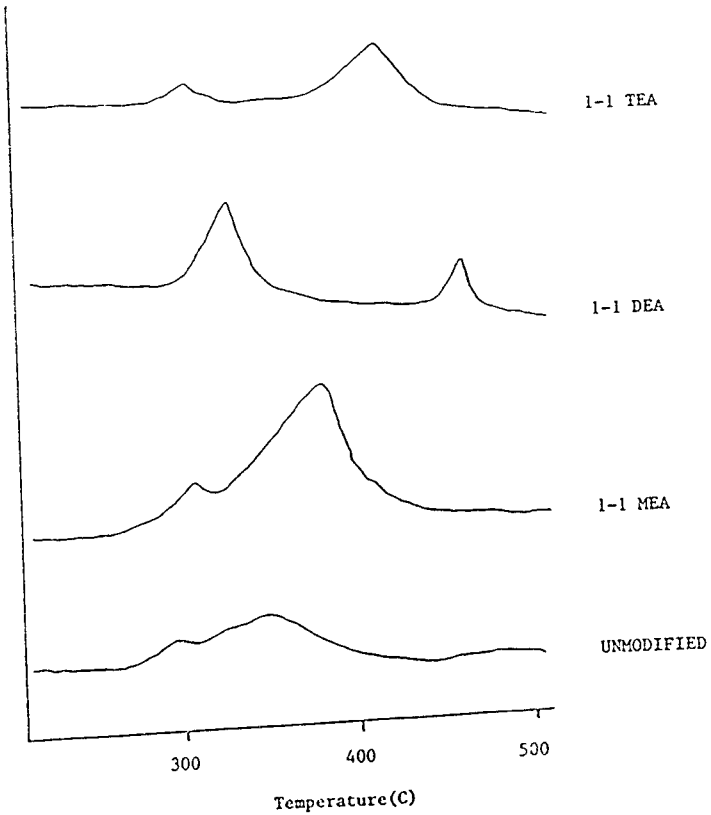

Table 17 - Locations of DTA Exothermic Peaks for Unmodified & Modified PZT (53/47) Gels, Heating Rate 10C min^{-1}

Additive	Temperatures (C) of DTA Exothermic Peaks	
MEA	310	390
DEA	330	460
TEA	310	430
AcAc	285	390
EtAcAc	310	355
DEEA	310	345
EAE	310	360
DMEA	320	380
MAE	315	360
Unmodified	300	360
$Pb(OAc)_2 \cdot 3H_2O$	320	390

Table 18 - Effects of DEA Concentration on DTA Exothermic Peaks of PZT (53/47) Gels, Heating Rate 10C min^{-1}

Molar Ratio of Alkoxide to DEA	Temperatures (C) of DTA Exothermic Peaks	
1-0.5	330	430
1-1	330	460
1-2	280	480

650C for 30 mins. The resulting spectra are shown in Figures 25 - 28. A comparison of the spectra for gels heated at 650C is shown in Fig. 29.

After firing at this temperature (650C) the DEA- and TEA-modified gels had much lower hydroxyl contents compared to unmodified and MEA-modified gels as evident by the lack of absorption at ~3500 cm^{-1} in the former cases. In addition, no absorption attributable to organic species are present in the DEA- and TEA- derived gels indicating the ease of organic burn-out when these modifiers are used in sol-gel systems.

iv) Phase Development of Gels

To investigate phase development during heat treatment, X-ray diffraction (XRD) patterns were obtained for unmodified PZT (53/47) gels, as well as for gels modified with MEA, DEA and TEA. In all cases, the modifications were effected at a molar ratio of alkoxide to modifier of 1-1, and the diffraction patterns were taken after heat treatment for 30 mins. at temperatures of 300, 400, 450, 550 and 650C. The diffraction data were obtained using a GE diffractometer at a scan rate of 4^{o} min^{-1}.

The results are shown in Figures 30-33. In considering these results, it should be recalled that the major X-ray diffraction peaks for perovskite PZT occur at $2\theta = 22^{o}$ and 31^{o} for CuKα radiation; while those for pyrochlore occur at $2\theta = 28^{o}$ and 34^{o}.

In all cases, single phase perovskites were found at firing temperature of 650C. For the MEA-modified, TEA-modified and unmodified gels, the following phase development was observed as a function of increasing heat treatment temperature: amorphous → pyrochlore → pyrochlore + perovskite → perovskite. In contrast, for the DEA-modified gels, the transformation sequence was: amorphous → pyrochlore + perovskite → perovskite. Both the MEA-modified and unmodified gels showed closely similar phase development with temperature, whereas the DEA-modified and TEA-modified gels showed easier conversion to perovskite.

Figure 34 compares the XRD patterns of various gels heated at 500C for 30 mins. As can be seen, only the DEA-modified gel gave single-phase perovskite PZT at this low temperature, demonstrating the significant advantage of this additive in promoting perovskite formation. That is, the

Figure 25- Diffuse Reflectance Fourier Transform Infra-Red Spectra of PZT (53/47) Gels [1 Mole MEA - 1 Mole Alkoxide] Heated at the Indicated Temperatures for 30 Minutes

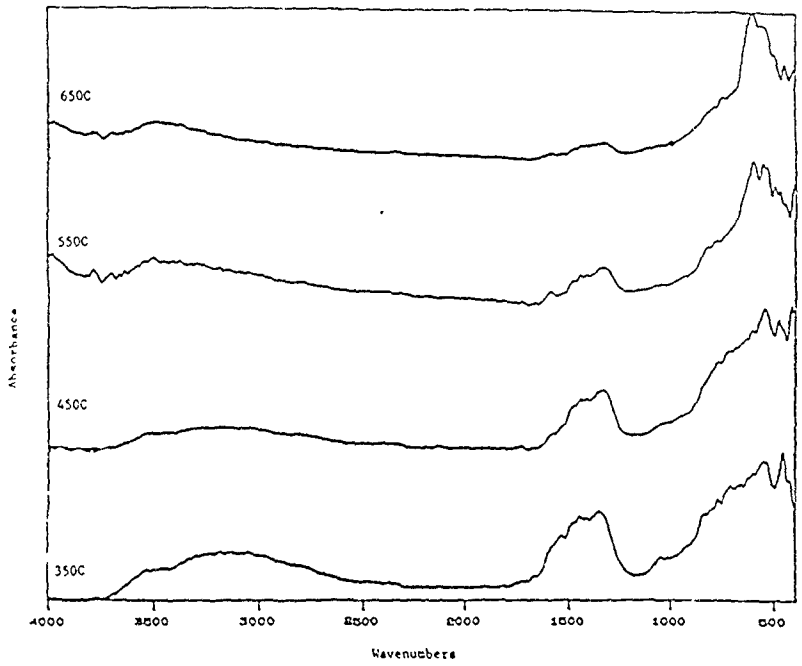

Figure 26 - Diffuse Reflectance Fourier Transform Infra-Red Spectra of PZT (53/47) Gels [1 Mole DEA - 1 Mole Alkoxide] Heated at the Indicated Temperatures for 30 Minutes

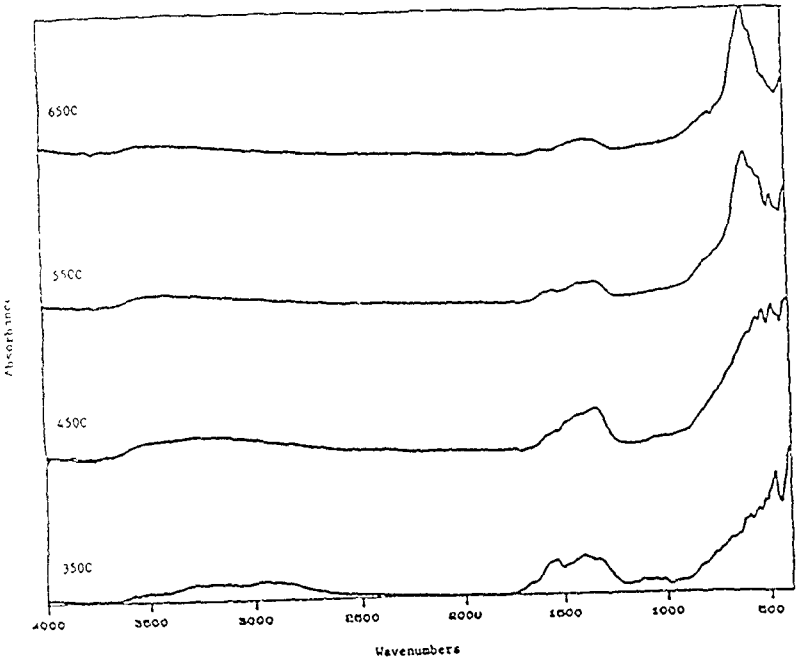

Figure 27 - Diffuse Reflectance Fourier Transform Infra-Red Spectra of PZT (53/47) Gels [1 Mole TEA - 1 Mole Alkoxide] Heated at the Indicated Temperatures for 30 Minutes

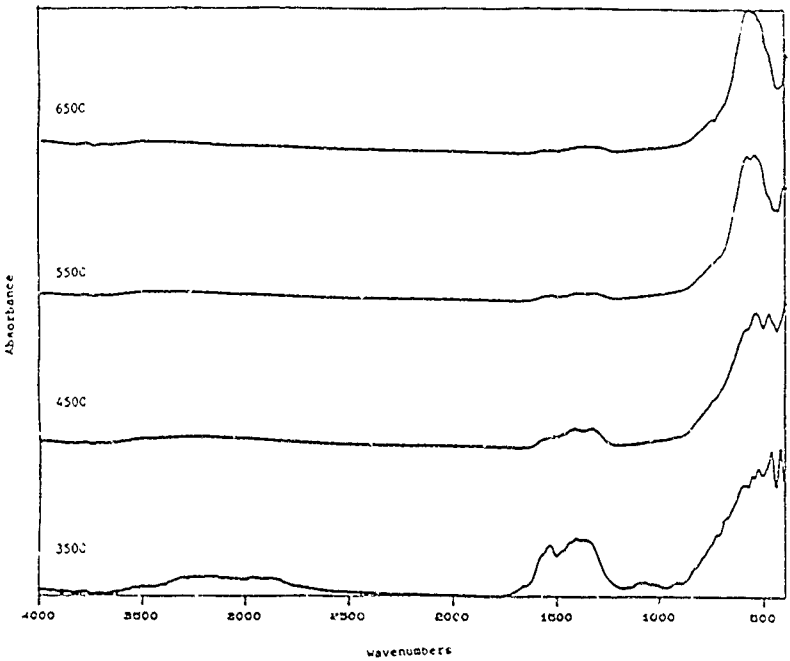

Figure 28 - Diffuse Reflectance Fourier Transform Infra-Red Spectra of PZT (53/47) Gels [Unmodified] Heated at the Indicated Temperatures for 30 Minutes

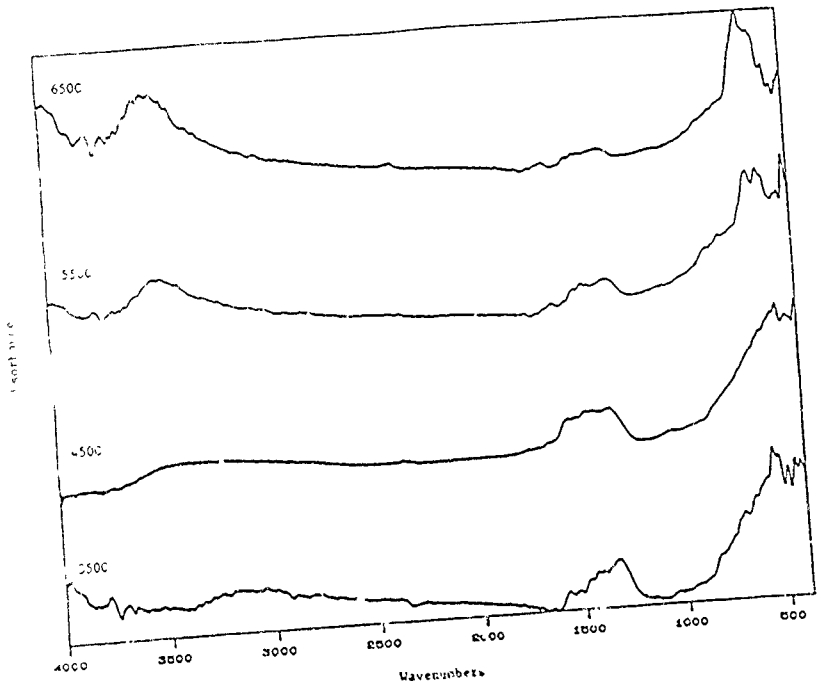

Figure 29 - A Comparison of the Diffuse Reflectance Fourier Transform Infra-Red Spectra of PZT (53/47) Gels Heated at 650C for 30 Minutes

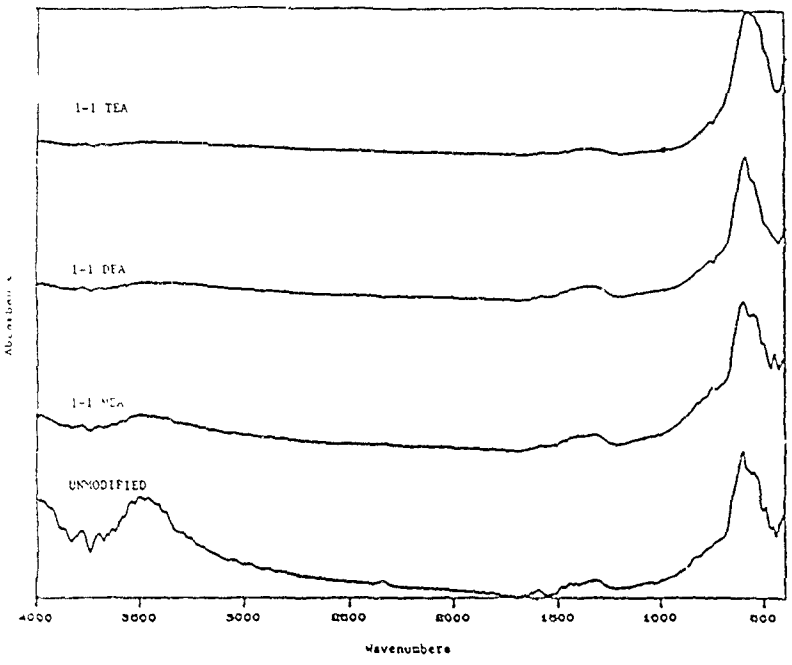

Figure 30 - X-Ray Diffraction Patterns of PZT (53/47) Gels [1 Mole MEA - 1 Mole Alkoxide] Heated at the Indicated Temperatures for 30 Minutes [6 Moles H_2O -1 Mole Pb]

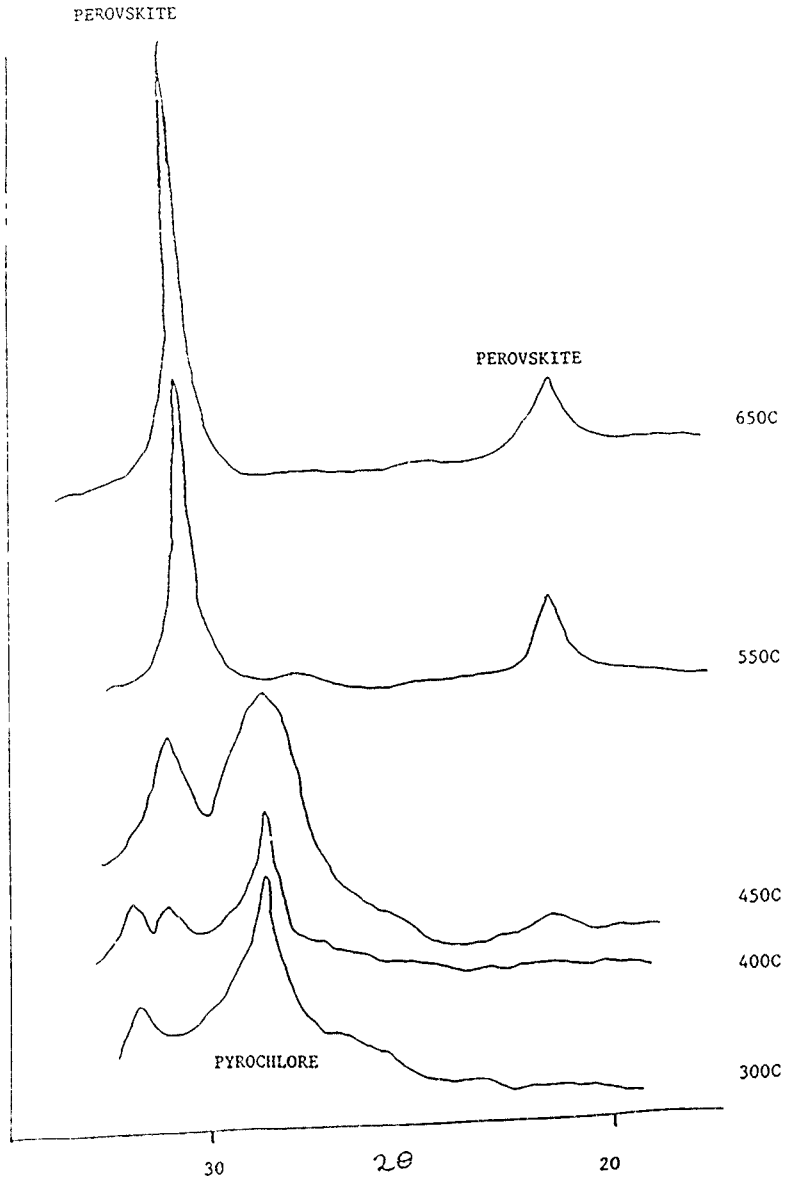

Figure 31 - X-Ray Diffraction Patterns of PZT (53/47) Gels [1 Mole DEA - 1 Mole Alkoxide] Heated at the Indicated Temperatures for 30 Minutes [6 Moles H_2O -1 Mole Pb]

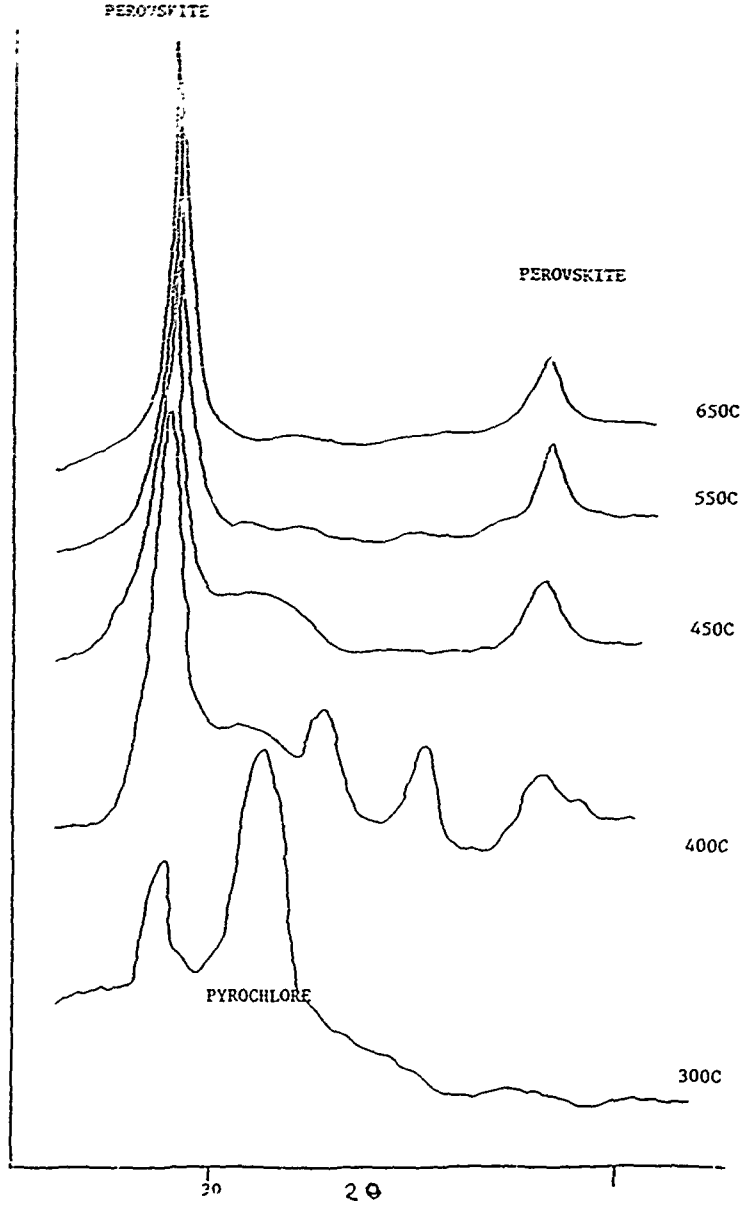

Figure 32 - X-Ray Diffraction Patterns of PZT (53/47) Gels [1 Mole TEA - 1 Mole Alkoxide] Heated at the Indicated Temperatures for 30 Minutes [6 Moles H_2O -1 Mole Pb]

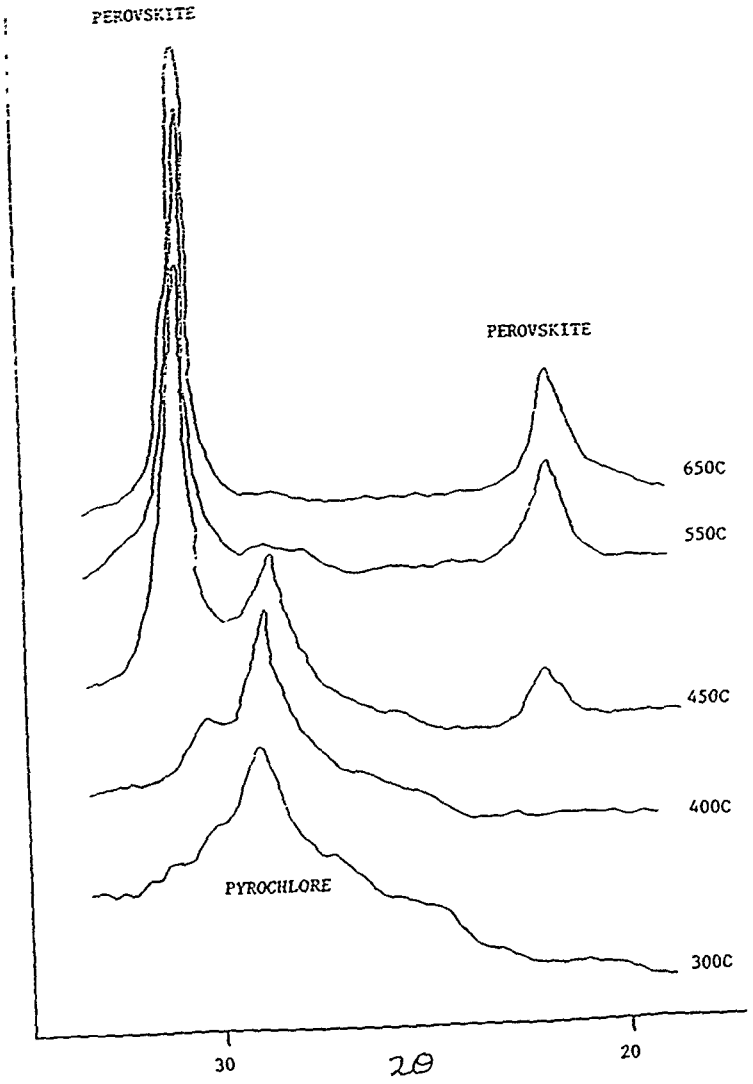

Figure 33 - X-Ray Diffraction Patterns of PZT (53/47) Gels [Unmodified] Heated at the Indicated Temperatures for 30 Minutes [6 Moles H_2O -1 Mole Pb]

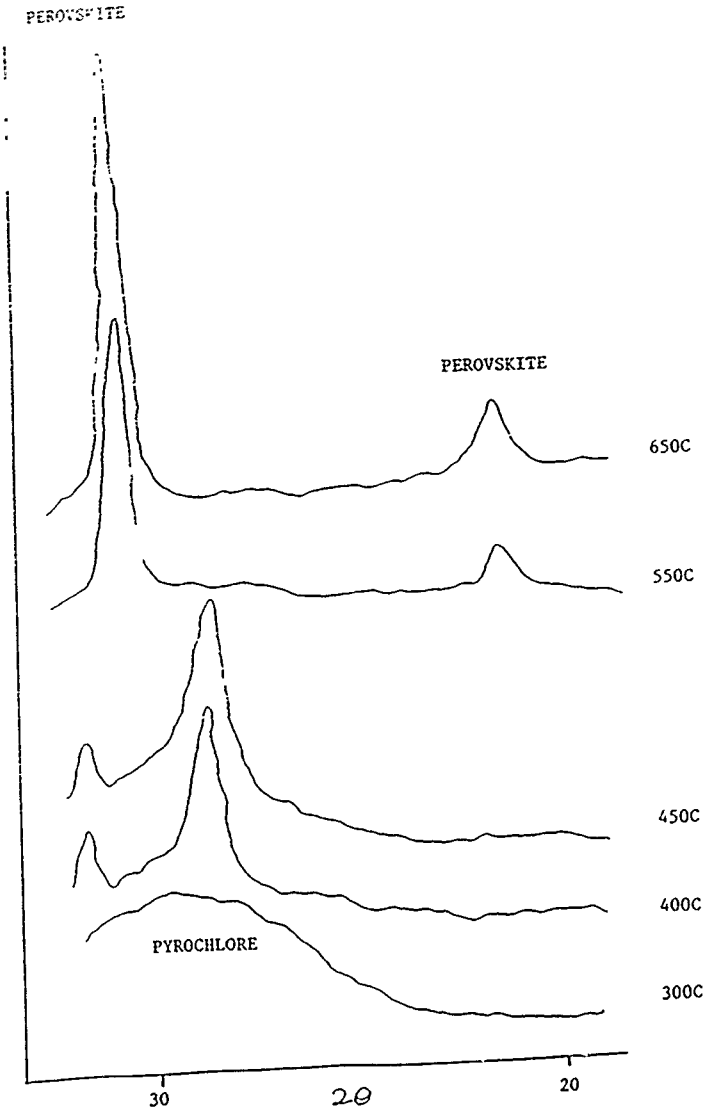

Figure 34 - A Comparison of the X-Ray Diffraction Patterns of PZT (53/47) Gels Heated at the Indicated Temperatures for 30 Minutes [6 Moles H_2O-1 Mole Pb]

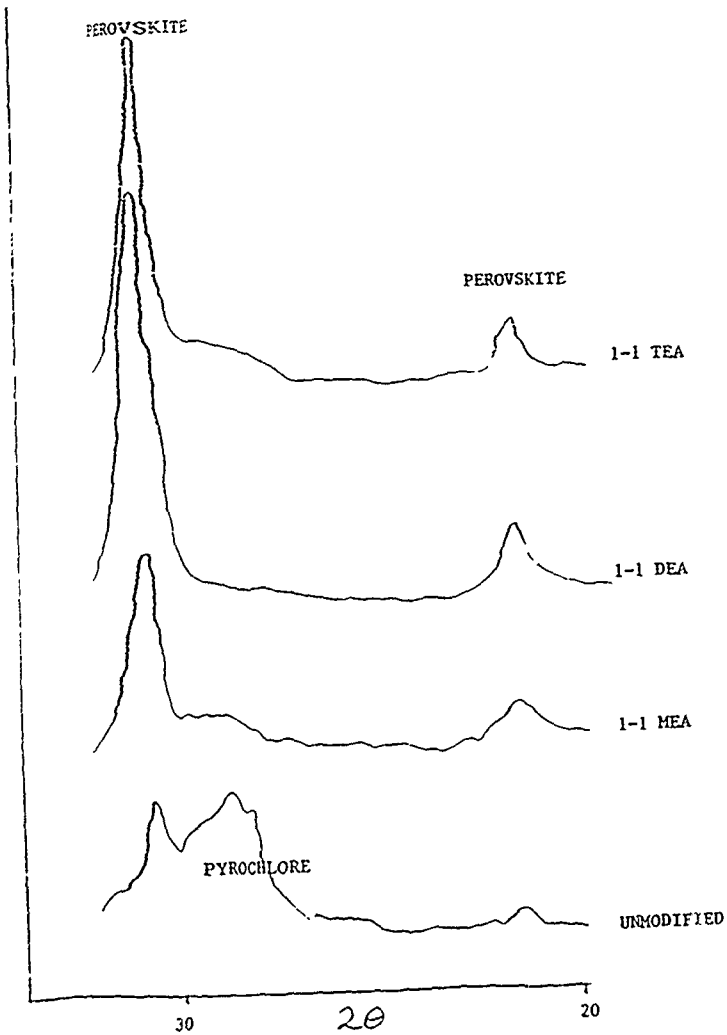

DEA-modified gels can convert completely to the desired perovskite PZT phase at temperatures as low as 500C. This is a remarkable finding.

The effects of the concentration of hydrolysis water on phase development are illustrated by the XRD data on 1-1 DEA-modified gels shown in Figures 35 and 36. Comparing the data shown in Figure 35 (on fired gels prepared with 3 moles H_2O/mole Pb) with those in Figure 31 above (on fired DEA-modified gels prepared with 6 moles H_2O/mole Pb) and those in Figure 36 (for fired gels prepared with 9 moles H_2O/mole Pb), it is seen that increasing amounts of H_2O promote the formation of the perovskite phase at lower temperatures - i.e., the relative heights of the pyrochlore and perovskite phases decrease with increasing water content used in the initial synthesis. At higher temperatures (>450C), however, similar perovskite contents are obtained regardless of the H_2O content used in the synthesis.

To explore the effects of DEA concentration on phase development, PZT (53/47) gels were modified with different ratios of alkoxide to DEA. XRD patterns obtained after heat treating for 30 mins. at various temperatures are shown in Figure 37 for 1-0.5 modified. Comparing these results with those shown in Figure 31 above for a 1-1 DEA-modified gel, it is seen that the lower concentration of DEA gives less perovskite at heat treatment temperatures of 450C and below. At both DEA concentrations, only perovskite is present after heat treatment at 550C. From these results, it is concluded that a 1-1 modification ratio is preferred for obtaining perovskite at low temperatures.

Pb-based ceramics can suffer from Pb loss at elevated temperatures. A classical method to overcome this problem is to incorporate excess Pb into the system. However Pb loss may not be significant from sol-gel derived systems due to the relatively low firing temperatures involved. In spite of this, we have explored the effects of excess Pb on phase development. Various lead concentrations (resulting in superstoichiometric PZT) were incorporated in gels modified 1-1 with DEA. XRD data on samples prepared with 10 mole% excess Pb and fired for 30 mins. at various temperatures are shown in Figure 38. Even for samples heated to 650C, a persistent pyrochlore phase whose peak is located about $2\theta = 29^{\circ}$is observed. Comparing these results with those obtained with excess Pb concentrations of 5 and 20 mole%, it was found that the pyrochlore peak becomes stronger with higher excess lead contents. The excess Pb introduced into the gels seems to be incorporated in a pyrochlore phase and does not appear as a PbO phase or as a Pb-rich perovskite PZT.

Figure 35 - X-Ray Diffraction Patterns of PZT (53/47) Gels [1 Mole DEA - 1 Mole Alkoxide] Heated at the Indicated Temperatures for 30 Minutes [3 Moles H_2O -1 Mole Pb]

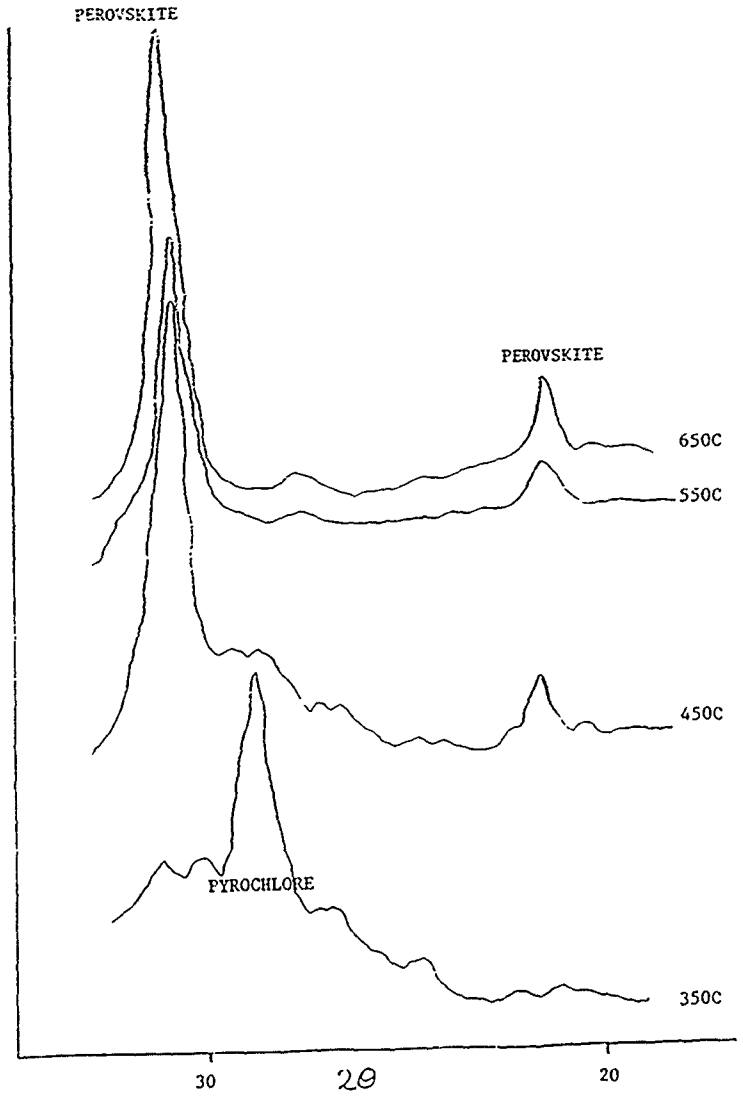

Figure 36 - X-Ray Diffraction Patterns of PZT (53/47) Gels [1 Mole DEA - 1 Mole Alkoxide] Heated at the Indicated Temperatures for 30 Minutes [9 Moles H_2O -1 Mole Pb]

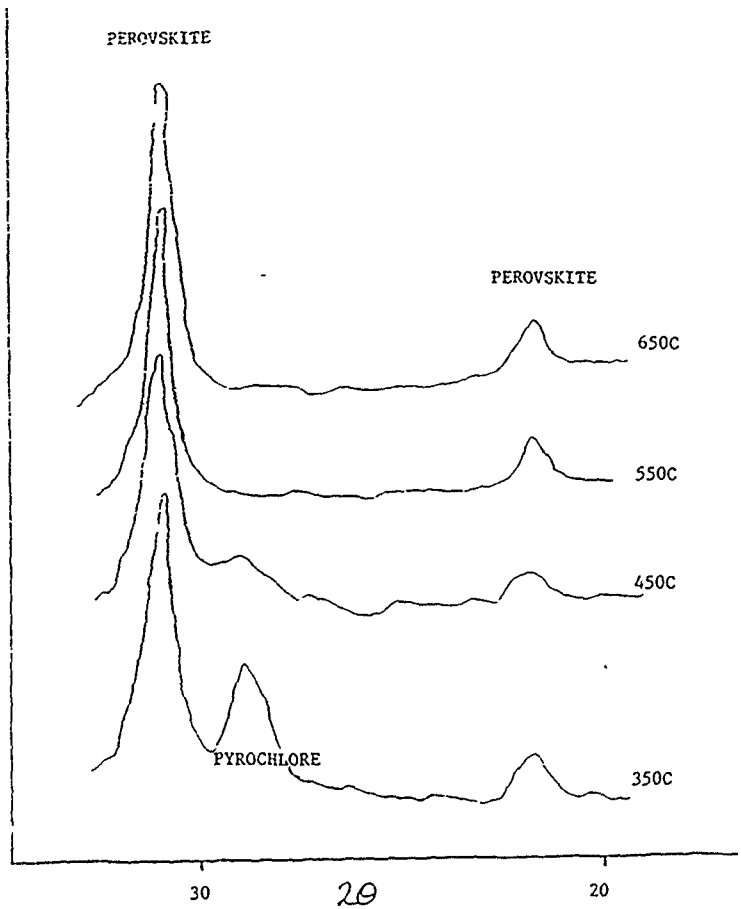

Figure 37 - X-Ray Diffraction Patter . of PZT (53/47) Gels [0.5 Mole DEA - 1 Mole Alkoxide] Heated at the Indicated Temperatures for 30 Minutes [6 Moles H_2O -1 Mole Pb]

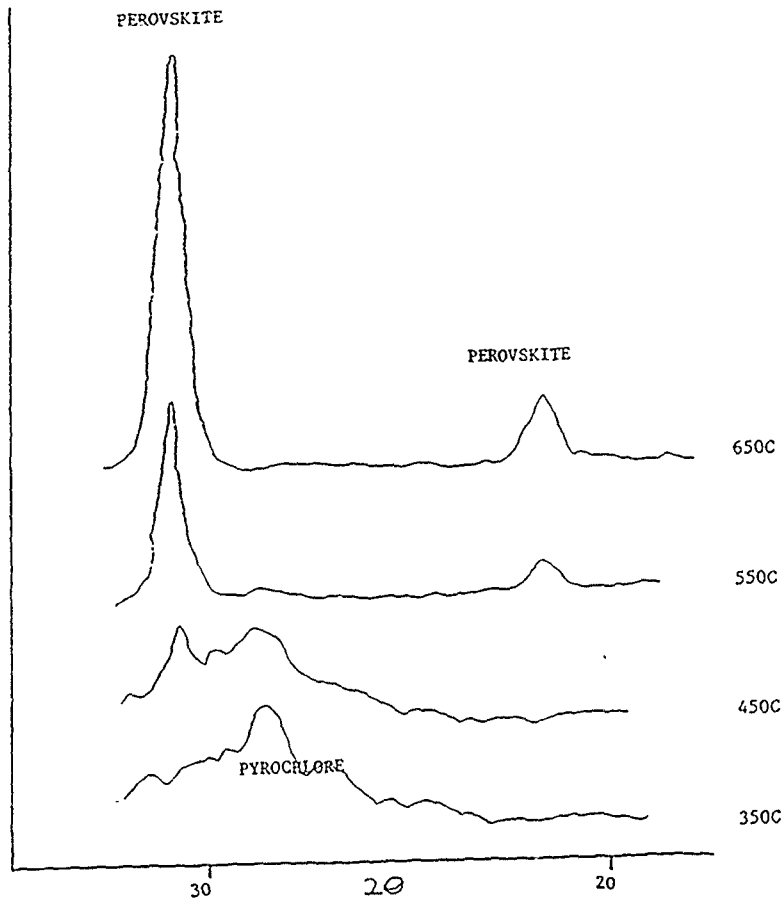

Figure 38 - X-Ray Diffraction Patterns of PZT (53/47) Gels [1 Mole DEA - 1 Mole Alkoxide] Heated at the Indicated Temperatures for 30 Minutes [10 Mole % Excess Pb]

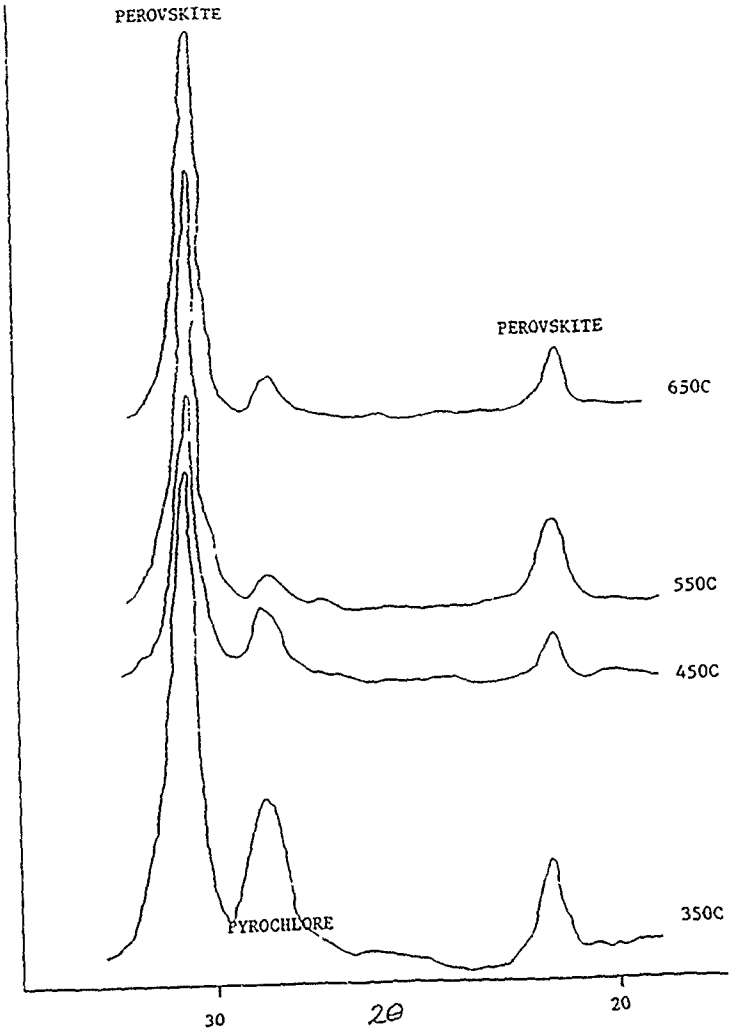

One noteworthy feature of all the present results is the absence of secondary phases such as Pb, PbO or ZrO_2. Such secondary phases have frequently been reported by other sol-gel researchers; and their absence in the present work indicates that the synthesis route employed here leads to highly homogeneous materials (the formation of Pb or PbO phases would effectively result in the final phase assembly being dependent on solid state reactions and on diffusion, thereby requiring higher firing temperatures or longer processing times to obtain the desired product).

C. Synthesis and Characterization of 53/47 PZT Spray-Dried Powder

i) Synthesis and Experimental Procedure

A saturated aqueous NH_4OH solution was prepared by bubbling NH_3 gas into distilled H_2O. A 53/47 PZT precursor solution prepared from methanolic Pb acetate trihydrate and modified Ti and Zr alkoxides (1 mole of alkoxide to 1 mole of DEA) was then slowly added to this basic solution (heated to 60C) with vigorous stirring, resulting in immediate precipitation of hydroxide species. The precipitate was stirred overnight with continued bubbling of NH_3 gas, followed by filtration and washing with MeOH. Filtration and washing was repeated until the precipitate was substantially free of acetate (as verified by FTIR). Distilled H_2O was then added to the resulting slurry to give a solids content of ~5 wgt. pct.; and this slurry was spray-dried at 175C using Buchi Mini Spray Drier. The resulting fine powder was heated to selected temperatures in the range of 350-650C; and the heat treated powders were characterized using X-ray diffraction and scanning electron microscopy.

ii) Characterization

The as-spray-dried powders are amorphous and have a particle size of ~1 μm (see Figure 39). Slight agglomeration occurred on heating to the temperature required for conversion to perovskite. TGA scan showed that all organics were burnt out by 350C (Figure 40). After heat treatment at 350 and 450C, a large, broad XRD peak centered at $2\theta = 29^{o}$ (corresponding to pyrochlore) was observed. Perovskite and pyrochlore were seen after heat treatment at 550C and 650C; and single phase perovskite was obtained at 700C. DTA exothermic peaks occurred at 240 and 310C. TGA shows that final burn-out took place at 350C, with differential TGA showing peaks at 240C and 310C.

Figure 39 - SEM Micrograph of As-Prepared Spray Dried PZT (53/47) Powder [Derived from a 1 Mole DEA - 1 Mole Alkoxide Precursor Solution]

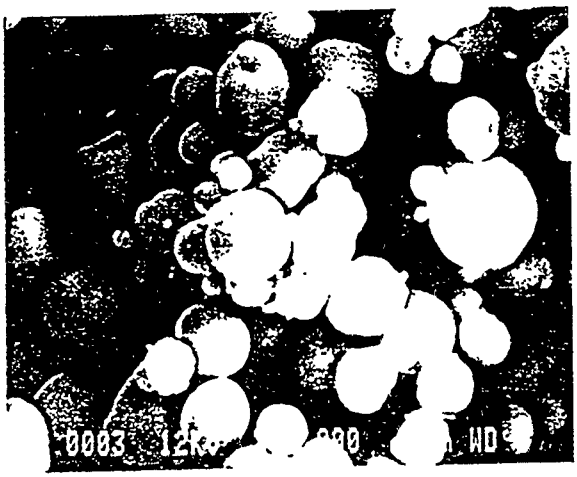

Figure 40 - TGA Scan of As-Prepared Spray Dried PZT (53/47) Powder [Derived from a 1 Mole DEA - 1 Mole Alkoxide Precursor Solution]

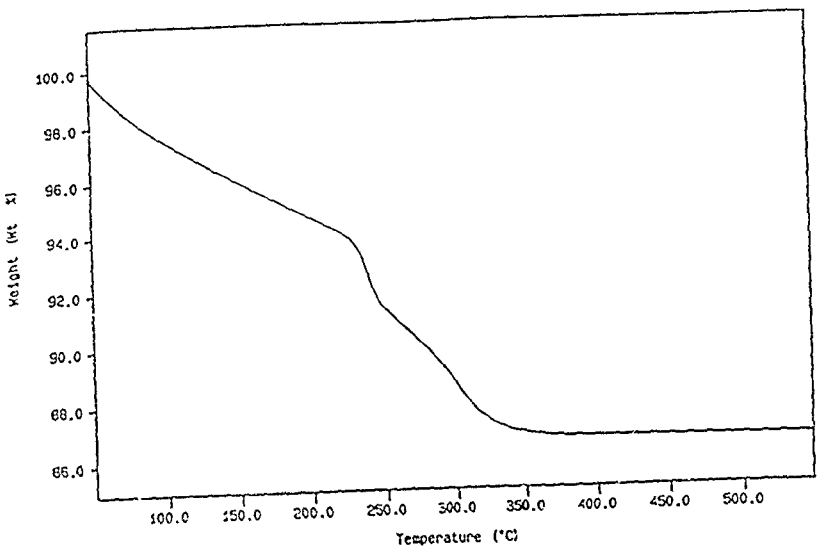

D. Synthesis and Characterization of 53/47 PZT Fibers

i) Synthesis and Experimental Procedure

Despite the desirability of ferroelectric fibers, especally those with highly anisotropic properties along their axes, for making composite transducers, there have been few reports of sol-gel derived ferroelectric fibers; and these have been concerned with $LiNbO_3$, $PbTiO_3$ and PLZT.

Utilizing DEA modification it has been possible to prepare PZT fibers. To our knowledge, this is the first time that PZT has been prepared in fiber form.

In the present work, use of precursor solutions with a molar ratio of alkoxide to DEA of 1-1 resulted in reasonable spinnability, but produced fibers with a high degree of tackiness. Reducing the DEA content to obtain a 1-0.5 alkoxide to DEA ratio enabled good fibers to be readily prepared. The fiber diameter ranged from 1 μm to 30 μm. Figure 41 shows a representative SEM micrograph of an unfired fiber. Thicker ones exhibited dog-bone cross sections, as illustrated in Figure 42. The addition of poly vinyl pyrrolidone (PVP) provided effective control of the sol rheology, and made it possible to draw long fibers of uniform diameter. Typically, a solution containing an alkoxide-to-DEA ratio of 1-0.5 with 2.5 wt% polyvinyl pyrrolidone was concentrated by rotary evaporation until it became spinnable. Fibers were drawn by hand with a glass rod and allowed to dry in air. These fibers were fired at various temperatures, varying from 550C to 750C, under O_2 and He atmospheres. Their microstructures were characterized using scanning electron microscopy.

After heat treatment for 30 mins. at temperatures of 350, 450, 550, 650, 700 and 750C, the fibers became quite brittle and often broke into smaller strands upon handling. Incipient crystallization on the fiber surfaces could be observed on samples fired at 650C. After heat treatment at 700C, the entire surface appeared crystalline. After heat treatment, at 750C, well-defined microstructures were clearly seen, sunburst crystallites being very prominent (see Figure 43). It is interesting to note that when heat treated for 4 hrs. under He, the fibers exhibited crystallite sizes which were notably smaller than those in fibers which were similarly heat treated under O_2 (see Figures 44 and 45).

Figure 41 - SEM Micrograph of Unfired PZT (53/47) Fiber [Derived from a 0.5 Mole DEA - 1 Mole Alkoxide; 2.5 wgt. % PVP-Oxide Equivalent Precursor Solution]

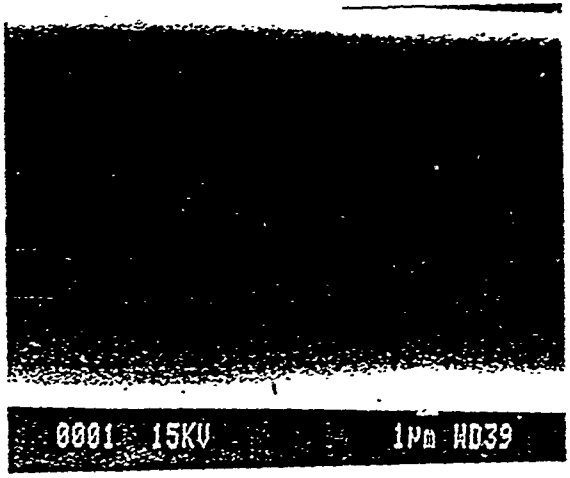

Figure 42 - SEM Micrograph of Unfired PZT (53/47) Fiber [Derived from a 0.5 Mole DEA - 1 Mole Alkoxide; 2.5 wgt. % PVP-Oxide Equivalent Precursor Solution]

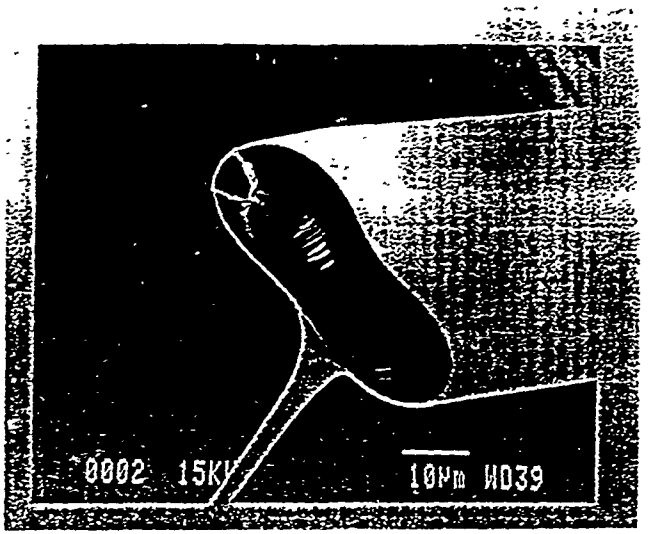

Figure 43 - SEM Micrograph of a PZT (53/47) Fiber Fired at 750€/30 mins. [Derived from a 0.5 Mole DEA - 1 Mole Alkoxide; 2.5 wgt. % PVP-Oxide Equivalent Precursor Solution]

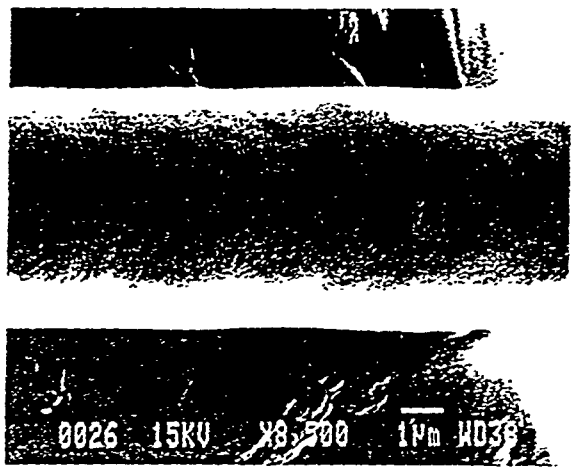

Figure 44 - SEM Micrograph of a PZT (53/47) Fiber Fired at 650C/4 Hours Under He [Derived from a 0.5 Mole DEA - 1 Mole Alkoxide; 2.5 wgt. % PVP-Oxide Equivalent Precursor Solution]

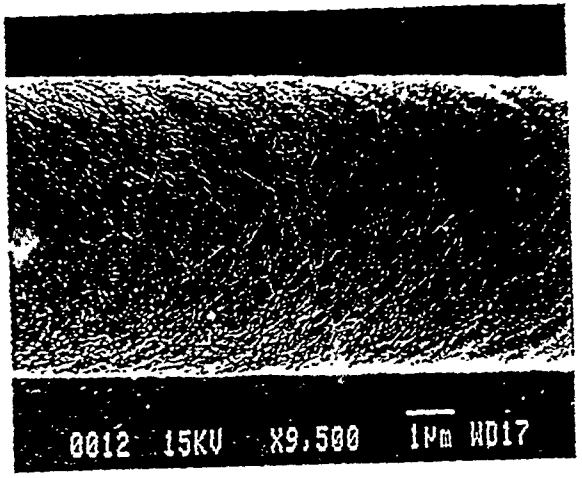

Figure 45 - SEM Micrograph of a PZT (53/47) Fiber Fired at 650C/4 Hours Under O_2 [Derived from a 0.5 Mole DEA -1 Mole Alkoxide; 2.5 wgt. % PVP-Oxide Equivalent Precursor Solution]

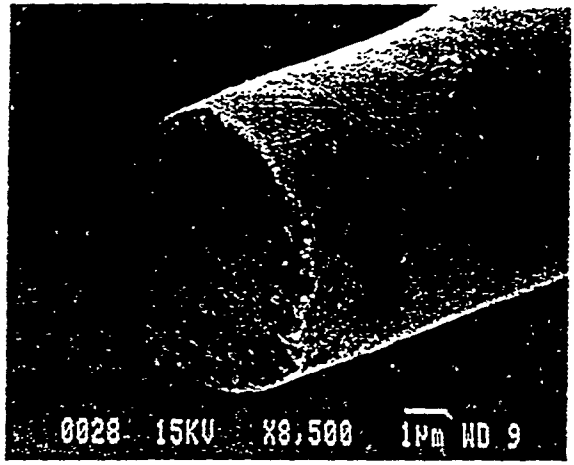

E. Synthesis and Characterization of PZT Thin Films

i) Synthesis and Experimental Procedure

Precursor solutions for spin-coating were prepared using an alkoxide to DEA molar ratio of 1-1. This specific modifier and degree of modification were chosen on the basis of our bulk gel results discussed earlier. In particular, gels of this composition gave a low decomposition temperature (480C) and the lowest observed temperature for formation of single-phase perovskite (500C). Additionally, this solution can be refluxed to ensure a high degree of mixing and molecular interaction. In thin film form a relatively low temperature (200C) post-deposition treatment is sufficient to ensure complete curing, whereas higher temperatures (300C) are necessary for TEA-based systems. DEA containing solutions were also stable for several months at room temperature when stored at room temperature. Experimental variables studied in the case of thin films included the effects of varying the water to alkoxide ratio and the addition of excess Pb (to compensate for Pb loss at elevated temperatures). The substrates were oxidized Si wafers which were electroded with Pt coatings deposited by sputtering.

A typical spin coating of the solutions led to films whose thickness was in the range of 500Å after firing at 500C. Multiple coatings were used to achieve thicker coatings. In such cases, each coating layer was fired at 200C for 5 min. prior to applying the next layer. Without such pre-firing, application of the subsequent layer was observed to produce partial dissolution of the underlying layer. After three coatings were applied, the overall film was subjected to a 500C heat treatment under O_2 for 30 mins. to oxidize and consolidate the film. The process was then repeated until the desired final film thickness was obtained.

The films were then fired at the final crystallization temperature, ranging from 550C to 750C, for various times (15 mins. to 2 hr.) either at a 5C/min heating rate or under rapid thermal annealing conditions. In rapid thermal annealing, the wafers were placed on a quartz plate, immersed directly into a furnace preset at a selected temperature, and after treatment for a desired time, were naturally cooled in the furnace. If removed immediately from the furnace after heat treatment, the films tended to crack. The atmosphere during the crystallization treatment was also varied. O_2, N_2, air, and He were explored here.

In determining the electrical properties of the films, Pt dots were sputtered via a shadow mask onto the films, forming the top electrical contact and resulting in numerous platinum - PZT - platinum devices. Figure 46 shows the device configuration. Back contact was established by partially covering the PZT film with wax, acid-etching the wafer and finally removing the wax with an organic solvent.

The thicknesses of the films were measured with a Sloan Dektak profilometer. Capacitance and dissipation factor as a function of frequency were obtained using a customized shielded probe station connected to a HP 4192A Impedance Analyzer. The measurements were carried out in a dry N_2 atmosphere. Dielectric constants were calculated from the capacitance data using the following equation:

$$E_r = \frac{Ct}{AE_o} \qquad (2)$$

where

E_r = relative dielectric constant
C = capacitance
t = film thickness
A = electrode area
E_o = permittivity of free space

A Sawyer-Tower (Figure 47) circuit was used to characterize the hysteresis loop formed at 60 Hz. X-ray diffraction, scanning electron microscopy and optical microscopy were used to investigate the evolution of microstructural features and phase development. Rutherford backscattering was utilized to determine compositional profiles. Electrical fatigue of the films was studied by recording the hysteresis loop after selected numbers of polarization reversals.

ii) Phase Development and Microstructural Characterization

Optical microscopy and SEM observations were used to study microstructural development during the processing of thin films. Amorphous PZT films were transparent but turned slightly hazy upon crystallization at elevated temperature due to grain boundary scattering. For films heated at 5C/min., large isolated grains appear first. These subsequently impinge on one another, resulting in interconnected grains across the film surface. See

Figure 46 - Device Configuration of a PZT Thin Film Capacitor for Electrical Characterization

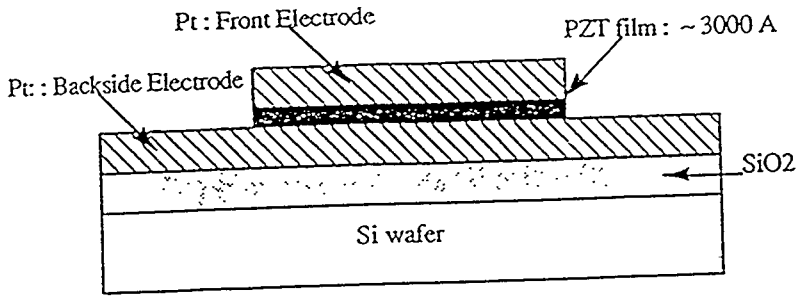

Figure 47 - Sawyer-Tower Circuit for Obtaining Hysteresis Loops of Ferroelectric PZT Capacitors

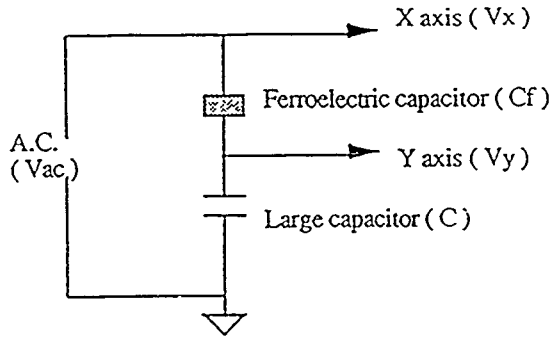

Figure 48 for an optical micrograph of a film heated at 650C for 30 mins. under O_2. Energy dispersive X-ray analysis indicated that the dark background material in Figure 48 has substantially lower Pb content than the lighter grains (see Figure 49). It is likely that the light grains represent the perovskite ferroelectric PZT, while the dark background material consists of lead-poor pyrochlore. The perovskite phase appears brighter due to its higher Pb content, emitting a higher yield of electrons under SEM illumination.

Under high magnification (see Figure 50), the perovskite grains are seen to consist of spherulitic rosettes. The background pyrochlore material appears fine-grained, but definitely crystalline. The perovskite grains are surprisingly large, about 2-4 μm in diameter (and thus much larger than the film thickness). They represent, however, polycrystalline units, as the various lamellae oriented radially from the center are believed to be single crystals.

Upon further heat treatment, the amount of pyrochlore (the dark material) compared with perovskite was observed to increase. This can be attributed to lead loss at elevated temperatures, leading to the formation of the lead-poor pyrochlore phase.

When He was used as the heat treatment atmosphere, the microstructure appeared richer in perovskite (see Figure 51). The proportion of pyrochlore was less and the grains exhibited a higher degree of packing. The presence of He thus appears to enhance densification and to inhibit lead loss.

A different microstructure was formed on rapid thermal annealing (RTA) compared to conventional heat treatment. Figure 52 shows a typical dense, perovskite microstructure. No dark pyrochlore areas are observed. Note that the grain size is also substantially smaller (~1μm) than that in the rate-heated films. At prolonged soak times, the pyrochlore phase starts to appear again reflecting the loss of lead from the surface.

It is concluded at this point that the starting materials and synthesis conditions have a profound effect on subsequent microstructure development, as do the post-gelation heat treatment conditions. Previous reports by researchers using the methoxyethanol route showed a smaller grain size (0.1-0.2 μm) and no appearance of the rosette crystallites.

For stoichiometric PZT (53/47) films, XRD results indicated that the following phase transformations occurred:

Figure 48 - Optical Micrograph of a PZT (53/47) Film Fired at 650C/30 Mins. Under O_2 [Derived from a 1 Mole DEA - 1 Mole Alkoxide Precursor Solution] (x500)

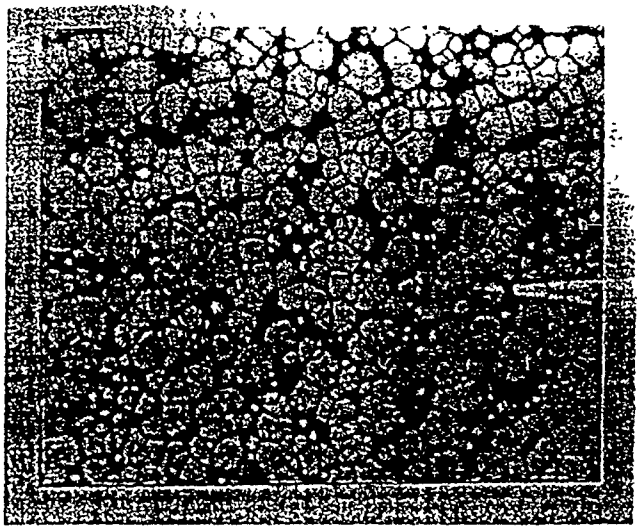

alysis of a PZT (53/47) Film Fired at 650C/30 Mins.
$)_2$ [Derived from a 1 Mole DEA - 1 Mole Alkoxide
r Solution]

red at 650C/30 Mins.
. - 1 Mole Alkoxide

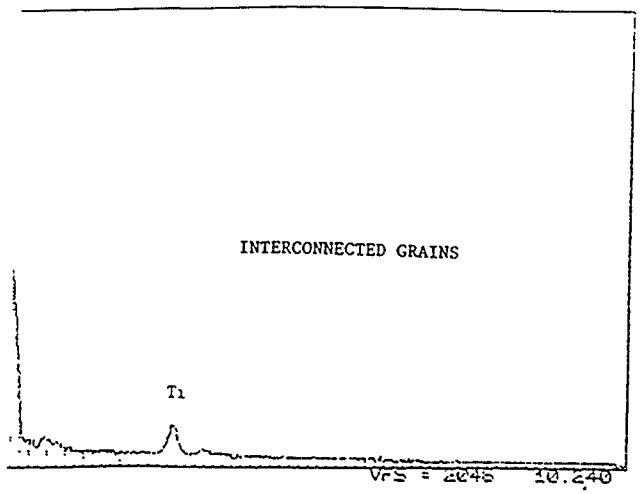

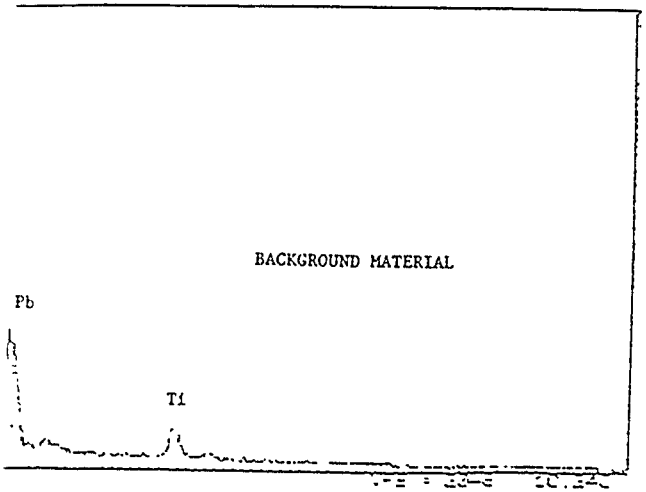

AD-A241849

Figure 51 - Optical Micrograph of a PZT (53/47) Film Fired at 700C/30 Mins. Under HE [Derived from a 1 Mole DEA - 1 Mole Alkoxide Precursor Solution] (x500)

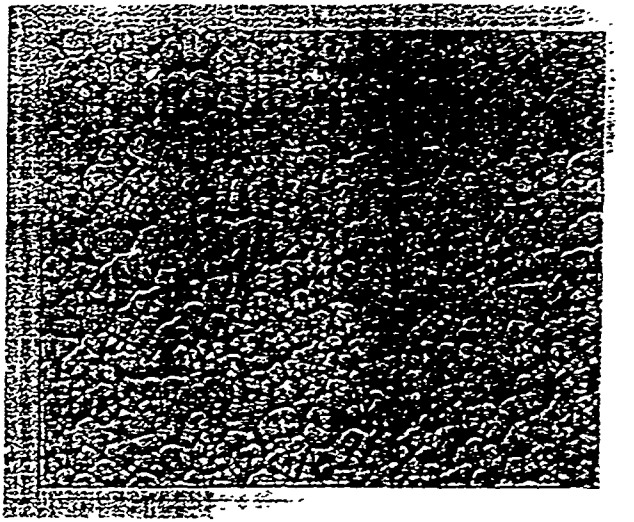

Figure 52 - Optical Micrograph of a PZT (53/47) Film Fired by Rapid Thermal Annealing at 650C/30 Mins. Under O_2 [Derived from a 1 Mole DEA - 1 Mole Alkoxide Precursor Solution] (x500)

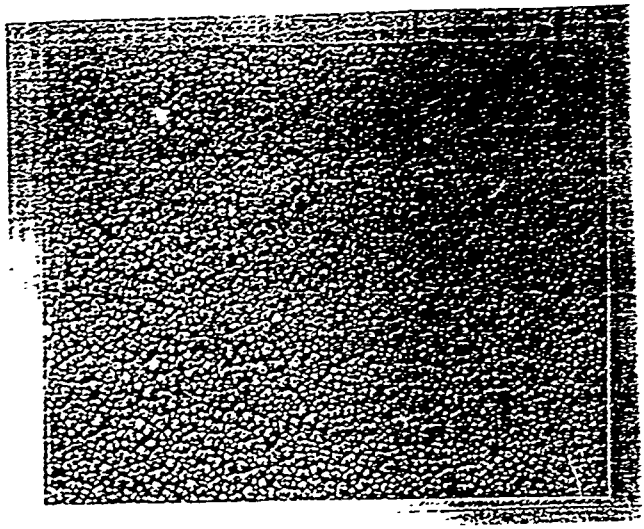

amorphous→perovskite + pyrochlore→perovskite. Table 19 shows the ratio of the intensity of the perovskite (200) and pyrochlore (222) peaks as a function of heat treatment temperature for RTA and rate heating treatments. It is seen that perovskite formation was sluggish at lower temperatures in RTA films compared with films treated with constant heating rates. At higher temperatures, the transformation kinetics of the pyrochlore→perovskite conversion were higher, as evident by the lack of pyrochlore in films which were rate heated to 700C. The origin of the continued presence of pyrochlore in the RTA films treated at 700C is not completely understood at the present time, but may be attributable to the smaller time experienced by the RTA films at elevated temperatures.

Table 19 shows that films either rate heated or subjected to RTA have essentially the same pyrochlore content at 650C (as evidenced by X-ray diffraction). In contrast, optical microscopy of the RTA sample shows dense perovskite grains and the absence of pyrochlore on the film surface. This difference reflects the presence of remanent pyrochlore phase beneath the surface perovskite grains. The pyrochlore is detected by X-ray diffraction as the penetration depth of the X-rays is sufficiently large that the entire thickness of the film is sampled. Longer soak times and/or higher temperatures are required to convert this bulk pyrochlore into a single-phase perovskite film.

Note that the height of the (200) peak is used for perovskite rather than that of the (110) peak which is the strongest peak in a randomly polycrystalline PZT sample. According to the JCPDS file #33-784 for PZT (52/48), the ratio of intensity of (100) and (110) peaks should be 0.12. In the present films, however, there exists a strong preferred (100) orientation. As a manifestation of this preferred orientation, the (100) peak is the strongest line in the diffraction pattern shown in Figure 53. Such preferred orientation has not been reported previously for any chemically derived PZT films. The orientation in the PZT films is likely associated, at least in part, to a preferred orientation of the underlying platinum coating on the oxidized Si wafers. This is shown by the XRD data in Table 20. The orientation of the Pt is an intrinsic effect of the sputtering conditions since annealing the wafer did not greatly affect the orientation of the Pt film. It is believed that the preferred orientation developed in the present PZT films was responsible for the exceptionally high dielectric constants and excellent ferroelectric properties observed (see next section).

Table 19 - Ratio of XRD Peak Intensities of Perovskite and Pyrochlore for PZT 53/47 Films

	$\frac{I(200)\ perovskite}{I(222)\ pyrochlore}$	
Temperature (C) for 30 mins.	RTA	5C $min.^{-1}$
550	0.13	6.64
650	6.13	6.07
700	7.50	---*

*No pyrochlore present.

Figure 53 - XRD Pattern of a PZT (53/47) Film Fired at 750C/45 Mins. Under O_2 [Derived from a 1 Mole DEA - 1 Mole Alkoxide Precursor Solution]

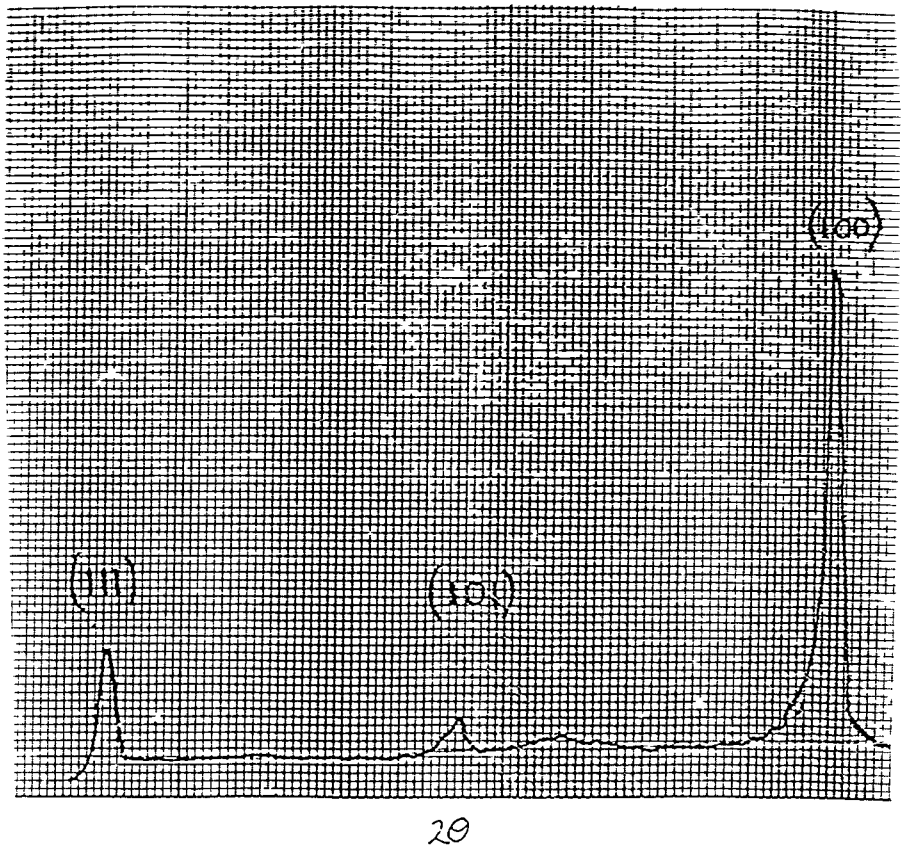

Table 20 - Preferred Orientation of Sputtered Pt Films on SiO_2/Si Wafers

Condition	I_{200}/I_{111}
As-sputtered	2.08
Annealed 700C 1/2 hr. in O_2	2.22
JCPDS File #4-0802 (random orientation)	0.53

When 10 mole% excess lead is incorporated into the films, the pyrochlore content in the RTA films decreased dramatically. Films heated at 650C were single phase perovskite with no pyrochlore being observed.

It is interesting to note that the degree of preferred orientation, indicated by the ratio of the I(100)/I(101) diffraction peaks, increases at higher temperatures and at longer heat treatment times in RTA-treated films. This likely reflects the development of preferred orientation as a result of the pyrochlore-perovskite transformation, either directly during the transformation or subsequently by structural rearrangement. Of these, the former seems more reasonable. The presence of excess lead compensates for lead loss associated with the high surface area during heat treatment, thereby avoiding the formation of a lead-poor pyrochlore phase.

iii) Electrical Characterization of Thin Films

Before discussing the electrical characterization of the present chemically-derived PZT films, it is important to note the lack of standard or universally accepted protocol in reporting ferroelectric film properties. Such properties are functions of film thickness, grain size, preferred orientation or texture, applied dc bias, amplitude and frequency of the probe signal, as well as the measurement geometry and dimensions.

The measured dissipation factor, tan δ, is actually the composite tan δ of the device (usually a capacitor structure) under test and consists of the intrinsic material tan δ plus a contribution from the series contact resistance, ωRC. The present authors have noted an increase in tan δ at high frequencies and near the resonance frequency of the bridge. Further, the series or parallel equivalent circuit mode used during measurement should be duly noted, particularly in lossy systems.

The level of the signal amplitude influences the dielectric constant and, loss as demonstrated in Figure 54 for a PZT film synthesized in our laboratory. At higher amplitudes, polarization reversals occur and lead to anomalous increases in the dielectric constant and loss due to the nonlinear contribution from the hysteresis loop. Even in the case of a non-ferroelectric film, the signal level influences the impedance, notably when a barrier is present. The barrier impedance dominates at low signal levels, and the bulk impedance at higher signal levels.

Figure 54 - Effect of Signal Amplitude on a PZT (53/47) Film Fired at 650C/30 Mins. Under O_2-2100Å Thick [Derived from a 1 Mole DEA - 1 Mole Alkoxide Precursor Solution]

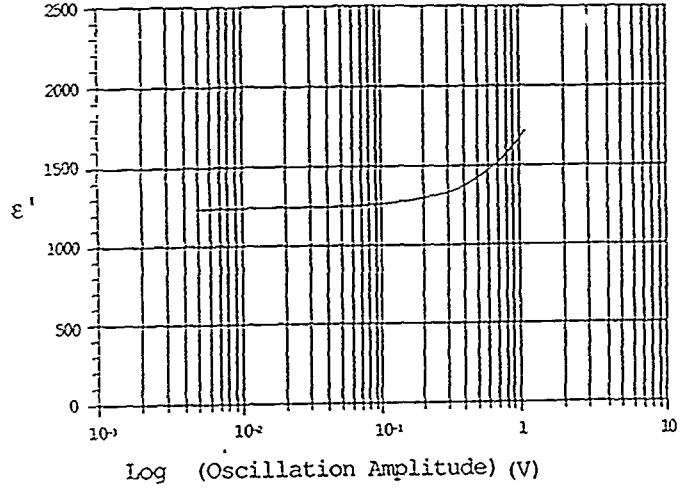

The choice of electrodes is important, particularly if the ferroelectric (FE) film is doped with off-valent dopants leading to semiconducting properties. The contacts formed may be rectifying or ohmic, thus affecting the electrical characteristics. While a metal-FE-Si structure is simple (notwithstanding interfacial reaction layers), the resulting electrical characteristics (e.g., hysteresis loop) are asymmetric. The voltage drop across the Si depletion region makes difficult the task of determining accurately the coercive field. Under suitable conditions, Si can also inject carriers into the film affecting the loss. A symmetrical metal-FE-metal structure, where the same metal is used on both sides of the FE layer, is always preferred. In close detail, even such a configuration is not symmetrical, since the FE film is deposited first on the bottom electrode layer and then heat treated. This interface is expected to behave differently (e.g. due to interfacial reactions) than the top metal-FE interface, where the electrode is deposited later.

Platinum sputtered on oxidized Si wafers was used as the back electrode of the PZT films in the present study due to its chemically inactive character, and its service as a barrier between the PZT film and the underlying substrate. The melting point of Al is too low; and Au shows poor adherence to SiO_2. Additionally Au reacts with Si at high temperatures (~650C), forming grossly heterogeneous regions. Other conductive materials which might be studied include ITO and Ti-W.

A dispersion of the dielectric constant as a function of frequency usually occurs due to various dielectric relaxation mechanisms, each dominating in a particular frequency range. Figure 55 shows a plot of the dielectric constant, E_r, vs. frequency where E_r is almost independent of frequency for one of the present PZT films (unlike many vapor-deposited films). This demonstrates the absence of any relaxation or dispersive phenomena and attests to the high homogeneity of the films. The higher the value of E_r, the higher is the dispersion with frequency in the films.

All of our dielectric data (Er and tan δ) were measured at 1 kMz, 5mV rms signal oscillation level with no applied D.C. bias unless indicated otherwise.

For films heated at intermediate temperatures (1ess than 650C), the dielectric constant increases with heat treatment time and then saturates. At higher temperatures (> 650C), the dielectric constant decreases with time (see Table 21) due to lead loss and interfacial reaction causing a degradation

Figure 55 - Dielectric Dispersion of a PZT (53/47) Film Fired by Rapid Thermal Annealing at 700C/1 Hour Under O_2-3230Å Thick (Composition Contains 10 Mole % Excess Pb) [Derived from a 1 Mole DEA - 1 Mole Alkoxide Precursor Solution]

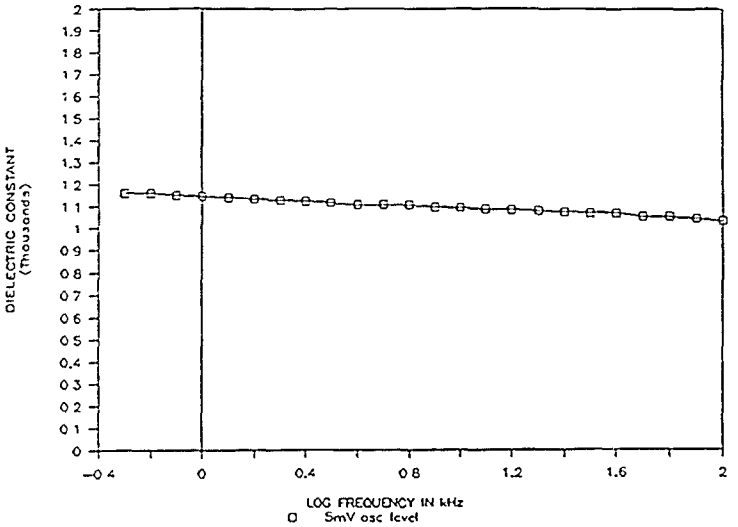

Table 21 - Dielectric Constants of PZT 53/47 Films RTA at 650C: O_2 for Various Times

Time (min.)	Er
15	1058
45	946
60	904

Table 22 - Dielectric Constants of PZT 53/47 Films Heated at 5C Min^{-1} to the Indicated Temperatures and Held at Temperature for 30 Min.

Temperature (C)	Er
500	82
533	483
550	648
650	942
700	954
750	1102

in dielectric properties. At high temperatures even the Pt reacts with lead compounds. For fixed heat treatment times, the treatment temperature determines the value of E_r, with E_r increasing with temperature, as illustrated in Table 22. This is attributed to the formation of a denser microstructure at higher temperatures, as well as conversion of the secondary pyrochlore phase to perovskite. For films heat treated at 650C for 30 mins, use of He rather than O_2 as the furnace atmosphere resulted in an increase in E_r from 942 to 1124. This increase can be attributed to improved densification, which was apparent in SEM micrographs of the fired films.

It is heartening to notice that in the present films, even those as thin as 2000Å, the values of E_r are exceptionally high at about 1000. The dependence of E_r on thickness of ferroelectric films is well known. Thinner films tend to exhibit lower value of E_r; and this phenomenon is associated with the grain size effect on bulk ferroelectrics. Typical literature values of E_r for 2000Å thick PZT (53/47) films are less than 300.

Figure 56 shows the plot of E_r vs. frequency for one of our films with a particularly high value of E_r. It is seen that E_r for this film is in the range of 2000 at 1 kHz and 1 V rms signal amplitude. This is much higher than the values for bulk ceramics and can be attributed to the presence of preferred orientation in the film. This value is the highest reported value of E_r published anywhere for this composition (see Tables 12 and 13 above).

Results obtained on films which were heat treated at 650C showed that the Pb activity in the heat treatment atmosphere was not crucial in determining the dielectric properties. Lead loss seemed to be insignificant at this temperature. Further tests are being carried out to study the effect at higher temperatures, with the Pb activity being varied by placing the films in powder beds consisting of PbO, $PbZrO_3$, $PbTiO_3$, or PZT 53/47.

A representative, well saturated hysterisis loop for one of the present films is shown in Figure 57. It shows a remanent polarization value of 18.3 μC/cm and a coercive field of 37.5 kV/cm. The value of coercive field is notably higher than the bulk value of 17 kV/cm. This is to be expected due to substrate clamping effects exerted during polarization reversal and the additional energy necessary to effect domain switching. There also exists a thickness dependence of the coercive field (Ec), and thicker films are expected to demonstrate lower values of E_c. Films treated at lower temperatures tend to exhibit higher values of E_c, e.g., films heated at 550C showed an E_c of 56.25

Figure 56 - Dielectric Dispersion of a PZT (53/47) Film Fired at 700C/15 Mins. Under O_2-3730Å Thick [Derived from a 1 Mole DEA - 1 Mole Alkoxide Precursor Solution]

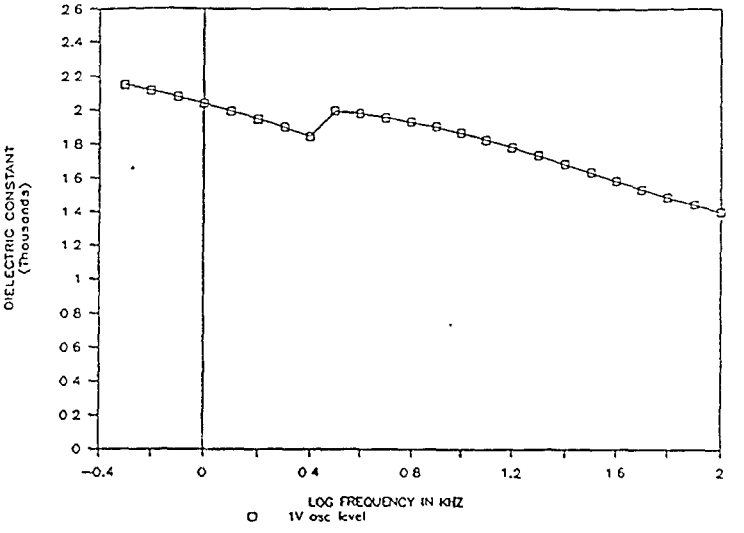

Figure 57 - Hysteresis Loop of a PZT (53/47) Film Fired at 700C/15 Mins. Under O_2-3730Å Thick [Derived from a 1 Mole DEA - 1 Mole Alkoxide Precursor Solution]

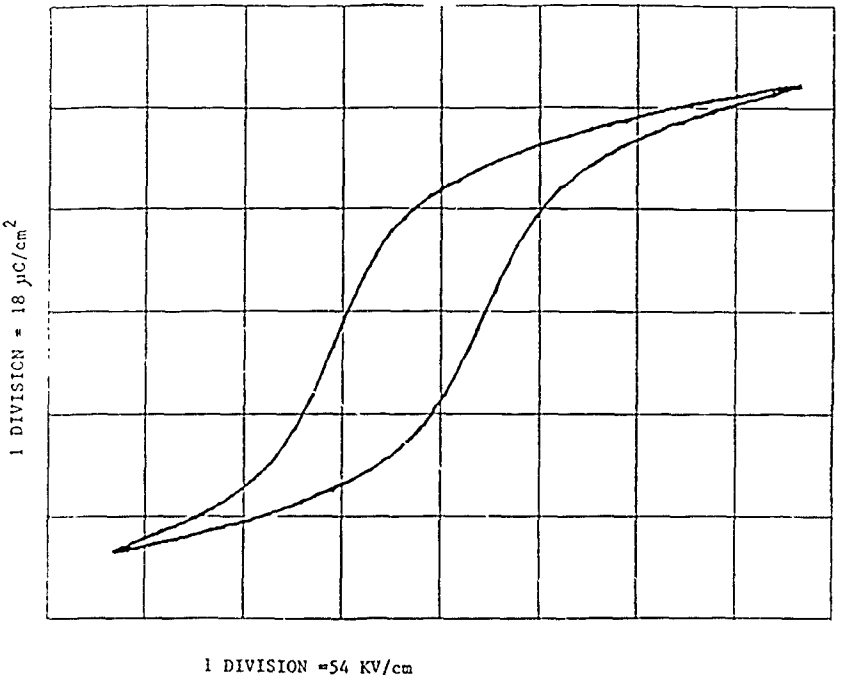

kV/cm. The presence of secondary phases notably pyrochlore, provides a hindrance towards polarization reversal.

The uniformity in thickness of the spin-coated films on platinized wafers was high. Some films showed a variation in thickness of only 1.4% across a 2-inch wafer surface.

TEA-modified precursor solutions maintained their thermoplastic nature upon drying. A spincoated film placed upright in a furnace flowed downwards at ~200C. Such solutions have potential for planarization applications, which are currently being actively studied.

iv) Fatigue

The phenomenon of fatigue is one of the greatest obstacles to the use of ferroelectric films in memory applications. This phenomenon is reflected in a decrease in the remanent polarization and an accompanying increase in coercive field as the polarization is reversed many times. In addition, the amount of charge switched during the reversals becomes increasingly small.

Various mechanisms have been suggested as the cause of fatigue. These include: the formation of conductive dendrites arising from a localized reduction of Ti^{4+} to Ti^{3+} ions; microcracking within the film itself; and delamination of the electrode at the interface due to the high degree of piezoelectric strain encountered during switching. There has to date been no report of dendrites being observed directly as a result of fatigue, although some preliminary observations linked such dendrites to an artifact of electron beam damage.

In the present films, as illustrated in Figure 58 for a chemically derived PZT (53/47) film heated at 700C, fatigue does occur. The figure indicated that the value of the remanent polarization decreases to 50% of its initial vaue after about $3x10^8$ reversals. There was also an increase in the coercive field, as expected. Improvements in fatigue behavior are expected to result from more optimized processing (see Proposal).

v) Time-Dependent Dielectric Breakdown

Another reliability issue when considering the eventual adoption of ferroelectric films for memory applications is time-dependent dielectric

Figure 58 - Effect of Fatigue on the Hysteresis Loop of a PZT (53/47) Film Fired at 700C/15 Mins. Under O_2-3730Å Thick [Derived from a 1 Mole DEA - 1 Mole Alkoxide Precursor Solution]

INITIALLY:

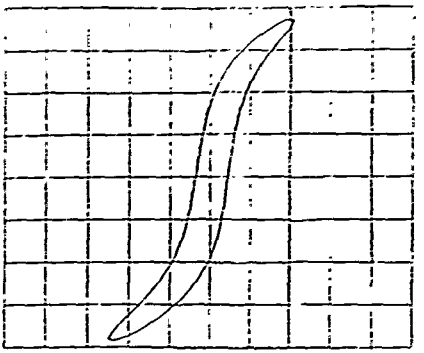

AFTER 3×10^8 REVERSALS:

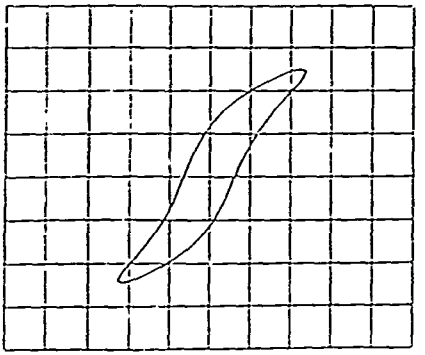

VERTICAL SCALE = 10 uC/cm^2 per division

HORIZONTAL SCALE = 134 KV/cm per division

breakdown. Such breakdown is irreversible and catastrophic. Figure 59 shows the time dependent leakage characteristics of a chemically derived PZT (53/47) which had been heat treated at 700C for 15 mins. The data shown in the figure were gathered by Prof. R. Schrimpf and Mr. S.C. Lee of the ECE Department, University of Arizona, on a film prepared by our group. While the leakage current was high, no breakdown occured for voltages applied at 10 and 15V within the lifetime of the experiment (1000 sec). For a conventional oxide capacitor (e.g., SiO_2) the leakage current will initially decrease with time (due to filling of traps within the oxide) until breakdown occurs, at which time the current increases dramatically by orders of magnitude. In the particular film shown in Figure 59, the leakage current increased gradually rather than decreased.

It is recognized that the conduction of charge in a ferroelectric film is a complex phenomenon and involves grain boundary scattering, domain switching and polarization saturation at higher applied voltages, ionic motion, traps within the film and localized film-electrode electrochemical reactions. Clearly more work needs to be done to explore further this phenomenon in order to achieve highly reliable PZT films.

vi) Rutherford Backscattering, Radiation Effects and Optical Properties

A chemically-derived PZT (53/47) film which had been heated to 750C for 45 Mins. was subjected to RBS analysis, primarily to determine if any migration of Pb towards the surface occurred at elevated temperatures. This has been reported by various researchers on sputtered films. Results (see Figure 60) show that the Pb concentration was quite uniform throughout the film profile with no lead-rich surface layer. The fact that our film does not exhibit any lead segregation at the surface is very encouraging. The role of the precursor materials, in particular the DEA modifier, in maintaining the constant profile needs to be explored further.

To explore the effects of radiation on the device characteristics of our chemically derived films, sample PZT (53/47) films were subjected to radiation doses from a Co^{60} source. The work was carried out in collaboration with Professor R. Schrimpf and Mr. S.C. Lee of the ECE Department, University of Arizona. The results to date showed no significant effect on E_c at radiation doses of up to 17.5 kRad. Further experiments are ongoing to determine whether any effect will be evident at higher doses.

Figure 59 - Time Dependent Leakage Characteristics of a PZT (53/47) Film Fired at 650C/30 Mins. Under O_2-3100Å Thick [Derived from a 1 Mole DEA - 1 Mole Alkoxide Precursor Solution]

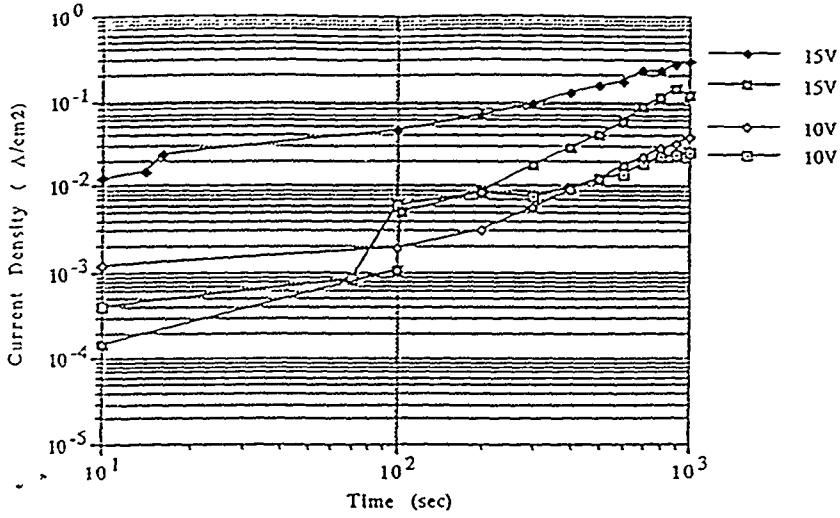

Figure 60 - RBS Analysis of a PZT (53/47) Film Fired at 750C/45 Mins. Under O_2-3300Å Thick [Derived from a 1 Mole DEA - 1 Mole Alkoxide Precursor Solution][2]

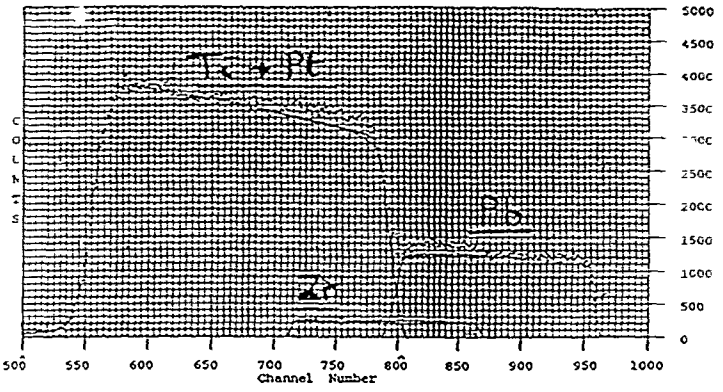

In further work, the refractive index of our chemically derived PZT (53/47) films as determined as a function of heat treatment conditions. As shown in Table 23, the results indicate that the refractive index increases with increasing heat treatment temperature, likely reflecting the effect of film densification. At temperatures above 400-500C for films deposited directly on Si, the refractive index begins to decrease. This decrease is likely due to interfacial reactions at the PZT-Si interface leading to the formation of SiO_2 and/or lead silicate species.

In contrast to the latter behavior, when the PZT films are deposited on platinized wafers, the refractive index continues to increase (and to increase significantly) above 500C. The difference is likely associated with the absence of interfacial reactions when platinized wafers are used as the substrates.

It has also been found that selected dopants have a considerable effect on the refractive index of the PZT films. For example, incorporation of only 2.4 atom % Ta increases the refractive index by 13%, to a value of 2.26.

F. Summary and Conclusions

The present work on the wet chemical processing of PZT has demonstrated clearly that the precursor chemistry, solution processing parameters, and post-gelation treatment have a profound effect on the microstructures and phase assemblages of the final PZT ceramics. Careful variations of the chemistry and processing conditions have yielded dense PZT thin films with large grain size, which exhibit the highest dielectric constants reported to date. In addition it has been found that films exhibiting strong (100) orientation can be prepared using wet chemical methods. Such orientation maximizes the ease of switching during polarization reversal, which is highly advantageous in memory applications. To our knowledge, there have been no previous reports of such a high degree of (100) preferred orientation.

The precursor chemistry can be readily altered by introducing modifying or chelating ligands into the system. Conventional chelates, such as 2,4-pentanedione (AcAc), have been widely used to tailor the reactivities of many transition metal alkoxides in preparing compositions such as SiO_2-TiO_2 glasses; but they have received little attention in ferroelectric systems. In the present study, some fifteen modifying agents have been investigated, ranging from alkanolamines to ethylacetoacetate. Inhomogeneous gels were obtained when

Table 23 - Variation of Refractive Index with Heat Treatment Temperature for PZT (53/47) Films on Silicon and Plastic Silicon Substrates

Temp. (C)	n_f	Substrate
As-dried	1.32	Si
200	1.57	Si
300	1.71	Si
400	1.73	Si
500	1.65	Si
650	2.00	$Pt/SiO_2/Si$

conventional bidendate chelates such as 2,4-pentanedione and ethylacetoacetate were used. Inhomogeneity also resulted when alkonalamines other than DEA and TEA were used. DEA and TEA modification enabled transparent homogeneous materials to be obtained readily.

Modifying agents function by effectively reducing the rate and degree of the hydrolysis and condensation reactions of the individual chemical species. The effectiveness of the modifying agent is dependent on its chemistry and its molar concentration relative to that of the reacting species. In this regard, the functionality of the modifier is critical. For example, MEA is essentially monofunctional, DEA bifunctional and TEA trifunctional. Modification of the reactivity of the chemical species will be reflected in the final gel structure in terms of homogeneity, degree of cross-linking and amount of residual organics.

The homogeneity is directly related to the condensation rate - slower condensing species will give rise to material with a higher degree of chemical homogeneity. The use of slower-reacting species also has distinct physical advantages, namely ease of handling due to a reduced tendency towards precipitation (rigorously controlled dry atmospheres are not required) and a long shelf-life (changes of viscosity with time are minimized ensuring reproducibility of coating thickness).

The most widely investigated wet chemical route to PZT uses 2-methoxyethanol as a solvent to dehydrate the $Pb(OAc)_2 \bullet 3H_2O$ prior to reaction with Ti and Zr alkoxides. The toxic nature of this solvent would, however, severely curtail its widespread use because of health and environmental concerns. In the present synthetic route, the modified reactivity of the alkoxides permits the use of methanol as the solvent.

While suitable choice of modifying agents can be used to prepare homogeneous materials, the physical form of the material (whether powders, densified pellets, thin films or fibers) has a significant effect on subsequent phase evolution. A brief summary of some of the present findings on the phase development of PZT in various physical forms with respect to chemistry, processing, and firing temperature is presented in Table 24.

Several interesting trends can be seen from the results in Table 24. A molar ratio of 1 alkoxide-1 DEA appears to be the preferred choice of chemistry and degree of modification to ensure enhanced perovskite formation. With such modification, single-phase perovskite can be formed at temperatures

Table 24 - Phases Found in PZT (53/47) Powders and Films
as Functions of Processing, Chemistry, Physical Form and Temperature

Temperature (C) Hold for 30 Mins.	Unmodified Gel	Gel 1-2 DEA or 1-1 TEA Modification	Gel 1-0.5 DEA Modification	Gel 1-1 DEA Modification	Spray-Dried Powder in 1-1 DEA Modification	Thin Film RTA 1-1 DEA Modification	Thin Film Rate Heated 1-1 DEA Modification
350	Pyrochlore	Pyrochlore	Pyrochlore	Pyrochlore + Perovskite	Amorphous	*	*
450	Pyrochlore + Perovskite	Pyrochlore + Perovskite	Pyrochlore + Perovskite	Pyrochlore + Perovskite	Amorphous	*	*
550	Perovskite	Pyrochlore + Perovskite	Perovskite	Perovskite	Perovskite + Pyrochlore	Pyrochlore + Perovskite	Pyrochlore + Perovskite
650	Perovskite	Perovskite	Perovskite	Perovskite	Perovskite + Pyrochlore	Pyrochlore + Perovskite	Pyrochlore + Perovskite
700	Perovskite	Perovskite	Perovskite	Perovskite	Perovskite	Pyrochlore + Perovskite	Perovskite

* Films were heat treated at 500C before final crystallization treatment. They are X-ray amorhpous after heat treatment at 500C.

as low as 500C. With the 1 alkoxide-1 DEA modification, the following phase transformations occur on firing gels: amorphous→pyrochlore and perovskite→perovskite. When different molar ratios of DEA to alkoxide are used, however, or when other modifying agents are employed, or when no modification is used, the formation of perovskite is hindered; and the following sequence of phase transformations is observed: amorphous→pyrochlore→pyrochlore and perovskite→perovskite. These findings illustrate clearly the importance of precursor chemistry in modifying phase development during later processing.

The phase development in PZT spray-dried powders also demonstrates the importance of precursor chemistry. Here, much higher temperatures (~700C) are required to form single-phase perovskite, even when a molar ratio of 1 alkoxide-1 DEA is employed. This reflects the very rapid condensation and almost instantaneous precipitation which occurs in the concentrated aqueous ammonia solutions. The rapid formation of mixed hydroxide species, possibly with micro-heterogeneous regions, negates the beneficial effects of tailoring the reactivity of the alkoxides with DEA.

With thin films, the effect of the substrate on subsequent crystallization behavior must be considered. Also important is whether the film is nucleated in the bulk or at either surface. If bulk nucleation is dominant, then phase development in the film should be similar to that in the bulk. Nucleation at either the film-substrate interface or at the free surface would generally be expected to result in a lower crystallization temperature. In contrast to this expectation, the results shown in Table 24 indicate that the films require a higher temperature for crystallization. The observation of preferred orientation in the films, associated with the epitaxial effect of the underlying Pt substrate, suggests that the nucleation was taking place at the film-substrate interface. This leaves as a puzzle the fact that nucleation in the films appears to be heterogeneous, yet is deferred to a higher temperature than nucleation in the bulk. Also puzzling and likely related is the observation of grain sizes in the films which are much larger than the film thickness.

It is also seen from Table 24 that the formation of single-phase perovskite was particularly inhibited in films subjected to rapid thermal annealing. This phenomenom can be attributed to the lessened effective times which these films experience at elevated temperaturs compared to rate-heated films. It was therefore necessary to resort to longer soak times at lower temperatures to ensure complete formation of single-phase perovskite.

Surprisingly, the incorporation of 10 mole% excess Pb in films subjected to rapid thermal annealing resulted in the formation of single-phase perovskite even at short heat treatment times. In bulk material, however, such incorporaton invariably led to the formaton of a persistent pyrochlore phase. This difference in behavior is currently being investigated in detail.

Careful optimization of both the precursor chemistry and subsequent thermal processing has permitted the preparation of PZT films exhibiting the highest dielectric constants reported in the literature even for films as thin as 3000Å. That is, other workers with films in the 1 μm range have reported inferior values to those of the present work. It is anticipated that increasing the thickness of the present PZT films would result in even better dielectric properties. This is currently being pursued. It is important to note, however, that films with thicknesses in the range of 2000-3000Å and with attractive ferroelectric properties are needed to accommodate the current high level of microcircuit packing density (due to scaling considerations).

Precursor modification with DEA has also permitted the preparation of PZT fibers. To the best of our knowledge, this is the first time that PZT has been prepared in fiber form. One outstanding advantage in preparing fibers via the present chemistry is that fibers can be drawn from concentrated viscous solutions. This suggests the presence in the solution of stable linear chains of polymeric species. In many other sol-gel systems, fibers can only be drawn near the gelation point; and hence the processing window is severely limited. Further efforts are on-going to investigate the applicability of such DEA modification chemistry in other ferroelectric fiber systems for potential composite applications.

VIII. SECOND HARMONIC GENERATION FROM FERROELECTRIC THIN FILMS

Second harmonic generation (SHG) - frequency doubling - is an important non-linear optical phenomena. It is displayed by non-centrosymmetric compounds as typified by ferroelectric materials. Polarization in an optical medium can be expressed by the following equation: $P=x^{(1)}E+x^{(2)}EE+x^{(3)}EEE+....$ The coefficient $x^{(2)}$, a quadratic electric field term, is the second order non-linear susceptibility and is a third-rank tensor. The value of this coefficient determines the strength of the SHG signal observed.

In this study, SHG from various wet chemically derived ferroelectric thin films has been investigated. SHG was measured using a modified Kurtz-Perry powder method (25). The measurement technique involved rotation of the films with excitation by a Nd-YAG laser (1.06 μm wavelength) while the second harmonic signal (green light, 530 nm) was measured in the transmission mode with a photomultiplier tube. Various Pb-based ferroelectric compositions were studied, namely lead titanate (PT), lead zirconate titanate (PZT), lead lanthanum titanate (PLT) and lead lanthanum zirconate titanate (PLZT). The precursors for these systems were methanolic solutions of $Pb(OAC)_2 \cdot 3H_2O$, $Ti(O^iPr)_4$, $Zr(O^nPr)_4$ and $La(O^nBu)_3$. Other ferroelectric compositions such as barium titanate, lithium niobate, potassium niobate, lithium tantalate, barium sodium niobate and bismuth titanate were also synthesized. For these compositions, alkoxide precursors were used except for the case of Bi where bismuth 2-ethylhexanoate was used. In all cases, films were deposited on fired SiO_2 substrates via spin-coating. Multiple coatings, with intermediate heat treatments, were employed to produce films with thicknesses in the range of 0.4-0.5 μm.

For the Pb-based systems, the phases identified by X-ray diffraction in films heated at 500C for 30 minutes are shown in Table 25. As seen there, $PbTiO_3$ films were comprised of pyrochlore + perovskite + amorphous after this heat treatment, as were $PbTiO_3$ films containing 7 mole % La. On increasing the La content to 15 mole %, pyrochlore was no longer observed. Changing from $PbTiO_3$ to PZT (65/35) in composition yielded amorphous films, and amorphous films were also obtained for PZT (65/35) containing 0 mole % La. The observed SHG from a $PbTiO_3$ film heated at 650C for 30 minutes is shown in Fig. 61, and the magnitudes of the maximum observed SHG signals for PLZT films of various compositions heat treated at 650C and

Table 25 - Phases Found in Films (4000A) on Silica

Heated at 500C for 30 Min.

x/y/z/ PLZT* Composition	Phases Found
0/0/100	Pyrochlore + Perovskite + Amorphous
7/0/100	Pyrochlore + Perovskite + Amorphous
15/0/100	Perovskite + Amorphous
0/65/35	Amorphous
9/65/35	Amorphous

* $Pb_{1-x/100}La_{1-x/100}(Zr_{y/100}Ti_{z/100})_{1-x/400}O_3$

Figure 61 - SHG from a 0.4 μm Thick $PbTiO_3$ Film Heated at 650C for 30 Min.

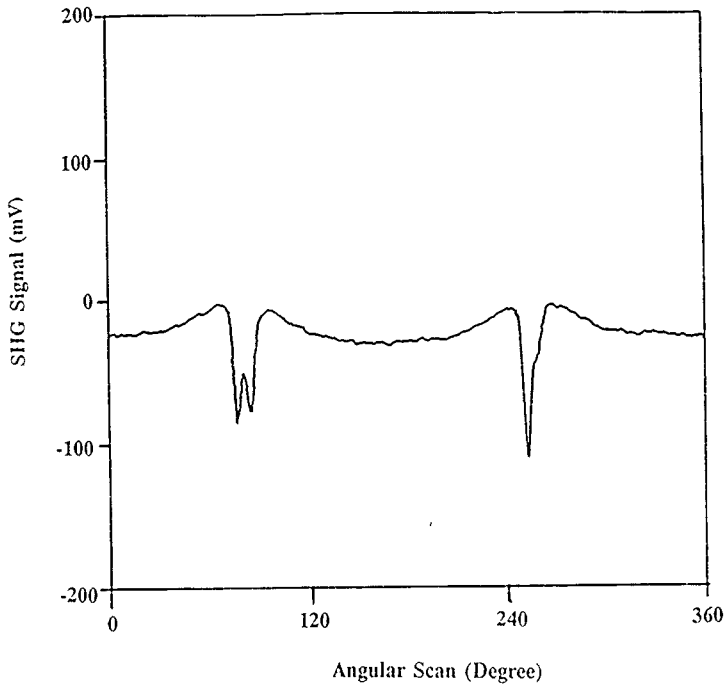

750C are shown in Table 26. As seen from the data in the Table, the maximum SHG intensity increases with increasing heat treatment temperature and is higher for $PbTiO_3$ than for any of the La- and Zr-doped materials. It is also seen that the incorporation of Zr has a considerable effect in decreasing SHG. The effect of heat treatment temperature on SHG from 7/0/100 PLZT films is shown in Table 27. A rather dramatic increase in SHG between 700 and 750C is noted, reflecting substantial densification of this film within this temperature range.

For a ferroelectric material such as $BaTiO_3$, whose Curie temperature lies not far above ambient, heating induced by a high intensity laser beam can lead to a decrease in the SHG signal - and even to its disappearance as beam heating raises the temperature above the Curie point (where the material is centro-symmetric). This behavior is illustrated by the results shown in Fig. 62. When the scanning was interrupted for 15 minutes and then resumed, the SHG intensity returned effectively to its original value (such as that depicted in the top left portion of Fig. 62).

SHG from lithium niobate, potassium niobate, lithium tantalate, barium sodium niobate and bismuth titanate films on fused silica was investigated as a function of post-deposition thermal treatment and the results are summarized in Table 28. In all of these cases, the desired ferroelectric phase was formed (as evidenced by XRD) on firing to 750C for 30 minutes. Further work is currently underway to study the effects on SHG from poled ferroelectric films and films deposited on various substrates.

To the best of our knowledge this is the first reported instance of SHG from sol-gel derived ferroelectric thin films.

Table 26 - Second Harmonic Generation from Various Films (0.4 μm Thick) on Silica

Composition (mV)	Maximum SHG Signal (mV) Treated at 650C	Maximum SHG Signal (mV) Heated at 750C
PLZT[(a)] 0/0/100	100	265
PLZT[(a)] 7/0/100	25	122
PLZT[(a)] 15/0/100	15*	120
PLZT[(a)] 0/65/35	None Detected	20
PLZT[(a)] 9/65/35	15*	20

(a) x/y/z PLZT: $Pb_{1-x/100}La_{x/100}(Zr_{y/100}Ti_{z/100})_{1-x/400}O_3$

* Within detection limits

Table 27 - Effect of Heat Treatment Temperature on Second Harmonic Generation from 7/0/100† PLZT Films (4000Å)

Annealing Temp. (C)	Maximum SHG Signal (mV)	Phases
500	13*	Pyrochlore + Perovskite
650	21	Perovskite
700	38	Perovskite
750	122	Perovskite

† x/y/z PLZT: $Pb_{1-x/100}La_{x/100}(Zr_{y/100}Ti_{z/100})_{1-x/400}O_3$

* Within detection limit

Figure 62 - Effect of Heating from Nd-YAG Laser on SHG from a $BaTiO_3$ Film on Silica. Film had been Heat Treated at 900C for 30 Min. Prior to Test.

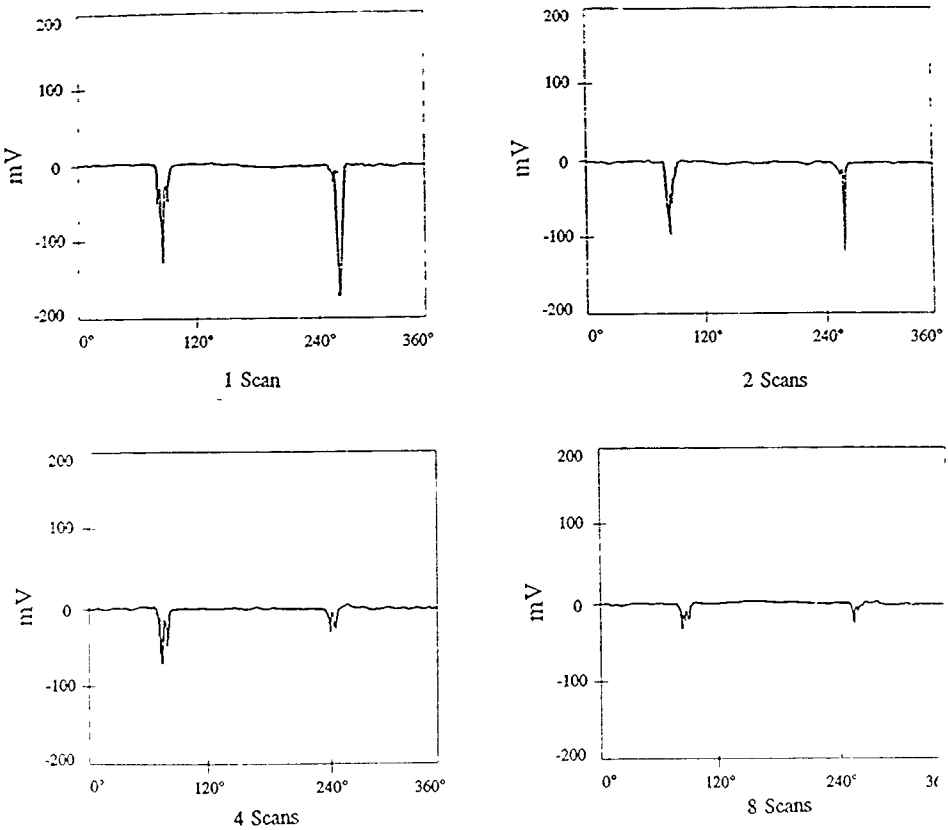

Table 28. Effect of Heat Treatment Temperature on Second Harmonic Generation from Various Ferroelectric Films

Composition	Maximum SHG Signal (mV)		
	750C	850C	950C
$LiNbO_3$	75	110	110
$KNbO_3$	*	*	*
$LiTaO_3$	*	*	115
$Ba_2NaNb_5O_{15}$	14	18	27
$Bi_4Ti_3O_{12}$	20	-	-

*Below detection limits

References

1. D.R. Uhlmann, G. Teowee, J.M. Boulton and B.J.J. Zelinski, to appear in Better Ceramics Through Chemistry IV. ed. B.J.J. Zelinski, C.J. Brinker, D.E. Clark and D.R. Ulrich (MRS,1990).

2. M.S. Ameen, T.M. Graettinger, S.H. Rou, H.N. Al-Shareef, K.D. Gifford, O. Auciello and A.I. Kingon: MRS Synp. Proc. Vol. 200, Ferroelectric Thin Films, Ed. E.R. Myers and A.I. Kingon (1990) p.65.

3. K.L. Saenger, R.A. Roy, K.F. Etzold and J.J. Cuomo, ibid. p.115.

4. C.K. Chiang, L.P. Cook, P.K. Schenck, P.S. Brody and J.M. Benedetto, ibid. p. 133.

5. A. Croteau, S. Matsubara, Y. Miyasaka and N. Shohata, pn. J. Appl. Phys. 26 (Suppl. 2) (1987) 18.

6. K. Sreenivas and M. Sayer: J. Appl. Phys. 64 (1988) 1484.

7. S.K. Dey, K.D. Budd and D.A. Payne, IEEE Trans. on Ultra, Ferro and Freq. Control 35, 80 (1988).

8. B. Yi, Z. Wu and M. Sayer, J. Appl. Phys. 64, 2717 (1988).

9. D.A. Payne, paper presented at Ultrastructure Meeting, Tucson, 1989.

10. C.J. Chen, E.T. Wu, Y.M. Xu, K.C. Chen and J.D. Mackenzie, Proc. First Symp. Integ. Ferroelectrics, Colorado Springs, 1989, pp 185-188.

11. S.K. Dey and R. Zuleeg, Ibid., pp. 189-194.

12. B.A. Tuttle, T.J. Garino, D.M. Doughty, S.L. Martinez and J.L. Yio, paper presented at Amer. Cer. Soc. Annual Meeting, Indianapolis, IN, 1989.

13. C.C. Hsuey and M.L. McCartney, Ibid.

14. R.A. Lipeles, N.A. Ives and M.S. Leung, in Science of Ceramic Chemical Processing (dited by L.L. Hench and D.R. Ulrich, Wiley, 1986) pp.320-326.

15. R.A. Lipeles and D.J. Coleman in Ultrastructure Processing of Advanced Ceramics (edited by J.D. Mackenzie and D.R. Ulrich) pp.919-924 (1988).

16. R. Moazzanni, C. Hu and W.M. Shepherd: 28th Annual PNC Ref. Phys 1990, p. 231.

17. J. Carrano, C. Sudhama, J. Lee, A. Tasch and W. Miller: Intl. Electr. Dev. Meet. 1989, p. 255.

18. Y. Xu, C.J. Chen, R. Xu and J.D. MacKenzie: Ferroelectrics 108 (1990) 47.

19. Y. Takahashi, Y. Matsuoka, K. Yamaguchi, M. Matsuki and K. Kobayashi: J. Mater. Sci. 25 (1990) 3960.

20. T. Yoshihara and I. Kikuchi: US Patent 4636908 (Jan. 13, 1987).

21. K.D. Budd and D.A. Payne: Inst. Phys. Conf. Ser. 103 (Part 1) (1989) 13.

22. B.A. Tuttle, R.W. Schwartz, D.M. Doughty and T.A. Voight, Ibid, p. 159.

23. L.E. Sanchez, S. Wu and I.K. Naik: Appl. Phys. Lett 56 (1990) 2399.

24. G.M. Haertling, Am. Ceram. Soc. Bull. 43, 875 (1964).

25. S.K. Kurtz and T.T. Perry, J. Appl. Phys. 39 (1968) 3798.